ESCUELA LATINOAMERICANA DE FISICA

ARGENTINA

1970

PROPERTIES OF ACCELERATED BEAMS;

SOME USES IN NUCLEAR PHYSICS.

M. J. SAMETBAND

PROPERTIES OF ACCELERATED BEAMS: SOME USES IN NUCLEAR PHYSICS

M. J. Sametband.

1.- Principles of operation of tandem electrostatic accelerators and cyclotrons.

2.- Beam transport systems.
Magnetic spectrographs.

3.- Temporal structure of beams.
Uses of bunching and of the beam microstructure in nuclear physics.

4.- Time of flight spectrometry.
Uses in nuclear physics with charged particles and with neutrons.

PROPERTIES OF ACCELERATED BEAMS; SOME USES IN NUCLEAR PHYSICS

M. J. SAMETBAND.

DESCRIPTION OF THE TANDEM ACCELERATORS AND CYCLOTRONS.

The tandem Accelerator.

This electrostatic accelerator has been developed during the last 16 years. Its basic concept: to use controlled atomic collisions to change the ion-charge in order to double the energy of the accelerator, has been discussed since 1932. At Winsconsin University, R. Herb developed a high current negative hydrogen ion source, which made possible the construction of the first tandem accelerator by the High Voltage Engineering Corporation directed by R. J. Van de Graaff. This tandem was succesfully operated in 1958, giving 1.5 μA of 13.4 MeV protons.

The accelerator consists basically of a cilindrical tank filled at high pressure with a dielectric gas; in its center there is a high voltage terminal charged with a moving belt to a potential V. The negative ions are injected into the tank and reach the energy ZeV when they pass trough the central terminal; there they are stripped of two or more electrons, so converted into positive ions which are accelerated by the terminal back to ground potential , to an energy of a least 2 ZeV, depending on the tandem type.

There are at present several tandem types; the most representative is the two-state tandem accelerator, like the HVEC Model EN istalled at the Comision Nacional De Energía Nuclear, in Mexico. Its main characteristics are: terminal potential 1.5-6 MV proton energy 3-12 MeV, analyzed beam intensity 2 μA for protons.

We will consider separately the following components:

1) Ion source and injection system.
2) Acceleration tube.
3) Stripper canal.

Ion source and injection system

The ion source is external and at ground potential, so there are no restrictions of space, cooling, etc. In principle it is possible to produce beams of all the isotopes of the periodic table either as negative ions or as accelerated neutral atoms.

To achieve the desired beam intensity it is necessary to use different types of ion sources, depending on the physical properties of the elements. Before discussing specific types, we will define the beam quality:

Emittance

The state of a particle in the ion beam can be described by a position vector in a six-dimensional phase-space, the components of which are space coordinates $q(t)$ and the canonically conjugate momenta $p_k(t)$, where $k = 1, 2, 3$. The particles density in the phase space is $\Psi(\bar{q}, \bar{p}, t)$, and the total number is $\Psi(\bar{q}, \bar{p}, t)\, dq\, dp$.

If none of the particles are lost from the beam, we apply Liouville's theorem from statistical mechanics:

In the phase space we express the conservation of matter by a continuity equation similar to the one used in hidrodynamics:

The density Ψ in phase space remains constant if the particles move due to forces which are not velocity dependent. The movements define a velocity $\bar{v}$ of components $\dot{p}_k$, $\dot{q}_k$, so

$$\dot{\Psi} = -\Psi \nabla \cdot \bar{v}$$

Since

$$\nabla \cdot \bar{v} = \sum_k \frac{\partial \dot{p}_k}{\partial p_k} + \frac{\partial \dot{q}_k}{\partial q_k}$$

, and Hamilton equations

introduced in $\nabla \cdot \bar{v}$ give

$$\nabla \cdot \bar{v} = 0$$

so

$$\dot{\Psi} = 0$$

If interacting forces are negligible and the paraxial aproximation applies, each two-dimensional subspace $(q, p)_k$ can be considered independent:

Since then

$$\Psi = \Psi_1 \cdot \Psi_2 \cdot \Psi_3$$

$$\dot{\Psi}(q_1, p_1) = \dot{\Psi}(q_2, p_2) = \dot{\Psi}(q_3, p_3) = 0$$

and so the area encompassing the points which represent the particles in each phase-plane remains constant, but it may change shape. If the beam moves in direction s, the areas occupied by the totality of particles in (x, p_x) and (z, p_z) phase-planes are beam invariants and called x and z emittance respectively (ε_x and ε_z)

Formally:

$$\varepsilon_x = \oint p_x\, dx \quad , \quad \varepsilon_z = \oint p_z\, dz$$

Generally p_x, p_z are inferred from the relationship

$$p_x \approx x' \sqrt{2meV} \quad , \quad p_z \approx z' \sqrt{2meV}$$

x', z' being the slopes of the trajectory, which is correct at non-relativistic energies for paraxial rays.

The distribution of x' and z' for the particles of a beam as a function of x and z, can be experimentally determined.

The emittance so obtained is usually circumscribed by an ellipse of minimun cross-section

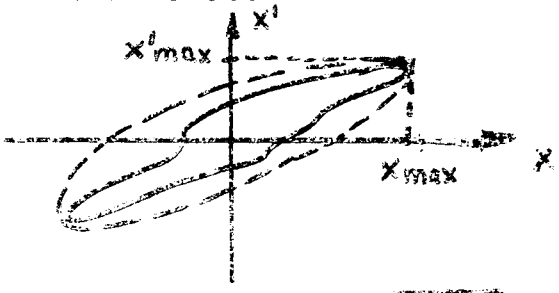

and written as: $\varepsilon_x < \pi x_{max} x'_{max} \sqrt{2mV}$

which is the area of that ellipse.

In most ion sources the beam has cylindrical symmetry, and one defines a phase plane depending only in radial coordinate r and p_r. The emittance is often called the brightness of the source, and is a figure of merit of beam quality.

The emittance of a source depends upon the temperature and mass of the positive ions in the emitting plasma. It is exressed in units of cm rad $MeV^{\frac{1}{2}}$, with the mass of the proton taken to be 1.

Beam Homogeneity

Measurements of the beam intensity of an ion source as a function of time show a "hash", due to plasma oscilations this "hash" has a continuous frequency spectrum with some peaks. The inhomogeneities in the plasma which cause this spectrum are caused by random processes, and produce an approximately gaussian energy distribution. The energy spread of the positive ion beam emerging from the source plasma is of the order of 40 eV for a Radio Frequency ion source, and 10 eV for a duoplasmatron. To this must be added the energy straggling due to ionizing collisions, and electron pickup in the attachment target, resulting in a total energy spread of about 50 eV in most ion sources.

Production of negative ions.

We may distinguish two methods of production:

a) Production by collisional attachment { with plasma focusing / with a separate lens system.

b) Production by direct extraction.

a) Negative ion production by collisional attachment occurs in two steps: 1.- Positive ions are extracted from a plasma, and 2.- They pass through an attachment canal where

they capture electrons.

A high current negative ion source of this type was developed by Brooks *et al* 5)

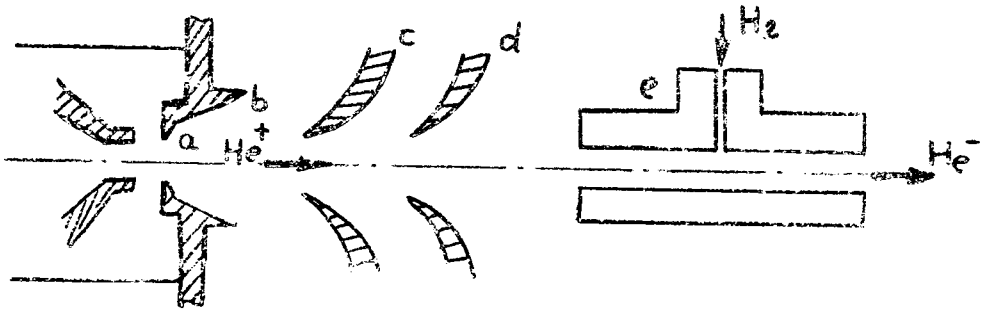

The geometry of the figure, were (a) is the anode aperture, (b) the plasma expansion cone, (c) the extractor electrode, (d) suppression electrode, (e) the attachment canal, gives a He^+ beam current of 30 mA. These positive ions pass through the charge-changing canal were they capture electrons from molecular hydrogen; the $H\bar{e}$ current is of 3 μA and the emittance of this ion source is 2 cm *mrad* $MeV^{1/2}$.

The disadvantage of this plasma focusing source is that once optimized for one element, it does not work as well for others.

This problem is eliminated by separating the functions of ion extraction and focusing, using a lens between the source and the canal to focus the positive ions into the attachment region. A source of that type was developed by Rose el al6) for the Tandem EN of 12 MeV. The H^+ beam through the canal is 7mA using a *duo*plasmatron.

The H^- output is 35 μA, and the emittance is 6 mrad cm $MeV^{\frac{1}{2}}$.

b) Negative ion production by direct extraction.

Since negative ion production by collisional attachment takes place in two steps, the emittance of the negative ion beam depends upon that of the initial positive ion beam and on the scattering produced by the attachment process. ~~Since it is important to produce by the attachment process~~. Since it is important to produce a beam of the smallest emittance, the direct extraction type of source has been developed, where the negative ions are taken directly from the plasma of the source. As an example, the one studied by Lawrence etal 7) gives 100 μA of H^- or D^-.

2) Acceleration tube

The negative ion beam goes through an analyzing magnet, and is injected into the accelerator, consisting of a cylindrical tank filled with SF_6 at 15 atmospheres.

Its lenght is about 10 meters and the diamater is 2,4 meters. The accelerating tube coincides with the tank axis, and is supported by glass and metal columns, which are in turn surrounded by equipotential rings in order to mantain constant the gradient of the electric field along the tube.

The HVEC developed the inclined-field tube in which the inclined fiel lines reduce the current of electrons produced during high-voltage discharges, since the electrons are

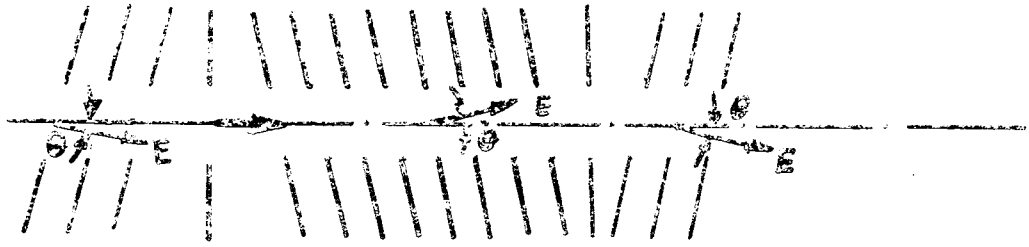

directed against the inclined electrodes. An important result is a great reduction of the electrons-load and of the X-ray background.

At the tank center there is a high-voltage terminal, supplied with current by a belt charging system, which collects charges from a system of points connected to a generator of + 30 KV. For a tandem of 12 MeV, the time needed for the terminal to reach 6MV is 3 seconds, and if there is a discharge, it needs a time of this order to recuperate the former voltage. A controlled corona discharge from a system of points which surround the terminal enables the stabilization of the high voltage up to ± 1 KV.

In several tandems there has been observed a voltage fluctuation, due to movements of the charge transporting belt, or to a non-uniform charge distribution on its surface [8]. Also particles and dust from the belt may cause discharges.

R.G. Herb, at National Electrostatics Corporation developed a new tipe of tandem, called Pelletron, and which should have a voltage fluctuation of only ± 50 V.

The Pelletron charging system consists of an endless chain made of alternate metalic cylinders and insulating sections, which connects a pulley in the terminal to a driven pulley at ground potential. The metalic cylinders are charged by induction when passing near a high voltage electrode, and transport the charges to the terminal which is in contact with the metallic pulley. In that way the collection of charges by means of a corona discharge is avoided, and there are no particles of dust generated by the gradual disintegration of the usual charging belt.

Each endless chain transports 100 μA of equivalent charge, and four chains are provided for each accelerator.

The accelerating tube is modular, formed with units of 18 inches, which are rated at a gradient of 1 MV over the 18".

The first version of the Pelletron is being installed at the Universidade de Sao Paulo, Brazil, and it consists of an injertor of 5 MV, and a two stages tandem of 8.5 MV. This combination results in a 3-stage beam energy of 22 MeV for a protons, with a current of 10 μA .

3) Stripper canal

The negative ions injected into the tandem, are accelerated by the negative ion acceleration type and focused into the stripper canal which is inside the high voltage terminal. There two or more electrons are removed in the gas or foil target, so producing a beam of positive ions which passes into the positive ion acceleration tube and is accelerated back to ground potential.

In the case of protons, the final energy E_f is

$$E_f = 2V_T e + E_i$$

where V_T is the terminal voltage, E_i the energy of the injected positive ions. With heavier elements, it is possible to remore more electrons, and E_f is:

$$E_f = (1+Z)V_T e + E_i$$

where Z is the efective charge of the positive ion.

The electrons are removed from the incident ions by successive collisions with the atoms of the stripping material. The fraction F_i of the incident beam which has the charge state i and can be converted to negative ions is a function of target thickness; as the thickness increasee, the attachment and loss process reach an equilibrium.

The variation of the charge state as a function of the thickness is given by a set of (K+1) linear differential equations [1])

$$\frac{dF_i}{d\Pi} = \sum_{n=0}^{i} F_{i-n}\,\sigma_{i-n,i} - F_i \sum_{n=1}^{K-i} \sigma_{i,i+n} - F_i \sum_{n=0}^{i} \sigma_{i,i-n} + \sum_{i=1}^{K-i} F_{i+n}\,\sigma_{i+n,i}$$

where Π is the number of atoms in the target per cm^2, $\sigma_{i+n,i}$ the cross-section for the remoral of n electrons from the i+h charge state.

In general those cross-sections remain to be measured the few data available show that σ_{ij} is maximun when the ion is moving with a velocity close to that of the orbital velocity of the electron i and the electron j.

Solid strippers give a greater fraction of high charge states than gaseous strippers. For example, for iodine ions of ^{127}I, it is possible to obtain a charge of 17+ using a molecular oxygen stripper, and of 24+ with a carbon foil. The reason for that is the fact that the spacing of atoms in a solid is so close that the positive ion does not have time to de-excise between collisions, and the

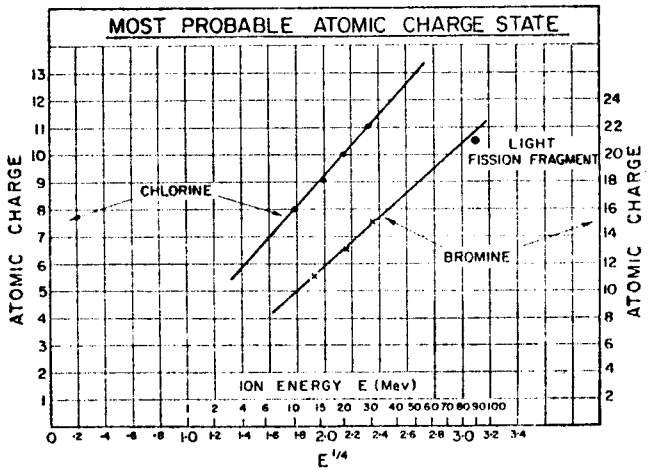

FIG. 6. Each point indicates the energy at which the corresponding atomic charge has maximum intensity. The straight lines are used to extrapolate the data as discussed in the text.

Population of charge state i

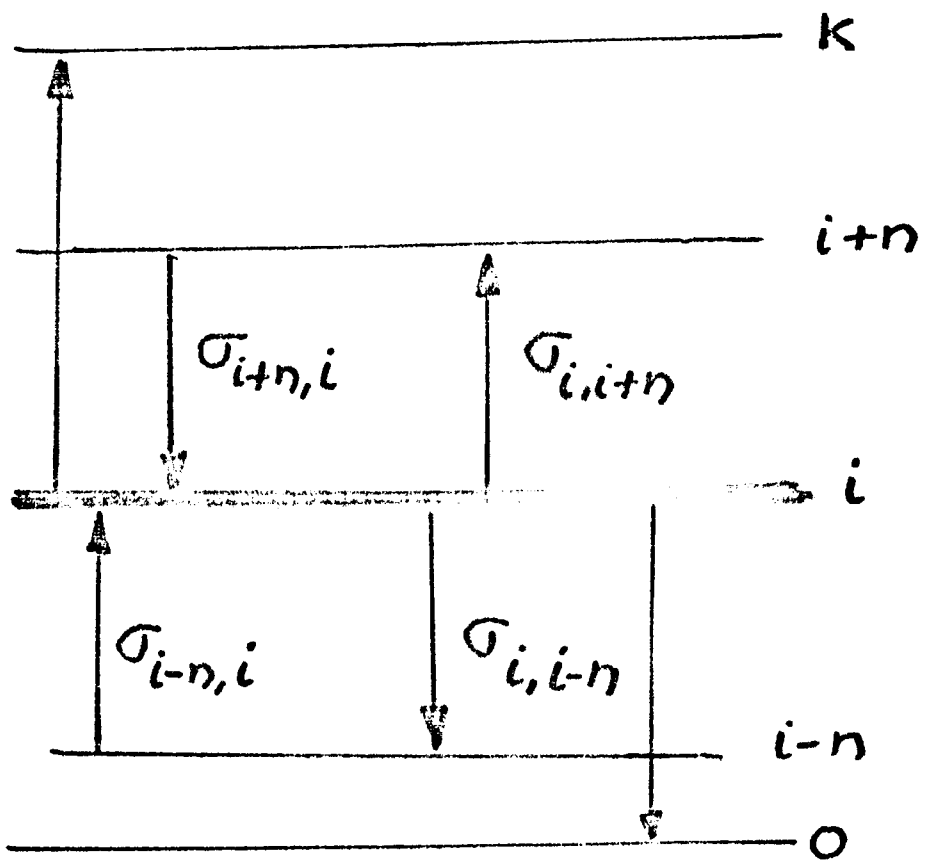

$$\frac{dF_i}{d\pi} = \sum_{n=0}^{i} F_{i-n}\,\sigma_{i-n,i} - F_i \sum_{n=1}^{K-i} \sigma_{i,i+n} - F_i \sum_{n=0}^{i} \sigma_{i,i-n} + \sum_{n=1}^{K-i} F_{i+n}\,\sigma_{i+n,i}$$

electrons are stripped from the excited states.

If after the stripper there were no change of the charge state of the ions, the spectra of the analized beam would appear as a series of well separated peaks

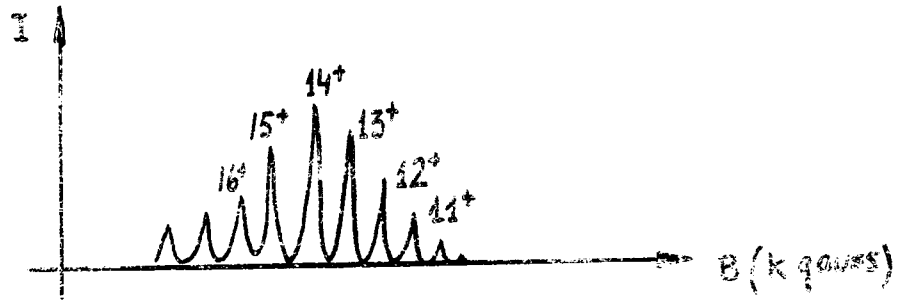

The distribution is gaussian, typical of a stripped beam, when the mean charge state is far from both extreme 0 and Z.

But since the analyzing system has a resolution better than 1/1000, and the beam which emerges from the tandem has an energy dispersion much smaller than 1/1000, any isotope of the element injected as a negative ion is well resolved:

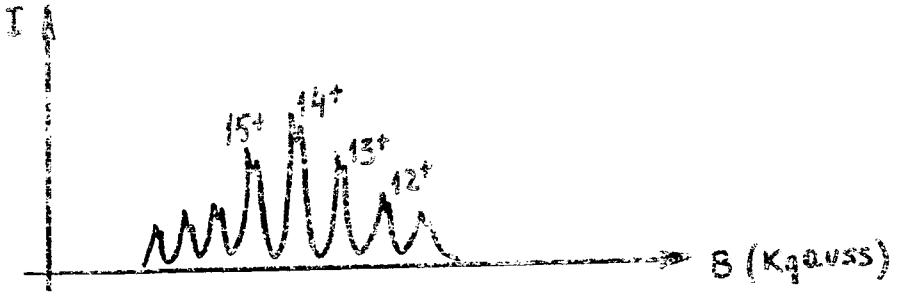

If it is desired to use only one isotope, it is necessary to introduce separated isotopes in the ion source, or to use an injection system with a high resolution analyzing magnet, in order to select the desired beam; but that means the problem of identifying the component.

In practice it is impossible to avoid charge-state changes after the stripper, and a continuum of particles of different charges and energies appears so giving the spectra of the figure:

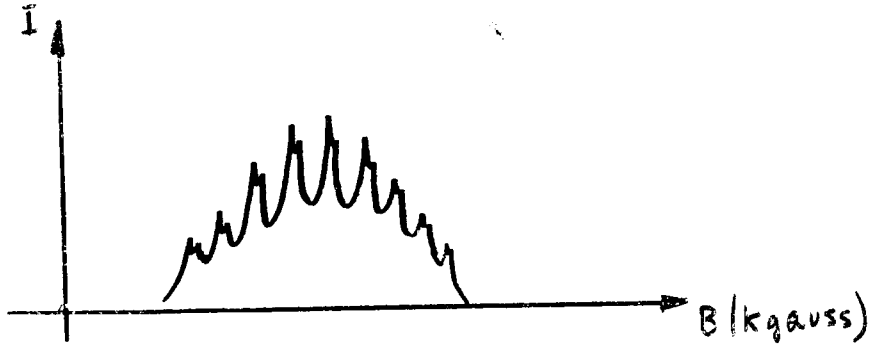

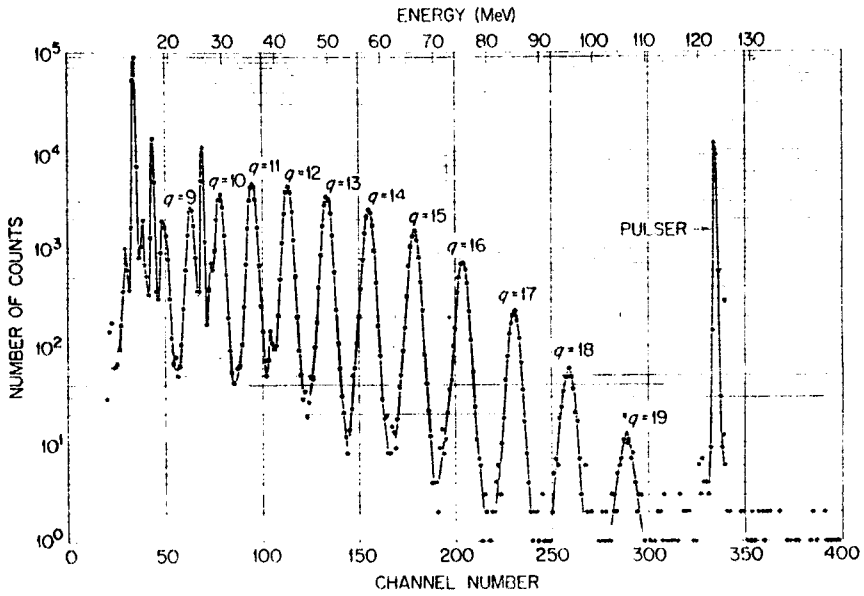

Fig. 2. Pulse height spectrum of iodine ions from the Oak Ridge Tandem Van de Graaff Accelerator. The ions are deflected through a 90° analyzing magnet onto a silicon surface barrier detector.

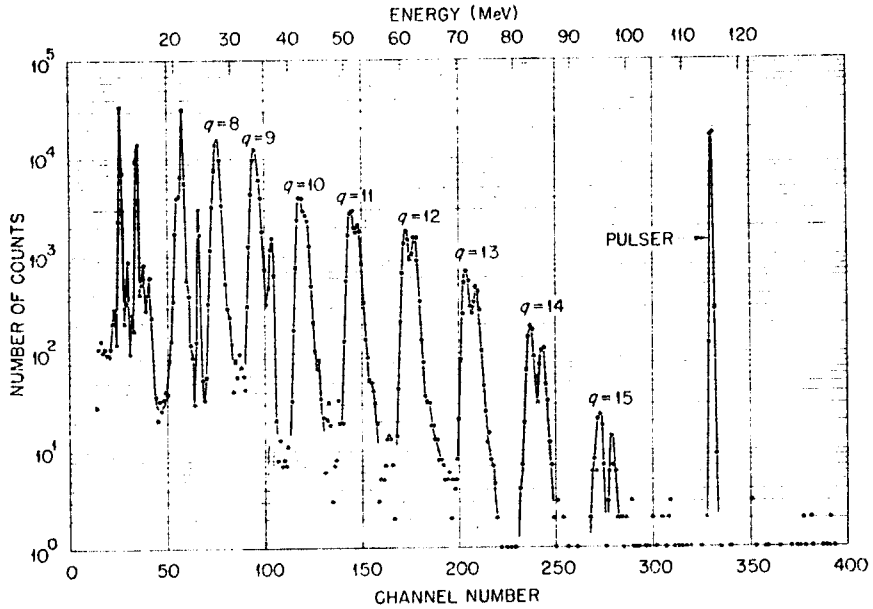

Fig. 3. Pulse height spectrum of bromine ions from the Oak Ridge Tandem Van de Graaff Accelerator. The ions are deflected through a 90° analyzing magnet onto a silicon surface barrier detector.

The cyclotron

In the cyclotron a magnetic field B is perpendicular to the trajectory of ions which have a velocity v, charge to mass ratio $\frac{e}{m}$. In that case the movement is practically circular, with a radius of curvature ρ and an angular frequency ω:

$$\omega = \frac{v}{\rho} = \frac{eB}{m}$$

This frequency is independent of the speed of the particles, for non-relativistic energies.

The ions are accelerated by an electric field between electrodes called dees; the alternating voltage has a frequency ω_E which coincides with ω, so a particle that starts at the right time will receive an increase on Kinetic energy of 2 e V each time it crosses the gap between electrodes.

It is possible to accelerate in that way protons or deuterons up to about 20 M e V. But the relativistic variation of mass with speed increases the mass in about 1% for protons of 10 M e V; the frequency ω of the ions does not coincide with ω_E, the particles traverse the gap out of phase with the electric field, and can not be accelerated at more than 25 MeV.

To increase the energy over 25 MeV, there are two possibilities according to eq. (1):

1) To keep constant the field frequency, so $\omega_E = \omega$ = const. means to increase B simultaneously with the relativistic increase of m.

That means that the magnetic field should increase from the center of the spiral trajectory to the maximum radius.

2) To vary ω_E and mantain it equal to ω, which diminishes when the ion energy increases.

The first possibility was abandoned due to the unstabilities appearing in the orbit when the magnetic field does not decrease with radius:

Let us consider a magnetic field $B(r)$ which weakens radially

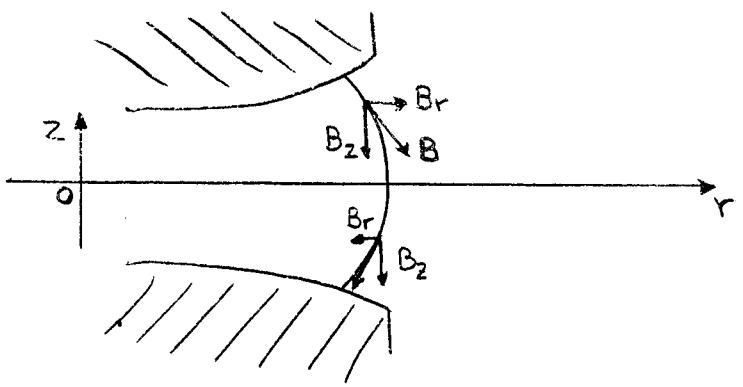

There is a radial component B_r outside the median plane, B_r increases with increasing axial displacement Z. The

relation B_r (Z), may be expressed as:

$$B_r = z\left(\frac{\partial B_r}{\partial z}\right)_{z=0} + \frac{z^2}{2}\left(\frac{\partial^2 B_r}{\partial z}\right) + \cdots$$

For small values of Z only the first term remains.
Since in a static magnetic field rot B=0

$$B_r = \frac{\partial B_r}{\partial z} z = \frac{\partial B}{\partial r} z$$

When a particle of velocity V moves in that field, appears a Lorentz force $e\bar{v}x\bar{B}$, which has a component toward the median plane, and therefore it acts as a restoring force F_z

$$F_z = e V_\theta \frac{\partial B_z}{\partial r} z = e w r \frac{\partial B_z}{\partial r} z = m w^2 \frac{r}{B_z} \frac{\partial B_z}{\partial r} z$$

Calling

$$K = \frac{r}{B_z} \frac{\partial B_z}{\partial r} \qquad F_z = m w^2 K z$$

we have Kerst-Serber equation for axial betatron motion;

$$\frac{d^2 z}{dt^2} - K w^2 z = 0$$

which gives a simple harmonic motion of frequency $w_z = w\sqrt{(-K)}$ if K is negative
We see that for axial stability $K < 0$, or $\partial B/\partial r < 0$
In that case the particle oscillates axially like a mass on a spring. The frequency of this axial motion is for the usual values of K

$$w_z = K^{1/2} w$$

one axial oscillation occurs in 10 or 20 particle revolutions.

In a similar way can be found the radial stability condition. Let us consider a small radial displacement x from the equilibrium orbit of radius r_e.

The equation of motion in the radial plane is

$$-e V_\theta B_z = -\frac{m v^2}{r} + m \frac{d^2 x}{dt^2}$$

The field off the equilibrium orbit can be written

$$B_z(r) = B_z(r_e) + \partial B_z/\partial r \; x + \cdots$$

so we have

$$-e V_\theta \left[B_z(r_e) + \frac{\partial B_z}{\partial r} x\right] = m\left(-\frac{v^2}{r_e + x} + \ddot{x}\right)$$

Since

$$\frac{1}{r_e + x} \approx \frac{1}{r_e}\left(1 - \frac{x}{r_e}\right), \quad -e V_\theta \frac{\partial B_z}{\partial r} x = \frac{m v^2 x}{r_e^2} + m \ddot{x}$$

If $x \ll r_e$

$$\ddot{x} + w^2 (1 + K) x = 0$$

where the radial oscillation frequency is

$$w_r = w\sqrt{1 + K}$$

The differential equation can be put in the form

$$d^2x/d\theta^2 + (1 + K) x = 0$$

In order to have a radial harmonic motion, $K > -1$
So in order to have stable orbits,

$$0 > K > -1$$

which means that if B increases with radius, there will be exponencial axial and radial growth of the particle motion for that reason the solution 2) was adopted to increase the energies to relativistic values, so developing the frequency modulated cyclotron, or synchrocyclotron.

If we define the radial and axial frequencies, ν_r and ν_z respectively:

$$\nu_r = \frac{\omega_r}{\omega} = \sqrt{1+K}$$

$$\nu_z = \frac{\omega_z}{\omega} = \sqrt{-K}$$

$$\nu_r^2 + \nu_z = 1$$

Plotting these parameters one against the other,

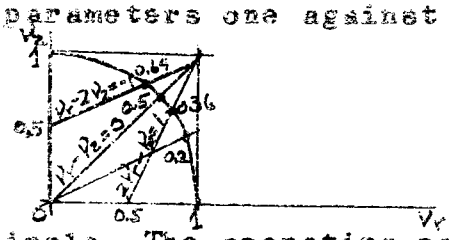

we describe a circle. The operating point moves along a quadrant, starting where K=0, ν_z=0 , ν_r=1 , and ending where K=-1 There is no orbit stability in those extreme points, neither at several other points of the circle, due to the fact that the axial and vertical betatron oscillations are in fact coupled, and there can be an energy transference from one motion to the other.

Those coupled resonances between the two modes of oscillation may be represented in the form;

$$A\nu_r - B\nu_z = C$$

where A,B,C, are integers, as represented in the graph.

There can be a loss of ion beam if the energy gain per turn is so small that the resonant condition is mantained for a time long enough to allow the energy transfer from one mode to another. This is specially so for the synchrocyclotron where the energy gain is of the order of 20 KeV per turn, and the first resonance encountered at K= -0.2 , where $\nu_r = 2\nu_z$, causes a big increase in the vertical amplitude.

At the Buenos Aires synchrocyclotron of 28 MeV deuterons, K=-0.22; for r=79 cm. The extraction of the beam starts at r= 76 cm, where K= -0.12; there $\nu_r = (0.88)^{1/2} = 0.98$ and $\nu_z = (0.12)^{1/2}$, so there are approximately 3 vertical oscillations per each turn, which coincides approximately with a radial oscillation.

Synchrocyclotrons

In those accelerators the frequency of the electric field is made to decrease as the particles gain energy in order to match the frequency of the particles. Since the oscillator frequency is modulated for that reason, it is easy to increase the degree of modulation to compensate for an increased

drop-off the field with radius, in order to increase the orbital stability of the ion trajectories; at B.A. cyclotron, the radio frequency voltage is 22 KV peak, with an initial frequency of 10.6 MHz.

The modulation frequency is 2 KH_z, and its amplitud is 4%. The mass increase is 1.6% for deuterons of 28 MeV, and the magnetic field decreases in 1.8% from r=0 to r=76cm. The total decrease of w is then

$$\frac{\Delta w}{w} = -\left(\frac{\Delta m}{m} - \frac{\Delta B}{B}\right) = -3,4\,\%$$

It takes 200 μs to accelerate a deuteron to maximun energy, and the number of revolution is $\omega \Delta t = 10^7 \times 200 \times 10^{-6} = 2 \cdot 10^3$, so each particle traverses 4000 times the gap between dees, and in order to reach 28 MeV it must acquire 7 KeV each time.

Isochronous cyclotrons

In 1938, L. H. Thomas [3]) gave the solution to the problem of making a cyclotron relativistic:"If the magnetic field is no longer rotationally symmetric, the orbits are not circular, and the orbital stability is achieved by means of a strong azimuthal variation of the magnetic field. In that way the field mean value along an orbit may increase with radius, without any defocusing of the beam".

But the concretion of such a field was impossible at that time. In 1950 two electron cyclotrons were built at Berkeley following Thomas principles. The first isochronous cyclotron to accelerate nucleons was operated at Delft, Holland, in 1958, and gave 12 MeV protons.

At the moment there are 20 functioning; the practical limit is 900 MeV for protons.

In the isochronous cyclotron the pole faces are divided in 3 or more sectors, of alternating strong and weak magnetic fields. The orbit of a particle changes its radius of curvature from one sector to another, and it has a radial velocity component directed alternatelly towards the center of curvature or in the opposite direction. This radial component forms a Lorentz force with the azimuthal component of the field, B_θ, which is called the Thomas force.

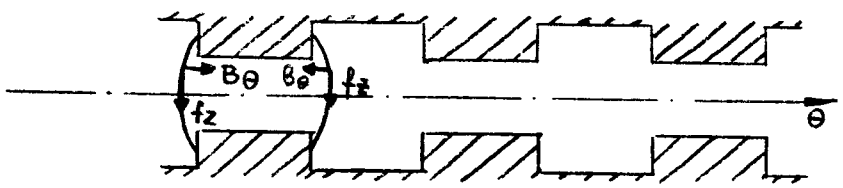

The magnetic fiel in the median plane Z=O can be described by a Fourier series:

$$B_z(r,\theta) = \langle B_z(r)\rangle \left[1 + \sum_n C_n(r)\left\{\cos n\theta - \varphi_n(r)\right\}\right]$$

If there are N hills or valleys and the field varies sinusoidally,

$$B_z(r,\theta) = \langle B_z(r)\rangle \left(1 + f\cos N\theta\right)$$

where f is the flutter amplitude $(f<1)$

The shape of a closed orbit can be calculated in the following way: the force F acting on a particle to deviate it from its circular trayectory is

$$m\ddot{x}_f = F = -qv\langle B\rangle - qv\langle B\rangle\left(1 + f\cos N\theta\right) + \frac{mv^2}{r} =$$

$$= -qv\langle B\rangle f\cos N\theta$$

If the radial displacement, x_f is $x_f << R$, we may write

$$-qv\langle B\rangle f\cos N\theta = m\ddot{x}_f$$

or $$-w^2 R f\cos N\theta = \ddot{x}_f = w^2\frac{d^2x_f}{d\theta^2}$$

Integrating twice

$$x_f = \frac{fR}{N^2}\cos N\theta$$

The orbital displacement has the same period of the magnetic field, and is positive in the hills. The radial velocity is

$$\dot{x} = v_r = w\frac{dx}{d\theta} = -\frac{wfR}{N}\operatorname{sen} N\theta$$

and is maximal in the border between hills and valleys.

Since there is an azimuthal component of magnetic field, B_θ :

$$B_\theta = \left(\frac{\partial B_\theta}{\partial z}\right)_{z=0} z + \ldots$$

and $$\nabla \wedge \bar{B} = 0$$

$$B_\theta = \left(\frac{\partial B_z}{R\partial\theta}\right)_{z=0} z$$

But

$$B_z = \langle B_z \rangle \left(1 + f \cos N\theta\right)$$

$$\frac{\partial B_z}{\partial \theta} = - \langle B_z \rangle N f \sin \theta$$

so

$$B_\theta = - z \frac{\langle B \rangle f N}{R} \sin N\theta$$

But B_θ and the radial component of the particles velocity, V_r, produce a force $-V_r B_\theta$ in the direction of Z:

$$F_z = - q V_r B_\theta = - m \omega^2 f^2 z \sin^2 N\theta$$

which is zero at the middle of a hill or valley and maximal at the border between them, but is alway directed towards the median plan, so it alwaye focusee the beam.

Usually the frequency of variation of F_z is large compared with the resulting particle oscillation, so $\sin^2 N\theta$ can be averaged between 0 and 2π, so get $1/2$, so

$$\langle F_z \rangle = \frac{1}{2} m \omega^2 f^2 z$$

The forces on the particle will then be $m\omega^2 kz$, as in the classical cyclotron, but with plus $\langle F_z \rangle$, and the equation for vertical movement

$$K = \frac{R}{\langle B \rangle} \frac{d\langle B \rangle}{dR}$$

$$\ddot{z} - \omega^2 K z + \tfrac{1}{2} \omega^2 f^2 z = 0$$

so

$$\omega_z^2 = \omega^2 \left(\tfrac{1}{2} f^2 - K\right)$$

or

$$\frac{d^2 z}{d\theta} + \left(\tfrac{1}{2} f^2 - K\right) z = 0$$

then,

$$\nu_z^2 = \left(\frac{\omega_z}{\omega}\right)^2 = \tfrac{1}{2} f^2 - K$$

which shows the new contribution to axial focusing, $\frac{1}{2} f^2$, proportional to the square of the flutter.

Condition for isochronism

The basic equation for the cyclotron in terms of the azimuthal averaged field $\langle B \rangle$ is

$$\omega = q \frac{\langle B \rangle}{m} = q \langle B \rangle \frac{c^2}{\gamma E_0} = q \frac{\langle B \rangle}{\gamma m_0}$$

The accelerator will be isochronous, that is, all ions will have the same frequency, if

$$\langle B \rangle = \gamma B_c$$

where B_c is the field at the center of the cyclotron.

The constant frequency will then be

$$w = \frac{q B_c}{m_o} = \frac{q B_c c^2}{E_o}$$

So an example,

For 100 MeV protons, where $E_o = 938$ MeV

$$\gamma = \frac{1038}{938} = 1.106$$ which means that

the magnetic field must increase in 10% from the center to the final radius.

The required magnetic field can be expressed as a Fourier series

$$B(r,\theta) = \langle B(r) \rangle \left[1 + \sum_N C_N(r) \cos N \left\{ \theta - \varphi_N(r) \right\} \right]$$

Radial stability is only possible when the two first harmonics are negligible ($C_1 \ll 10^{-3}$, $C_2 \ll 10^{-2}$) and to satisfy this condition the field has triple or gradruple symmetry around Z axis; the equation for B (r,θ) has them only terms with N multiple of 3 or 4.

To produce triple symmetry, 3 hills and 3 valleys of 60° each are built. The orbits have a greater curvature on the hills than on the valleys, and are not orthogonal to the boundary between them.

The stabilizing effect is greater if those boundaries spiral outward instead of being straight.

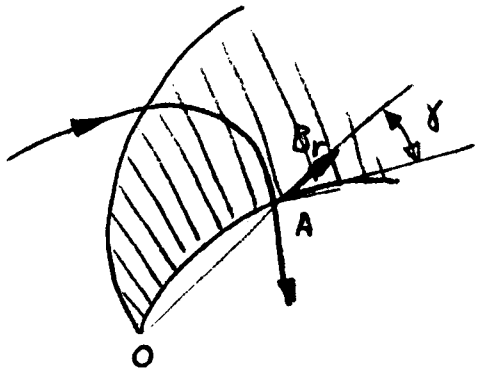

γ is the angle between radius OA and the tanget to the ridge at A, and it increases with radius; that means that out of the median plane there is a radial component B_r, which is directed outwards when the particle crosses the boundary from a valley to a hill, and inwards in the following boyndary.

That B_r and the momentum $m.v_\theta$ of the particle produces an axial force f_z which alternatively focuses and defocuses; the boundaries are so shaped that the focusing force is stronger.

Another axial focusing effect of the spiral is due to the diference between the axial forces on the boundaries, since the ones directed towards the median plane are slightly greater (see figure), because Thomas angle δ is smaller in boundary

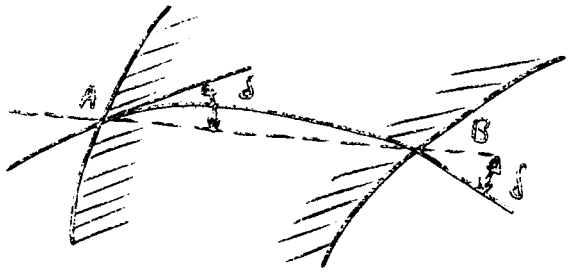

A. Each one of these forces is a separate term in the movement eqpations; Thomas's force and the other two ones are opposed to the defocusing action of the radially increasing magnetic field.

Correcting coil:

Several types of coils produce the desired field:

1) Principal coils
2) Trim coils- Those are individual rings, concentric, which cover the surface of each pole. They are used to produce a field which makes conetant the time for a complete revolution, independently of the radius.
3) Flutter coils- Covering the hills and valleys, control the focusing.
4) Harmonic coils- Situated on critical zonee, correct inhomogeneities and conform the initial orbits.

Variable Energy Isochronous Cyclotron

Since the isochronous cyclotron has its proper magnetic field shaped by means of several types of coils, as we have seen above, it seems feasible to optimize this field by varying the current of the coils, in such a way that several different energies can be reached at the final radius, and different particles can be accelerated, without correcting the field with iron pieces.

For each energy and kind of particle a different oscillator frequency is required, so ~~different~~ the radiofrequency must be variable. There are several possible plots which can be made to represent the required values of frequency and magnetic field for a range of energies of several different ions.

One of the most used ones is $\langle B \rangle r$ as a function of T/A, where T/A is the kinetic energy per nucleon, and r the final radius:

Since

$$\omega = \frac{e\langle B \rangle}{m} = \frac{v}{r}$$

and

$$\langle B \rangle r = \frac{E \beta c}{e c^2}$$

where

$$\beta^2 = \frac{E^2 - E_o^2}{E^2}$$

theh

$$\langle B \rangle r = \frac{(E^2 - E_o^2)^{1/2}}{zec}$$

since

$$E = T + E_o$$

$$\langle B \rangle r = \frac{(T^2 + 2 T E_o)^{1/2}}{zec}$$

multipying and dividing by the mass-number A

$$\langle B \rangle r = \frac{A}{zec}\left[\left(\frac{T}{A}\right)^2 + 2\left(\frac{T}{A}\right)\left(\frac{E_o}{A}\right)\right]^{1/2}$$

for

$$f.r = \frac{w}{2\pi} r = \frac{e\langle B \rangle r}{2\pi m} = \frac{zec^2}{2\pi E zec}\left[\left(\frac{T}{A}\right)^2 + 2\left(\frac{T}{A}\right)\left(\frac{E_o}{A}\right)\right]^2$$

$$f.r = \frac{c}{2\pi} \frac{\left[\left(\frac{T}{A}\right)^2 + 2\left(\frac{T}{A}\right)\left(\frac{E_o}{A}\right)\right]^{1/2}}{\left(\frac{E_o}{A} + \frac{T}{A}\right)}$$

where E_0/A is the rest energy per nucleon.

Hence if the $\langle B \rangle r$ for a proton is plotted against T/A, corresponding curves of $\langle B \rangle r$ for other particles can be obtained by multiplying $\langle B \rangle r$ by the radio A/Z. If the scale of f.r is added, parallel to that of kinetic energy, it is only necessary to multiply $\langle B \rangle r$ by $Zec^2/2\pi A\,(E_0/A + T/A)$ to get the different values.

In such a chart, as in the figure, for a machine of assumed radius and oscillator frequency, two vertical lines are drawn corresponding to the maximum and minimum f.R, and two horizontal lines at the highest and lowest values of $\langle B \rangle r$

The resulting rectangle shows the ions which can be accelerated and the energy range they will have:

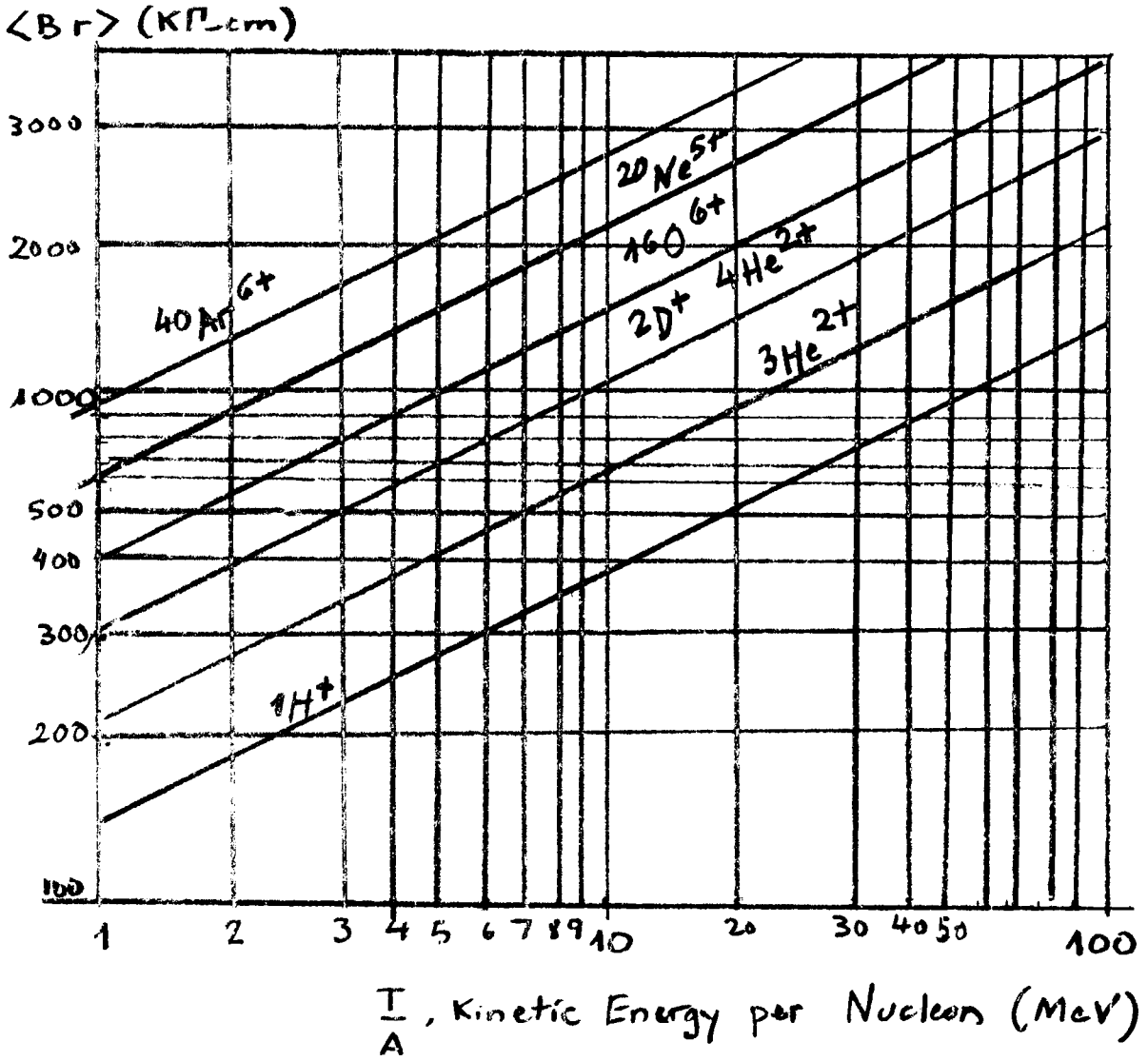

BEAM TRANSPORT SYSTEMS

We have been considering the motion of particles in the stages:

1) Injection
2) Acceleration

The stage:

3) Beam transport and analysis

is the displecement of the accelerated particles in order to perform physics experiments. Both stages 1) and 3) are important from the point of view of obtaining maximun beam intensity and the optimum conditions for performing the experiments. Along the tube which transports the beam out of the accelerator, there may be electrostatic and magnetostatic lenses, switching and analyzing magnets, for the purpose of focusing, deflecting and analyzing the beam during its travel from the source to the target.

After the target, there may be a spectrometer to analyze the reaction products.

We will first deal with the beam optics theory which gives the perfomance in all these elements.

Since we deal with systems with external electric and magnetic fields, where only conservative forces act on the charged particles, and we neglect radiative effects, beam scattering effects due to residual gas molecules in the evacuated tubes, and the space charge effects which are significant only in the region of the ion source, the beam displacement can be replaced by individual trajectories, and we can adopt the Hamiltonian formalism. Then, the total Hamiltonian for n particles is simply

$$\mathcal{H} = \sum_{i=1}^{n} \mathcal{H}_i$$

where, for the relativistic case:

$$\mathcal{H} = c\sqrt{m_0^2 c^2 + (\bar{p} - \frac{e}{c}\bar{A})^2} + e\phi$$

As has been seen when the emittance was defined, to each particle corresponds point in the six-dimensional phase space, with coordinates (p_k, q_k). Its movement is described by Hamilton's equations.

$$\dot{q}_k = \frac{\partial \mathcal{H}}{\partial p_k} \qquad \dot{p}_k = -\frac{\partial \mathcal{H}}{\partial q_k}$$

As a first approximation theory we consider the Hamiltonian as a sum of terms involving only canonically conjugate variables (p,q).

Let us consider an axially symmetric beam in a region where there are no accelerating forces, i. e, $p_s = m v_s =$ constant; then we may represent two particles in the beam with the position vectors $(r_1 p_1)$ and $(r_2 p_2)$, and we may apply Lagrange's invariant L to relate particle 1 to particle 2:

$$L = r_1 p_2 - r_2 p_1 = \text{constant}$$

If both particles are on the transverse phase plane $s=s_1$ and then pass to $s=s_2$, the relative position of the particles is preserved under a linear transformation between $s=s_2$ and $s=s_1$. This is the a form of Liouville's theorem, and is expressed as

$$L = r_1(s_1)\,p_2(s_1) - r_2(s_1)\,p_1(s_1) = r_1^*(s_2)\,p_2^*(s_2) - r_2^*(s_2)\,p_1^*(s_2)$$

If (r, p) is the position vector of a particle at the input of an ion optical element of the beam transport system, and (r^*, p^*) the vector at the exit, then the linear transfer properties of the optical element depend upon the component's geometry and working conditions, and can be given in terms of a transfer matrix with elements a_{ij}:

$$\begin{bmatrix} r^* \\ p^* \end{bmatrix} = \begin{bmatrix} a_{11} & a_{12} \\ a_{21} & a_{22} \end{bmatrix} \begin{bmatrix} r \\ p \end{bmatrix}$$

the determinant of the matrix being unity.

Transfer matrices for some optical elements

1) Space without any field (0)

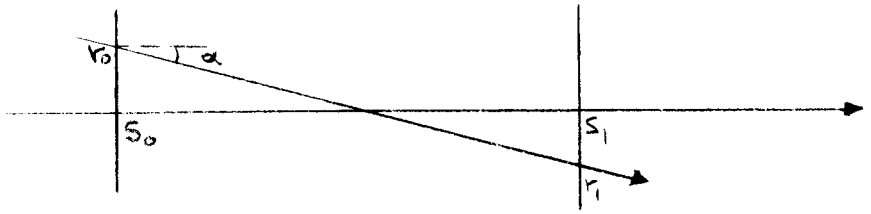

Let us consider a beam trajectory in a space without any field, (drift space) which has a longitude $\ell = s_1 - s_0$,

and an input position vector (r_0, p_0),

where $p_0 \equiv \frac{dr_0}{ds} = tg\,\alpha = r_0'$

We will geometrically determine the exit vector (r_1, p_1):

$$r_1 = r_0 + \ell\, tg\,\alpha = r_0 + \ell\, r_0'$$
$$r_1' = r_0'$$

The transfer matrix is then

$$O(r_1 \mid r_0) = \begin{pmatrix} 1 & \ell \\ 0 & 1 \end{pmatrix}$$

2) Magnetic sector.

In a focusing magnetic sector with a constant gradient the equation for the trajectories has the form

$$\frac{d^2y}{ds^2} + K(s)\,y = 0 \quad , \qquad K > 0$$

change enough to need a study for the optimization of the system.

The use of those systems is to determine momenta of charged particles emitted in nuclear reactions or scattering processes. If the rest mass of the particle is known it is possible to determine the energy. When the energies are of the order of some MeV, the magnetic spectrograph competes with several detectors: ionization chambers, scintillanting counters, solid state detectors. This last one is cheap, has a good resolution and may determine the energy and identity of the particle when combined with a dE/dx counter. But for high resolution work with low intensity beams, it cannot compete with the spectrographs. Usually* equal momenta, emitted in nuclear reactions.

The magnets which focus and analize the primary particles extracted from an accelerator are called analyzers, and are part of the transport system.

Usually the magnetic field is perpendicular to the trajectories, which means that the orbits are circular. Here $Br = P/q$ which is correct even for relativistic energies For high energies, one measures the momenta p in $\frac{Mev}{c}$ or $\frac{GeV}{c}$, which numerically is equal to the total energy of the particle in MeV or GeV.

For medium and low energies the mass-energy product ME/z^2 is used (M in atomic mass units, E in MeV).

For non-relativistic particles it is

$$E \sim \frac{p^2}{2m} = \frac{(Brq)^2}{2m}$$

$$Br = 144 \left(\frac{ME}{z^2}\right)^{1/2} \text{ KGauss cm}$$

The dispersion measures the capability to separate two particles with momenta p and $p + \Delta p$

$$D = \frac{\Delta y}{R} \frac{p}{\Delta p}$$

where Δp is the variation in p which produces a displacement Δy in the central ray going through an analyzer or spectrograph, and R is the radius of curvature of the central ray.

The resolution is determined by the size of the object: if it has an uniform brightness and a width o, an image is formed in the detector of $\Delta y = oM$ where M is the magnification for the analysing system. The resolving power is then

$$R_p = \frac{p}{\Delta p} = \frac{D}{M} \frac{R}{o}$$

Examples of beam analyzers

The analysis system for the Michigan State University cyclotron has been designed to provide doubly focused beams of 0.01 % energy widht, and it consist of two K=0 bending magnets each one bending 45°, combined with two quadrupole lenses to give vertical focusing such that $\nu_z = 2\nu_r$. In that system the

* the spectrographs focus on a detector the secondary particles of..

which is a linear equation of second order.

All the solutions of this equation satisfy the relation

$$\begin{pmatrix} y \\ y' \end{pmatrix}_{S_1} = M(S_1|S_0) \begin{pmatrix} y \\ y' \end{pmatrix}_{S_0}$$

Where the elements of the transfer matrix $M(S_1|S_0)$ may be obtained in terms of two linearly independent solutions of the differential equation, which we call C(s) and S(s). These "principal trajectories" are defined by their values and those of their derivatives at the input S=So:

$$C(S_0) = 1 \qquad S(S_0) = 0$$

$$C'(S_0) = 0 \qquad S'(S_0) = 1$$

where $C'(s) = \frac{d}{ds} C(s)$, $S'(s) = \frac{d}{ds} S(s)$

We call C(s) the cosin like trajectory, and S(s) the sin like trajectory.

The transfer matrix is then

$$M(S_1|S_0) = \begin{pmatrix} C(S_1) & S(S_1) \\ C'(S_1) & S'(S_1) \end{pmatrix}$$

where the matrix elements are the independent solutions for the exit $S=S_1$, and their derivatives.

a) Focusing sector (F)

For the focusing sector case, where $K>0$, the general solution contains the two initial conditions $Y(S_0)$ and $Y'(S_0)$ as independent constants. This solution is, for $S_1 - S_0 = \ell$:

$$Y(S_1) = Y(S_0)\cos \ell\sqrt{K} + Y'(S_0)\frac{1}{K}\sin \ell\sqrt{K}$$
$$Y'(S_1) = -Y(S_0)\sin \ell\sqrt{K} + Y'(S_0)\cos \ell\sqrt{K}$$

The transfer matrix is in the focusing case:

$$F(S_1|S_0) = \begin{pmatrix} \cos \ell\sqrt{K} & \frac{\sin \ell\sqrt{K}}{\sqrt{K}} \\ -\sqrt{K}\sin \ell\sqrt{K} & \cos \ell\sqrt{K} \end{pmatrix}$$

where $\ell\sqrt{K} > 0$

b) Defocusing (D)

The general solution in that case, in which $K<0$, is

$$Y(S_1) = Y(S_0)\cosh \ell\sqrt{K} + Y'(S_0)\frac{1}{\sqrt{K}}\sinh \ell\sqrt{K}$$
$$Y'(S_1) = Y(S_0)\sqrt{K}\sinh \ell\sqrt{K} + Y'(S_0)\cosh \ell\sqrt{K}$$

Therefore the linear effect of a defocusing sector is described by the transfer matrix

$$D(S_1|S_0) = \begin{pmatrix} \cosh l\sqrt{K} & \frac{1}{\sqrt{K}} \sinh l\sqrt{K} \\ \sqrt{K} \sinh l\sqrt{K} & \cosh l\sqrt{K} \end{pmatrix} \qquad l\sqrt{K} > 0$$

3) Series of optical elements

If the transformation operators are known for each element in a beam transport system, the total transfer matrix between source and target is the product of the individual matrices multiplied in the reverse order of application

$$[M_{TOTAL}] = [M_N][M_{N-1}] \ldots [M_2][M_1]$$

Where 1 is the index for the input plane, and N for the exit plane. Since these matrices do not commute, care must be taken not to interchange the order when perfoming the products. This linear theory applies quite generally to the beam transport for paraxial rays of most beam handling components, and it describes the particles motion in a plane perpendicular to the direction of the central axial ray. Given a known emittance at the input of the beam transport, and applying the matrices corresponding to the components along the beam for an adequate number of trajectories, the beam profile along the system may be determined. Generally the planes xz and yz are used when the beam has a plane symmetry instead of an axial one, and similar sets of equations for xz and yz held separately.

Beam analyzers and spectrographs

As nuclear physics moves into the region of heavier nuclei and higher excitation energies, the need of improvement in resolving power and accuracy increased. At this moment, there is a great variety of magnetic analysing systems for charged particles corresponding to the energy range of cyclotrons and tandem beams. The beam accelerate by a tandem Van de Graaff has an emittance of the order of 5 mm mrad, and an energy dispersion of 0.01%, which makes it an excellent instrument for nuclear structure studies. On the other hand, cyclotrons and synchrocyclotrons have an energy dispersion of 1% and an emittance for the external beam of about 50 mm mrad and isochronous-cyclotron an emmitance of 20 mm mrad and an energy dispersion of 0.2%.

The isochronous cyclotron compensates this poorer beam quality with a higher intensity and a greater energy.

At several laboratories analyzing systems for cyclotrons have been developed, which give an analyzed beam dispersion of 0.01% in the case of Michigan State University's cyclotron.

There the programing of the central orbits is being tried, by means of slits which define very well the first orbits and it is hoped to get a low dispersion beam (0.02%) without any analysing system.

Every accelerator, once built, needs a different design for the analysing system, since the beam characteristics in each case

change enough to need a study for the optimization of the system.

The use of those systems is to determine momenta of charged particles emitted in nuclear reactions or scattering precesses. If the rest mass of the particle is known it is possible to determine the energy. When the energies are of the order of some MeV, the magnetic spectrograph competes with several detectors: ionization chambers, scintillanting counters, solid state detectors. This last one is cheap, has a good resolution and may determine the energy and identity of the particle when combined with a dE/dx counter. But for high resolution work with low intensity beams, it cannot compete with the spectrographs. Usually* equal momenta, emitted in nuclear reactions.

The magnets which focus and analize the primary particles extracted from an accelerator are called analyzers, and are part of the transport system.

Usually the magnetic field is perpendicular to the trajectories, which means that the orbits are circular. Here $Br = P/q$ which is correct even for relativistic energies For high energies, one measures the momenta p in $\frac{Mev}{c}$ or $\frac{GeV}{c}$, which numerically is equal to the total energy of the particle in MeV or GeV.

For medium and low energies the mass-energy product ME/z^2 is used (M in atomic mass units, E in MeV).

For non-relativistic particles it is

$$E \sim \frac{p^2}{2m} = \frac{(Brq)^2}{2m}$$

$$Br = 144 \left(\frac{ME}{z^2}\right)^{1/2} \quad KGauss\,cm$$

The dispersion measures the capability to separate two particles with momenta p and $p + \Delta p$

$$D = \frac{\Delta y}{R} \frac{p}{\Delta p}$$

where Δp is the variation in p which produces a displacement Δy in the central ray going through an analyzer or spectrograph, and R is the radius of curvature of the central ray.

The resolution is determined by the size of the object: if it has an uniform brightness and a width o, an image is formed in the detector of $\Delta y = oM$ where M is the magnification for the analysing system. The resolving power is then

$$R_p = \frac{p}{\Delta p} = \frac{D}{M} \frac{R}{o}$$

Examples of beam analyzers

The analysis system for the Michigan State University cyclotron has been designed to provide doubly focused beams of 0.01 % energy widht, and it consist of two K=0 bending magnets each one bending 45°, combined with two quadrupole lenses to give vertical focusing such that $\nu_z = 2\nu_r$. In that system the

* the spectrographs focus on a detector the secondary particles of..

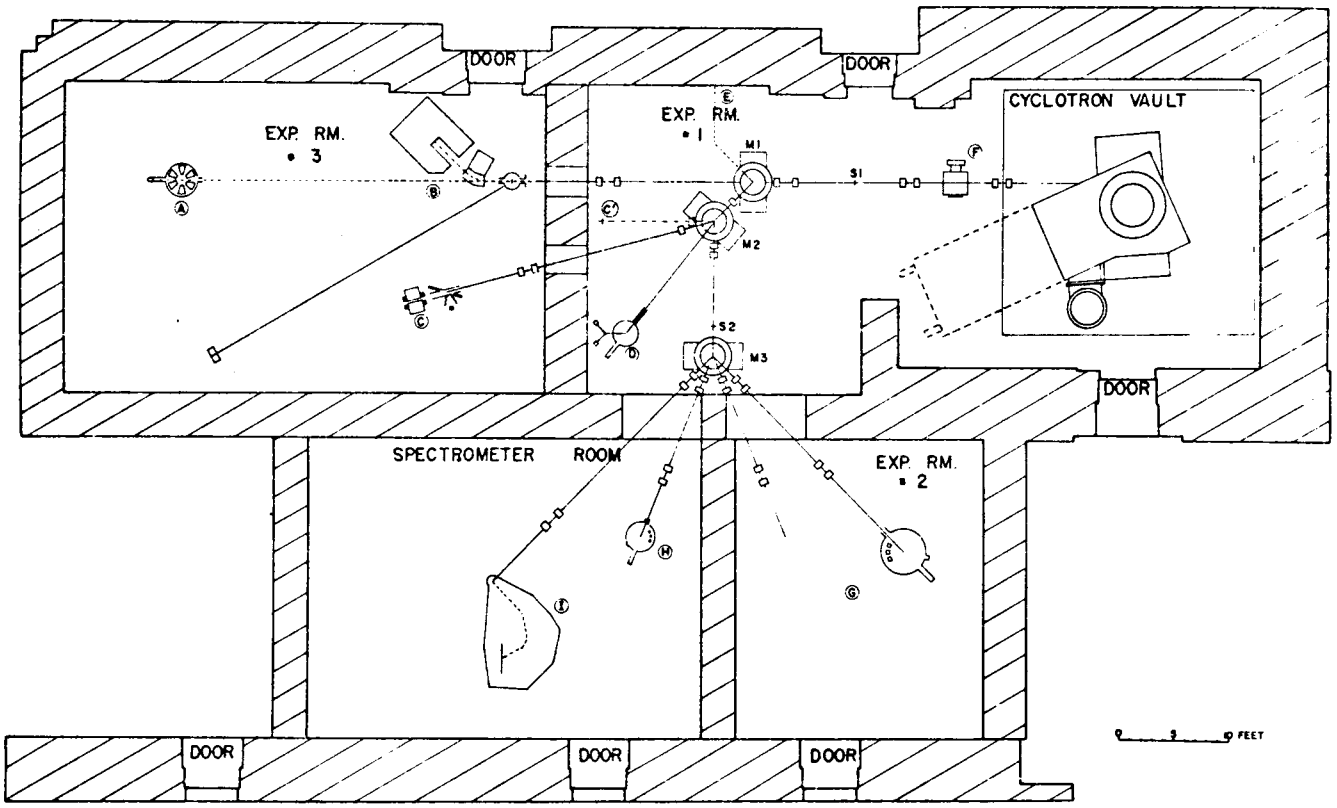

Fig. 1. The layout of the experimental areas. The items indicated in this figure are: (a) a multi-gap electron spectrometer; (b) beam stop assembly for the neutron time of flight program; (c) gamma ray facility with a bending magnet to send the beam into a well in the floor; (c') a beam of extremely small spot size to be used in biological studies; (d) polarization facility; (e) to possible future beam positions; (f) activation facility; (g) high precision scattering chamber; (h) low precision scattering chamber; (i) broad range, split pole spectrograph.

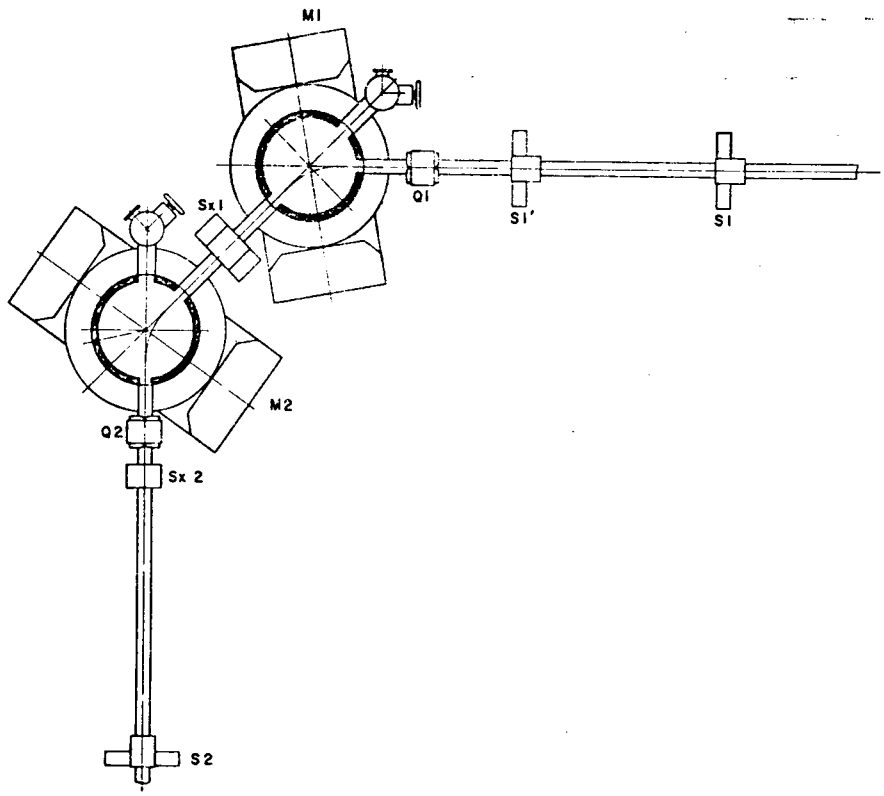

Fig. 2. The analysis system. M1 and M2 are n = 0 bending magnets, quadrupoles Q1 and Q2 provide vertical focusing, and second order aberrations are corrected by sextupoles Sx1 and Sx2. The slit S1 serves as an object for the system, the acceptance solid angle being controlled by S1', and an image is formed at slit S2.

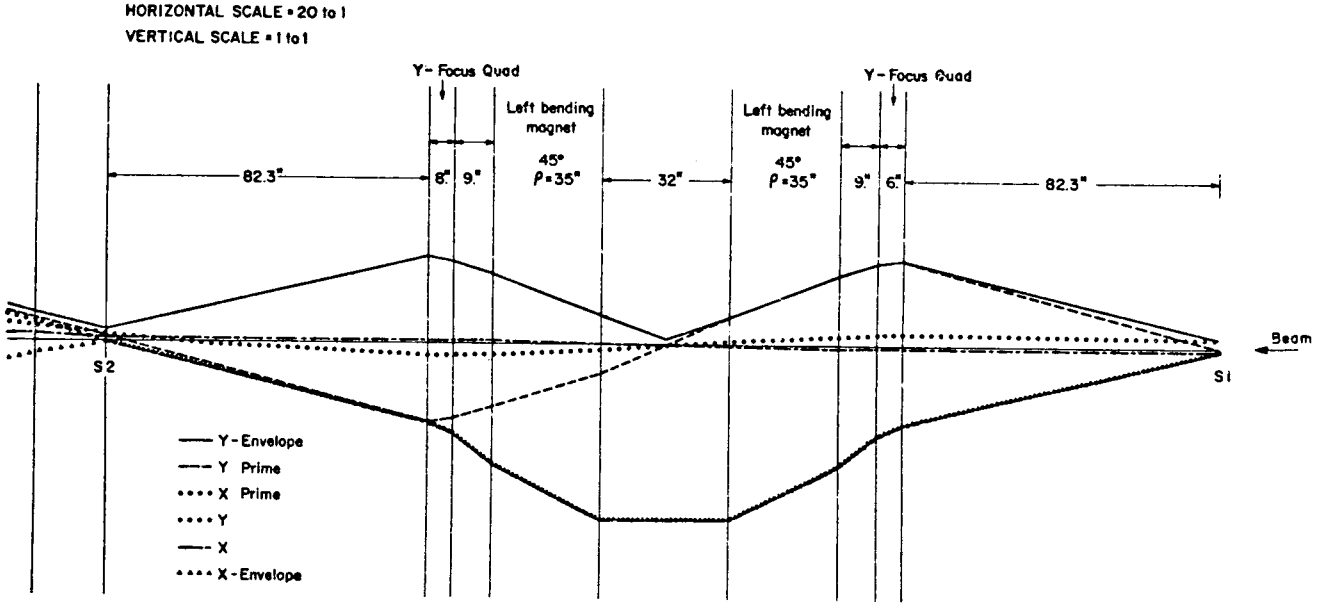

Fig. 3. The results of linear calculations on the analysis system of Figure 2. The positions of a representative set of rays are calculated at the beginning and end of each element (excluding sextupoles) and the positions joined by straight lines. Note the $\nu_z = 2\nu_r$ character of the system.

magnification is one, and the $\nu_z = 2\nu_r$ system, similar to a single magnet with $K = -0.8$, gives about twice the resolution of a $\nu_z = \nu_r$ system, which corresponds to $K = -\frac{1}{2}$.

The beam is extracted from the cyclotron and focused on the slit S_1 by means of four quadrupole lenses. When both magnets have the same polarity an energy dispersion of 0.03% is achieved; the sistem forms an image of S_1 at S_2. If the field in the second magnet is reversed, low dispersion is available at C, D and C', with a high intensity.

In the University of Michigan 83 inch cyclotron, the accelerator provides an affective source S, the magnets M_1 and M_2 are the dispersive elements,

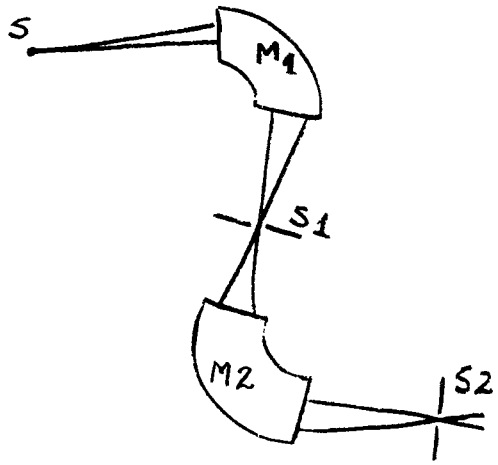

and slits S_1 and S_2 are placed at the image planes of P_1 and P_2. The beam through the slit S_2 at the focal plane of M_1 impinges on the target.

The magnets are $K = -\frac{1}{2}$, Magnification = 1, radius = 2m, E_0 = 40 MeV, and the dispersion is $D = 10$ keV/mm

The resolving power is RP= 4000

MAGNETIC SPECTROMETERS

Magnetic spectrometers are being widely used in measurements concerned with the energy level spectra of nuclei; they range from measurements of energies of a few MeV for beta particles emitted from radioactive nuclei, to measurements on the spectra of heavy ion reaction products, with energies of several GeV.

In an experimental facility consisting of an accelerator, a beam transport system, a scattering chamber containing the target, a magnetic spectrometer and a particle detector, the total resolution is affected by each one of these components. The beam transport system is designed to reduce the energy spread and emittance of the beam to match the requirements at the target. The resolution of the spectrometer is of the order of 0.01%-0.02% usually, and the resolution of detectors can be kept at the same order, when using spark chambers and emulsion plates.

There appears an energy spread due to effects on the target: the incident particles lose energy in the target stastiscally (Landau-Symon energy spread), so particles which incided with the same energy may emerge with different energies. Also, the nuclear reactions within a target produce scattered or reaction particles, which usually have different rates of energy loss than the original particles, and the emergent particles will have energies which depend upon where the particles originated in the target.

These effects can be reduced using thin targets.

Basic Theory

Various magnetic field configurations are used in spectrometers. For all cases, the radial motion of a particle can be described by the equation

$$\frac{d}{dt}(m\dot{r}) - mr\dot{\theta}^2 = er\dot{\theta}B_z - e\dot{z}B_\theta$$

The solution for small angles of divergence from the central ray is

$$x_1 = a_{11}x_0 + a_{12}x'_0 + a_{13}\frac{\Delta P}{P}$$

$$x'_1 = a_{21}x_0 + a_{22}x'_0 + a_{23}\frac{\Delta P}{P}$$

$$\left(\frac{\Delta P}{P}\right)_1 = \left(\frac{\Delta P}{P}\right)_0$$

x= displacement of the particle with respect to the central ray at the entrance to the magnet

x'= divergence of the particle.

Those equations can be summarised in a matrix form

$$\begin{pmatrix} x_1 \\ x_1' \\ \frac{\Delta p}{p} \end{pmatrix} = \begin{pmatrix} a_{11} & a_{12} & a_{13} \\ a_{21} & a_{22} & a_{23} \\ 0 & 0 & 1 \end{pmatrix} \begin{pmatrix} x_0 \\ x_0' \\ \frac{\Delta p}{p} \end{pmatrix}$$

The followings first order optical properties can be determined using this equation:

1) position of the radial focus ($\overline{BP}$)

The point where the particles trajectory crosses the central ray or optic axis after leaving the spectrometer is the position of the radial focus, at the distance $\overline{BP}$ from the magnet exit. From the figure

$$\overline{BP} = \frac{x_1}{x_1'} \qquad \overline{OA} = \frac{x_0}{x_0'}$$

Combining those equations, for $\frac{\Delta p}{p} = 0$

$$\overline{BP} = \frac{a_{11} x_0 + a_{12} x_0'}{a_{21} x_0 + a_{22} x_0'} = \frac{a_{12} + a_{11} \frac{x_0}{x_0'}}{a_{22} + a_{21} \frac{x_0}{x_0'}} =$$

$$\therefore \overline{BP} = \frac{a_{12} + \overline{OA}\, a_{11}}{a_{22} + \overline{OA}\, a_{21}}$$

2) Magnification (M)

The magnification is the ratio of the size of the image to that of the object.

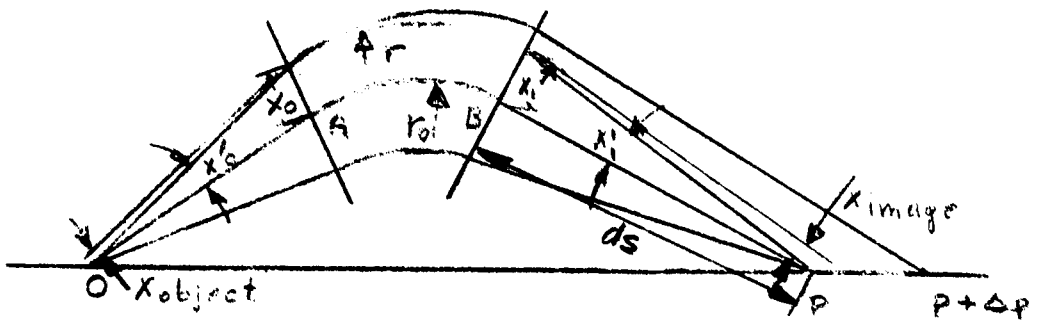

It is necessary to consider the trajectory with maximum displacement x_{object} (size of object) at the origin and zero divergence; the displacement x_{im} at the focal distance ds is the size of the image. Then the magnification is

$$M = \frac{x_{im}}{x_{obj}} = \frac{x_1 + ds\, x_1'}{x_0}$$

and sustituting from the trasfer matrix, where $x'_0 = 0$, $\frac{\Delta p}{p} = 0$

$$M = \frac{a_{11} x_0 + ds\, a_{21} x_0}{x_0}$$

then

$$M = a_{11} + ds\, a_{21}$$

3) Dispersion

To calculate the dispersion a trajectory is considered where initially

$$x_0 = x'_0 = 0 \qquad \frac{\Delta p}{p} > 0$$

Then we define the dispersion as the displacement at the focus divided by the fractional difference of momenta:

$$D = \frac{y}{\Delta p/p} = \frac{x_1 + ds\, x'_1}{\Delta p/p}$$

$$\therefore \quad D = \frac{a_{13} \Delta p/p + ds\, a_{23} \Delta p/p}{\Delta p/p} = a_{13} + ds\, a_{23}$$

The simplest spectrometer has an uniform field magnet; its disadvantage is that there are no focusing properties perpendicular to the median plane.

The image aberration is proporcional to a'_0 .

It is posible to produce a transversal focusing effect using the magnet's fringing-field; in that case, out of the median plane there is a component Bx, and if a particle comes in a trajectory which is not perpendicular to the magnets border; it has a velocity component Vy , and so it appear a Lorentz force Fz. The fringin field acts as a lens of focus $f_z = \frac{r}{\tan \chi}$

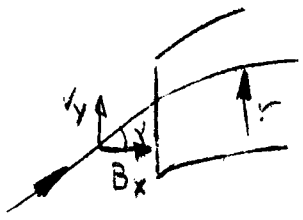

Another type of spectrometer consists in the double focusing spectrometer ($n = -\frac{1}{2}$). In that case, a transversal focusing can be obtained, and a point object gives a point image, so it is an astigmatic system, at least for gaps small relative to radius.

It is impossible to design a spectrometer which focuses all the point objects as point images, neither the points as line images, unless the acceptance angle is infinitely small;

for a high precision spectrometer, there is a limitation in the solid angle of acceptance, due to the several kinds of aberrations and their effects on the resolving power. Usually the aberrations are expressed as a series of powers of the acceptance angle X'_0 and the corresponding Z'_0 in the vertical plane, so

$$\Delta y_{image} = a_{10} X'_0 + a_{20} X'^2_0 + a_{30} X'^3_0 + \dots$$

It is possible to place the detector in such a way that the first order term disappears : $a_{10} = 0$ (first order focusing). If it is possible to make a_{20} negligible, the instrument has second order focusing; usually the focus in the transversal direction is not important, since it does not affect the momenta determination .

Different types of magnetic spectrographs

Usually in nucleas structure studies the cosmic rays or the neutrons background is low; the important background is the tail in the low energy side of every high intensity peak, due to:

Scattering at the defining slits, with loss of energy; scattering after the target. The first effect is made small using a very clean beam; the second one is much reduced by means of transversal focusing in the spectrograph, specially near the entrances since in that case the probability to do scattering on the pole faces or slits is lower.

Double focusing spectrograph at Caltech:

It has a $n=-\frac{1}{2}$ field, first used by Svertholm-Siegbahn who designed it to focus at 254°; at Caltech de deglecting angle is 180°. The main advantages of the double focusing (or $N\frac{1}{2}$) spectrometers over the uniform field type are its high resolution and acceptance solid angle; it is therefore very useful when there are experiments involving the separation of closely spaced energy levels or where differenctial cross-sections of a low cross section reaction is being measured. A spectrometer of that type was built by B.L. Cohen, for a 12 MeV tandem accelerator (Nucl. Instr. Meth. 10 p. 4(1961)).

Broad range spectrographs

It was suggested first in 1951 by C.P. Browne and W.W. Buechner and designed for M.I.T. and for University of Bergen, Norway.

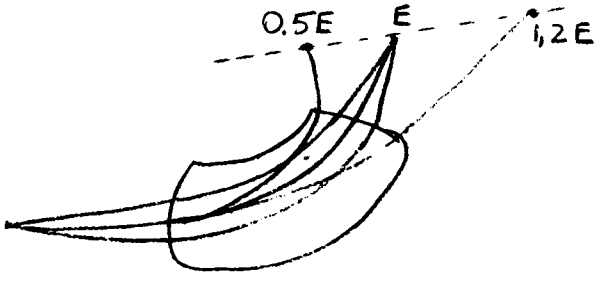

It has curved boundaries, which produces a second order correction ($a_{20} = 0$) for particles deflected 90°, but there are strong second order aberrations for the particles with lower and higher momenta. The total range of momenta is $\rho_{max}/\rho_{min} = 1.5$, and has a solid angle of about 0.4 millisteradian (msr). The theoretical resolving power at this solidangle for particles deflected 90° is $\rho/\Delta\rho = 36.000$, where $\Delta\rho$ is the full width of the peak at half maximum. Nuclear track plates are used as detectors, usually 3 plates of 2x10^{w} each. Since the trucks are counted in strips $\frac{1}{2}$ mm wide, one gets about 1520 data points per each set of plates.

The multigap spectrograph is equivalent to 25 broad range instruments working simultaneously. It has been conceived at MIT in 1955 and built at MIT, at Aldermaston in England, and at the Universidad Autonoma de Mexico.

The basic unit is the broad range spectrograph, with the difference that there are now 24 air gaps, producced by cutting a toroid shaped magnet from $7\frac{1}{2}$° wedges. There is a hole through which the incident beam impinges on the target, located in the center of the toroid. There are two 90° gaps, and in general the gap at 0° is not used. Since there are 24 gaps at which it is possible to put nuclear track plates, each one giving 1520 data points, in one exposure it is possible to get 36.500 data points. To scan the 18 m of nuclear track plates in $\frac{1}{2}$mm strips requires between 3 and 4 man-months.

The energy range as 2,3:1, so if 11.5 MeV protons are focused at one end of the plates, 5 MeV protons are focusedat the other.

Elbek Spectrograph

It was designed by Elbek for the tandem at Copenhagen; it is a homogeneous-field instrument, with entrance and exit of the particles not normal to the field boundaries, and it gives some axial

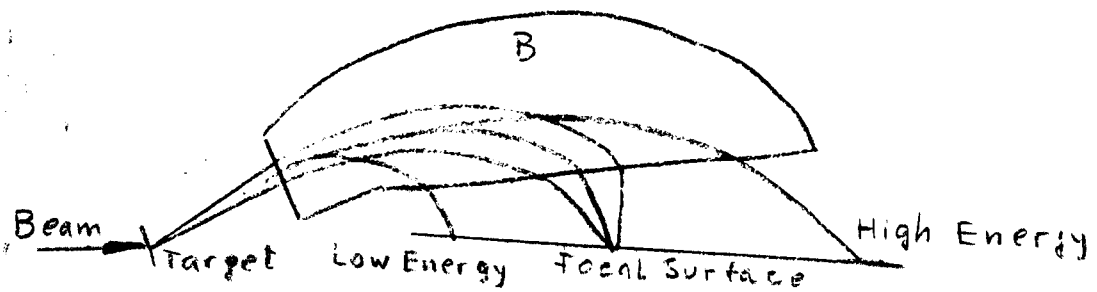

focusing. The acceptance angle is 35°, and it gives a median-plane magnification of 0.5,

which is important obtain a good resolving power (RP= $\frac{DR}{MO}$), and also because of the difficulty of mantaining the beam

spot constantly on the same point at the target. It has a broad range, of 6:1 in energy, with practically no second order aberration.

Split-pole spectrograph

It consists essentially of two pole-edge focusing spectrometers arranged in series. The object of this arrangement is is:

1) The larger area of the second set of pole pieces means that a wide energy acceptance is possible (6:1 as in broad rang spectrograph)
2) The focusing properties of the four variable pole edges enables second order focusing over the whole focal plane. The poles edges are shaped in such a way that the high energy particles are twice focused in the fringing fields, and the low energy ones are only once focused.

The split-pole spectrograph has the highest ratio D/n, since the magnification M is small at the medium plane: $M \sim 0.3$

One disadvantage of this instrument is that the Z plane magnification is 4 to 6 so that the image width on the focal plane is 4 times larger than the target spot size, which may make neccesary the use of wide detectors. In the table the parameters of several nuclear structure spectrographs.

The actual trend for magnetic spectrographs is to have as many adjustable parameters as possible; a deflecting magnet with straight boundaries has three parameters: entrance and exit angles, and the deflecting angle. The effect of a change in the entrance and exit angles is equivalent to the action of a quadrupole before or after the magnet, respectively, so these three adjustable parameters have the same action as putting two quadrupoles plus a dipole (a deflecting magnet with normal entrance and exit angles).

Using curved boundaries and varying the radius of curvature (three adjustable parameters for the design), the magnet will have five parameters; the curved boundaries are equivalent to sextupoles. In the split-pole spectrograph there are eight adjustable parameters.

Other desired features of a magnetic spectrograph are: a high resolving power, a high signal to background ratio, which may be better than 10^5, a reaction angle range θ of 0° to 180°, and the correction for Doppler effect.

Detectors used in the spectrographs

Most of the spectrographs use photographic emulsions as detectors, which are very reliable and do not worsen the resolving power of the instrument. If on-line or coincidence experiments are wanted, it is necessary to use other detectors. The time needed to get the information out of the nuclear track plates is long even using an automatic track-counter.

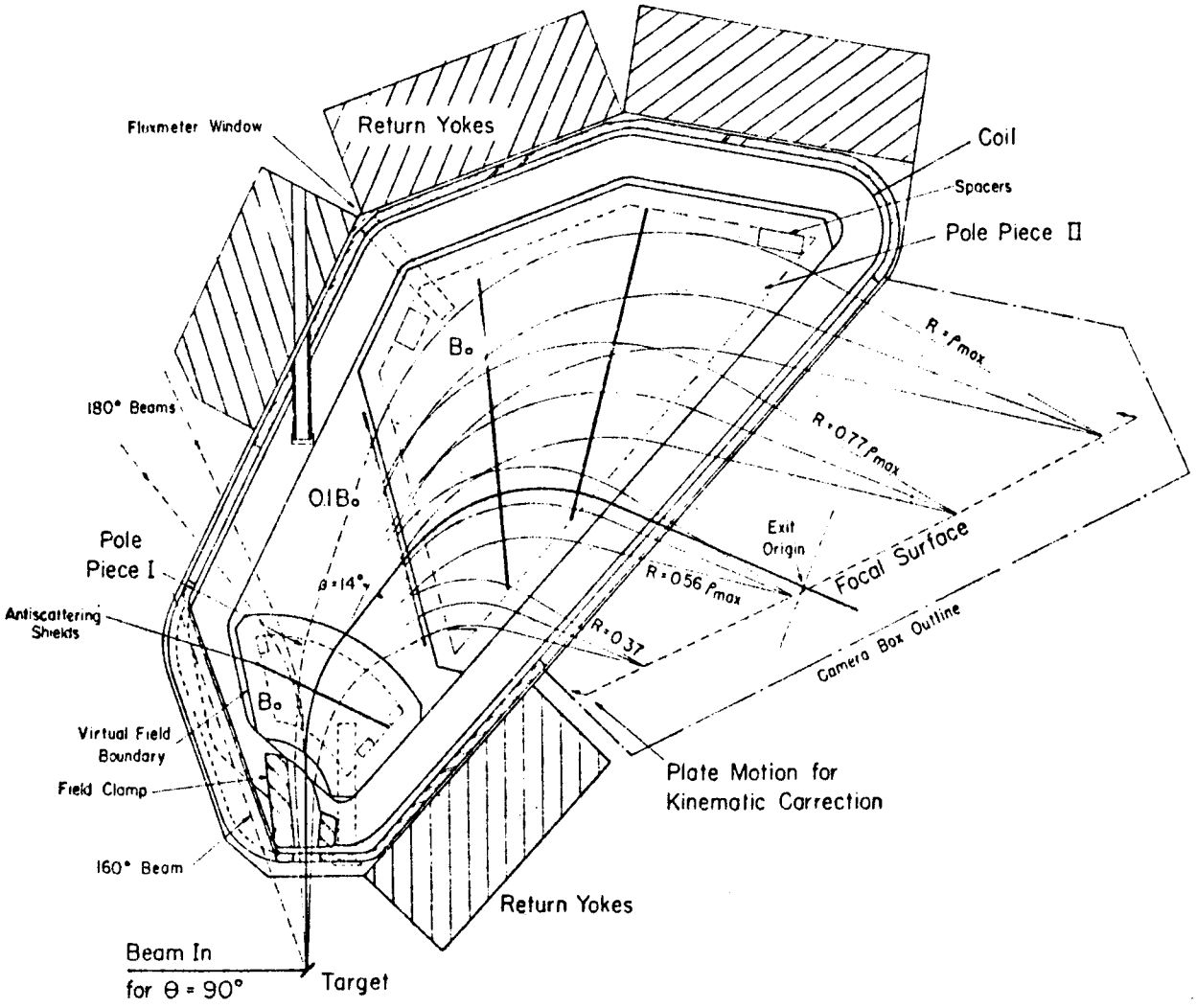

Fig. 1. (a) Top view of the split-pole spectrograph

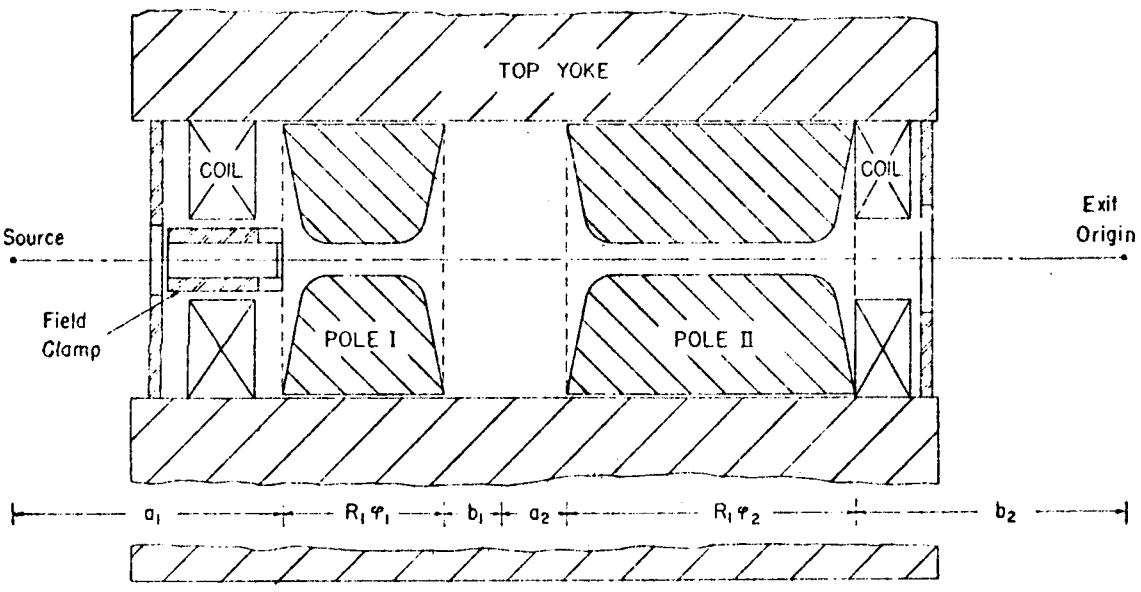

Fig. 1. (b) Folded-out cross section taken along the nonreal central ray, shown as a heavy line in (a). The vertical scale in the cross-sectional view is twice the horizontal scale.

To overcome these dificculties other detectors are being developed, like the position sensitive solid state detectors.

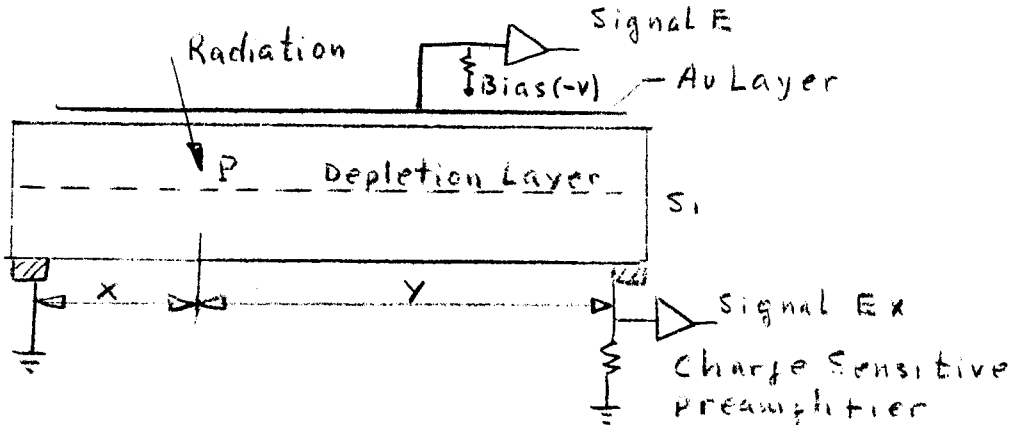

If a particle incides on P, a signal E is generated, which is proportional to the energy of the particles, and simultaneously a signal E_x proportional to $E \cdot x/x+y$, that is, to the energy and distance from the point of incidence P to the earth contact.

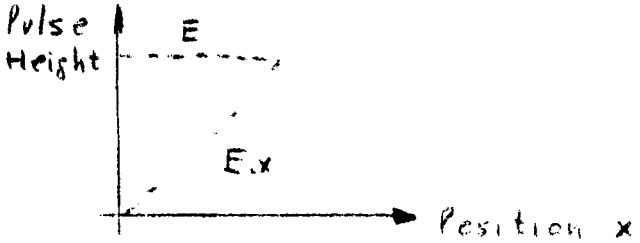

The detectors are prepared in strips of 5 x 1cm and 1 to 2 mm thickness, and put on the focal plane of the spectrograph.

Other devices, used before for the detection of high energy particles, are increasingly used in the range of 1 to 100 MeV like the spark chamber which consists of a number of metallic plates insulated from each other and with a neon-filled gap of the order of a few mm between them. Every other plate is grounded, and the voltage is such that sparks will occur at places where the gas is ionized, so the trail of ions left by a particle will trigger such sparks and a photograph give an outline of the path of the particle.

NUCLEAR RESEARCH WITH PULSED BEAMS

During the last decade there has been a continuous growth in the field of experimentation with pulsed beams of neutrons and charged particles. The techniques now in use can produce pulses of ions of the order of one nanosecond duration, and simultaneously there has been a development of electronics and detectors with speeds in the nanosecond range.

The general applications of nanosecond pulsed beams in the range from 1 MeV to 100 MeV are

1) Measurement of energies by the time-of-flight method
2) Use of the time information for the discrimination of events

1) Time-of-flight method

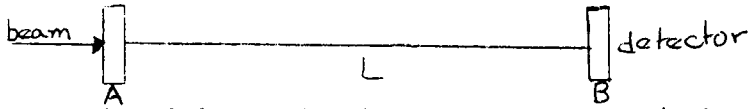

If a pulsed beam incides on target A during a burst of duration Δt, reaction products appear starting from the initial time of incidence t=o. The emitted particles travelling to the detector B located at the distance L will reach it after a time t which depends on L and their kinetic energy T.

$$t = \frac{L}{v} = L\sqrt{\frac{m}{2eV}}$$

The detector will then give pulses whose time separation depends on the particles mass and energy, and the spectra so obtained has an energy resolution $\frac{\Delta T}{T}$ which depends on time resolution $\frac{\Delta t}{t}$:

$$\frac{\Delta T}{T} = \frac{2\Delta t}{t}$$

This method, which we will discuss in more detail further-on, has been first used for investigation of the elastic and inelastic interaction between neutrons and various nuclei, so giving important information on MeV range neutron inelastic scattering (nuclear models and nuclear reactors). It is now being used also in KeV range neutron capture, which is important for fast reactors design and for nucleosynthesis. The neutron producing reactions in the light nuclei have been under investigation at several laboratories; for example the $D(d,n)^3He$ reaction for deuteron energies up to 20 MeV, which is important to determine the extent to which the continuum of neutrons due to the break-up processes D(d;n,p)D and D(d;n,n,p)P contribute to the total neutron yield.

Another application is the measurement of isobaric analogue states, which have been known for a long time in light nuclei, and recently in heavy nuclei, where they have been observed in charge-exchange reactions such as the (p,n) reactions.

2) Use of time information for the discrimination of events.

The study of gamma rays from neutron capture or inelastic scattering is greatly facilitated by the time separation of the gammas from the neutron-producing target from those arising from (n,γ) or $(n,n'\gamma)$

Most of the effort on $(n,n'\gamma)$ reactions has been directed toward the spectroscopy of excited levels. The properties of levels which are investigated are the excitation energies, gamma-ray decay-schemes, and their angular momenta. When the gamma-ray branching ratios and production cross sections are measured the neutron inelastic scattering cross sections are determined, and so the $(n,n'\gamma)$ reactions enables the comparison of those cross sections with the predictions of a statistical model.

Another application is the investigation of isomeric states: the pulse burst is used as a starting point in time, and then the frequency of γ - emission is measured in the energy range of interest, as a function of the delay following the burst.

The nanosecond pulsed beams used in those experiments are obtained from the following accelerators:

a) Electrostatic accelerators, like the tandem Van de Graaf, and the Cockroft-Walton.
Those are dc current machines, and in order to obtain nanosecond pulses it is necessary to introduce a radio frequency sweeping system which acts on the external beam.

b) RF accelerators, like the cyclotron, which give a naturally pulsed beam due to the phenomenon of phase grouping. The interval between two pulses is the inverse of the radiofrequency, usually around 100 nsec. When a longer time interval is required, a pulsed deflector in the neighborhood of the ion source is used, which interrupts some bursts. Another conventional method is to use an electric deflector for the external beam.

A synchrocyclotron has a double structure; as an example, the Buenos Aires FM cyclotron has the following structure.

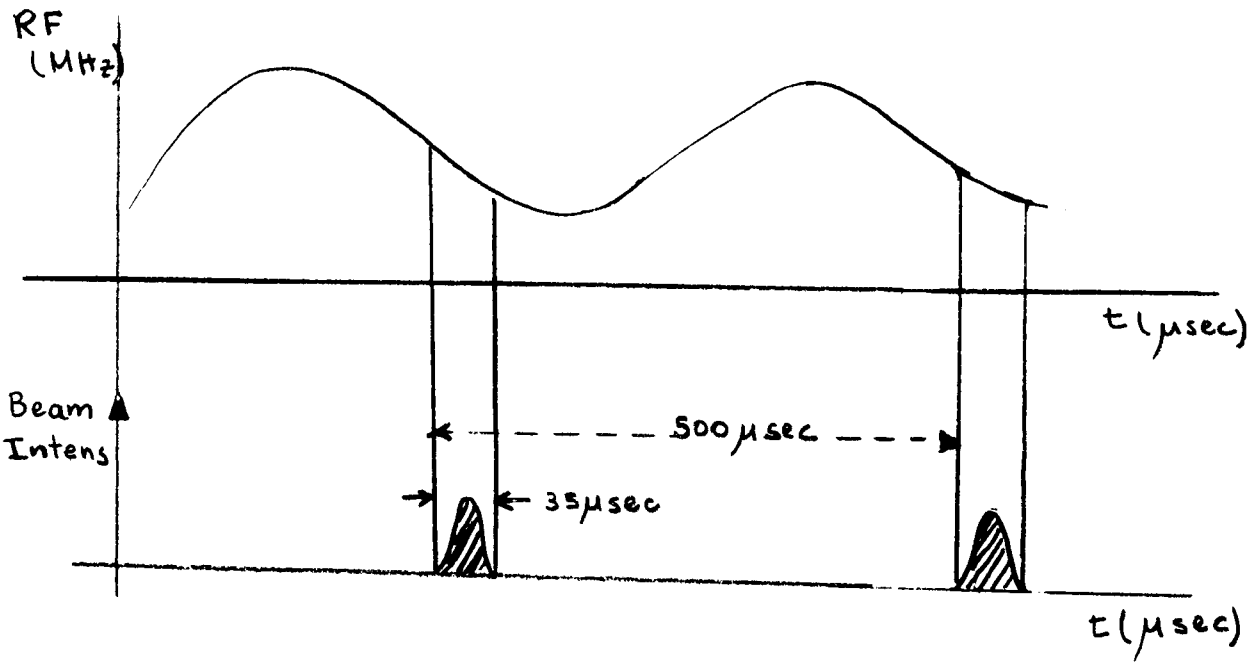

consisting of macroscopic bursts of 35 μsec widht and the repetition rate of the modulated frequency , 2 KHz.

Each macroscopic burst consists of pulses similar to those from a fixed frequency cyclotron or from an isochronous cyclotron,

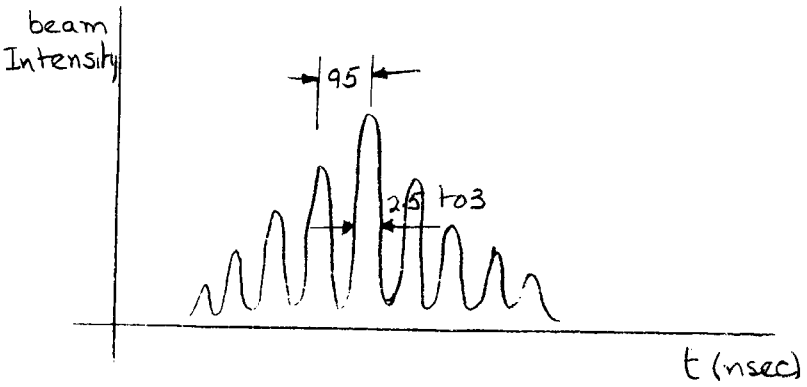

with a width of about 3 nsec separated by a time interval of about 95 nsec, which varies in 4% due to the frequency modulation. It is possible to alter the time structure of the beam in a synchrocyclotron, by means of a debuncher, consisting of a radiofrequency electrode which acts on the accelerate beam just before it starts to get extracted, spreading the particles in all the orbit, in such a way that the macroscopic bursts vanish and in turn new semi-microscopic bursts appear.

The interval between those bursts depends on the deflector frequency

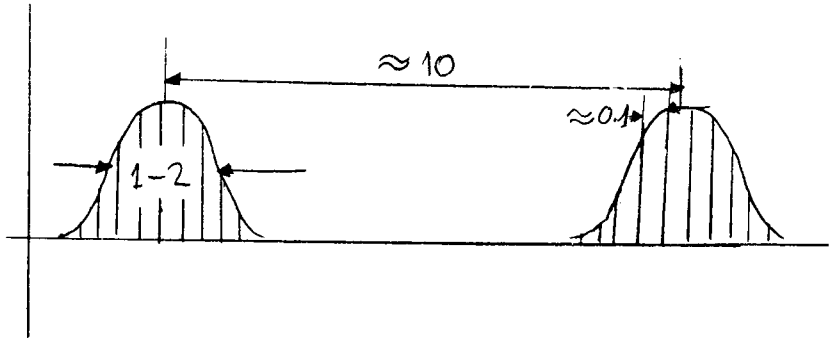

Before going into a more detailed study of the pulsed beams of tandems and cyclotrons, we will discuss the use of the pulsed beam for studies of short-lived isomers.

Studies of Short-Lived Isomers in the Range $t_{\frac{1}{2}} \approx$ μsec-nsec

We consider an isomeric state of mean life τ which is populated at t=o by a pulsed beam of width ΔT and interval T sec, which defines a duty factor $\frac{\Delta T}{T}$. The desintegration rate, or average number of states formed in the beam is I_o per second and $I_o T$ per pulse. The emitted gamma radiation is detected with a detector of overall efficiency ε, and time analyzed.

Usually the total counting rate in the detector system is 10^4 cp sec at the most; this

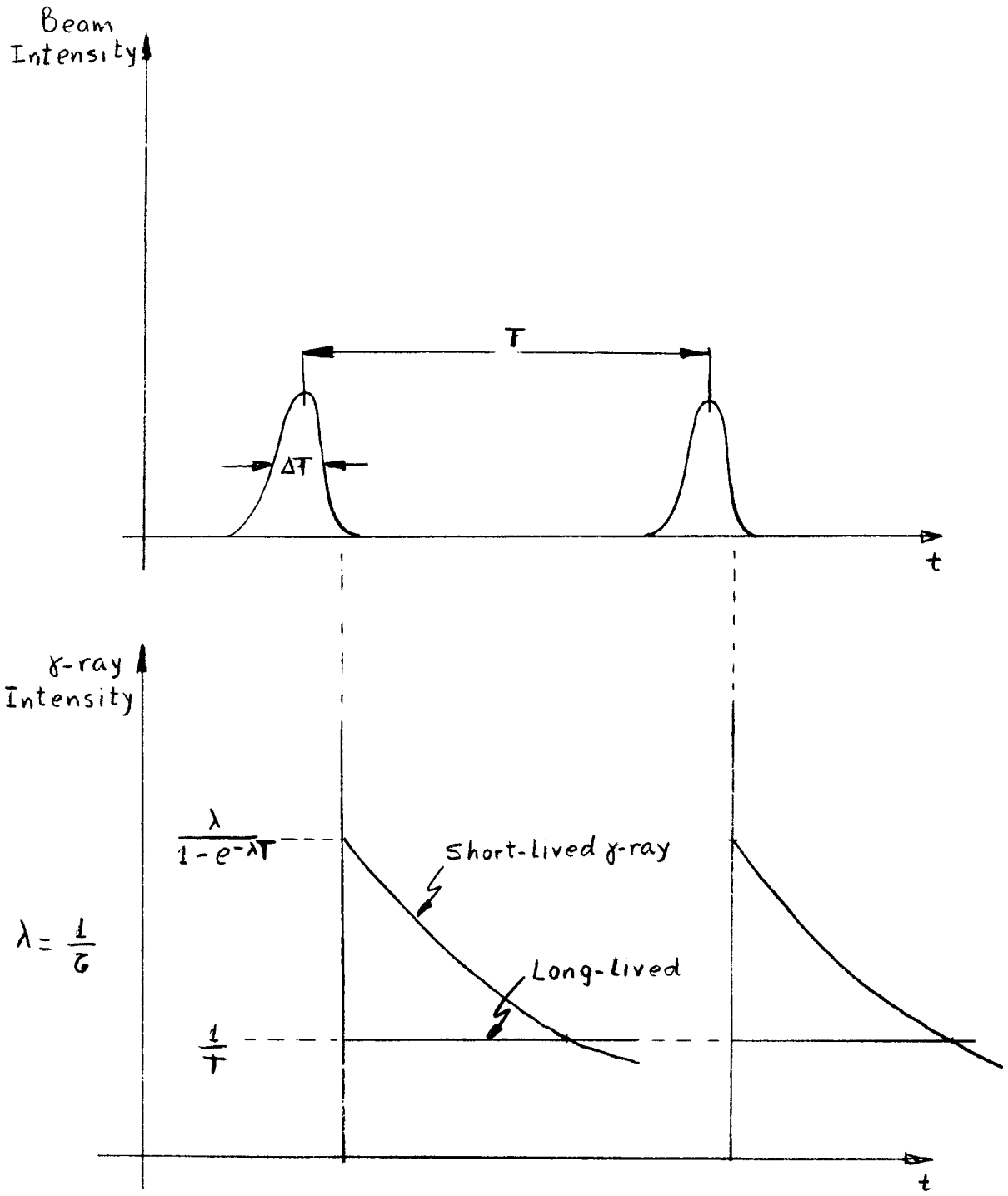
Beam Intensity
T
ΔT
t
γ-ray Intensity
λ / 1 - e^-λT
Short-lived γ-ray
Long-lived
λ = 1/τ
1/T
t

implies that the mean interval of detector pulses, t_d, shall be $t_d \geq 100\,\mu sec$. Generally $T \ll t_d$, and the beam is regarded as continuous regard less of its duty factor; then, if γ-rays are recorded only during each microscopic burst, the long-lived and background components are reduced by a factor T compared with the prompt components and the microscopic burst are useful even for taking prompt singles spectra.

The time differential counting rate of a γ ray is

$$N(t)\Delta t = \varepsilon I_0 \cdot \lambda e^{-\lambda t} \Delta t$$

for

$$T >> \tau >> \Delta T$$

Here the integrated counting rate is

$$\int_0^\infty N(t)\,dt = \varepsilon I_0$$

By measuring the time difference between the pulses given by the detector and the beam pulse, it is possible to obtain the time distribution* of all the preceding beam bursts must be taken into account, and in that case

$$N(t) = \varepsilon I_0 \sum_{n=0}^{\infty} \lambda e^{-\lambda(t+nT)} = \varepsilon I_0 \frac{1}{1-e^{-\lambda T}} \lambda e^{-\lambda t}$$

Measurements in the region $t_{\frac{1}{2}} \approx \mu sec$

Measurements in the region μsec-msec have been made by T.W. Conlon et al, at Harwell, and by H.F. Brinkmann et al, at Karlsruhe.

The method generally used to measure time distributions is to trigger a saw-tooth generator to each beam burst; the analog pulse height taken at an instance of a detector signal corresponds to the time delay between the beam burst and the detector pulse

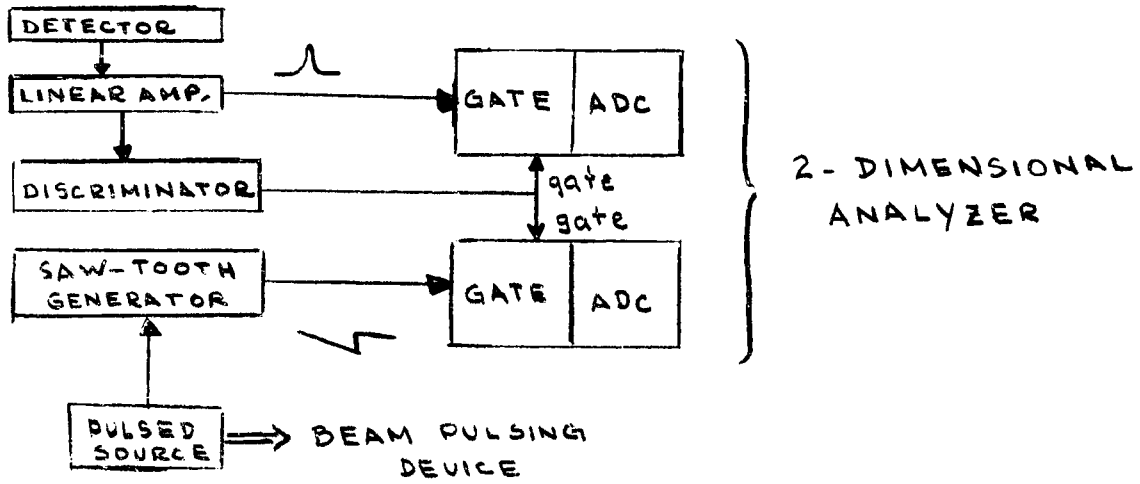

* N(t). Since not always is the condition $T >> \tau$ fulfilled, the contribution of *

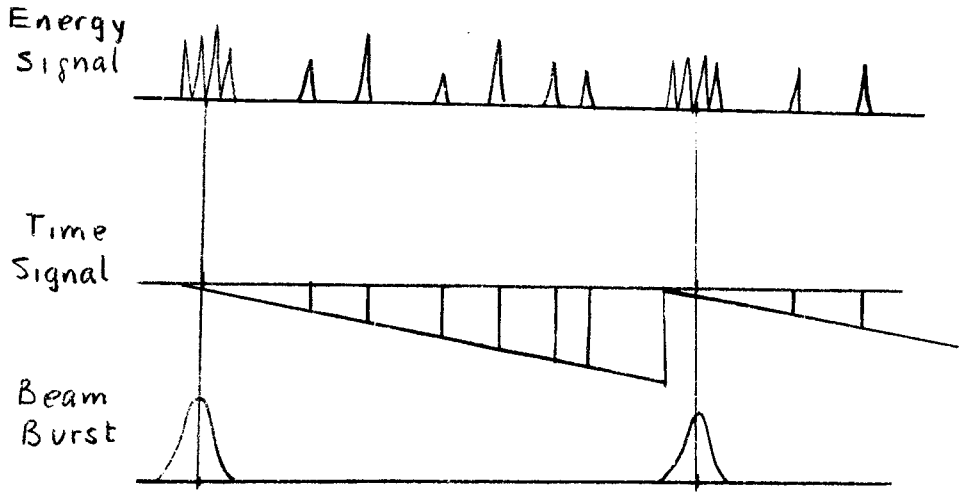

The time signal and the energy signal are then analyzed by a two dimensional pulse-height analyzer.

Another way to get the time difference is to use a clock pulse generator triggered by each beam burst, and count the number of the digital pulses.

Measurements in the region $t_{\frac{1}{2}} \approx$ nsec

Using a nanosecond pulsed tandem Van de Graaff or the natural beam bursts of a cyclotron it is possible to measure $t_{\frac{1}{2}} \approx$ nsec. Yamasaki and Ewan analyzed γ rays emitted in (α, X_n) reactions, using the Berkeley 88" isochronous cyclotron:

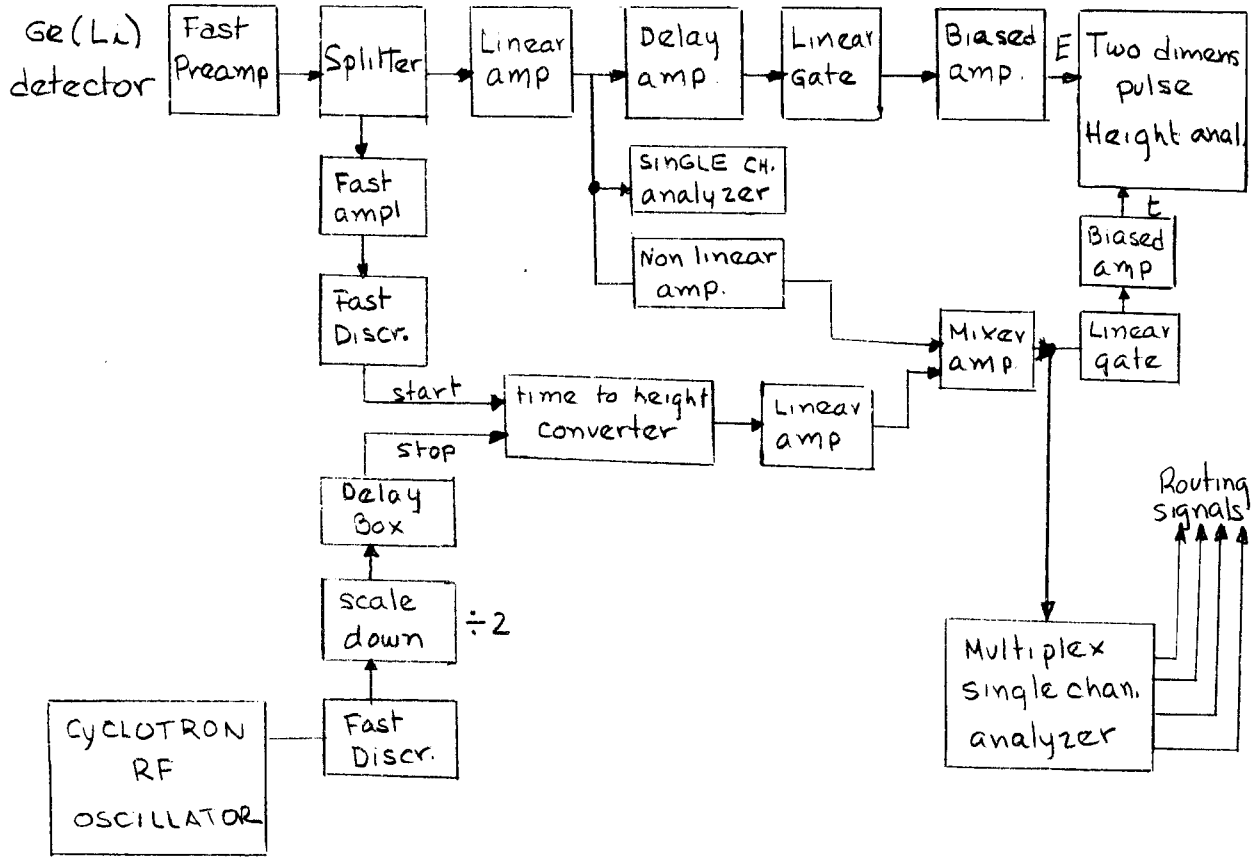

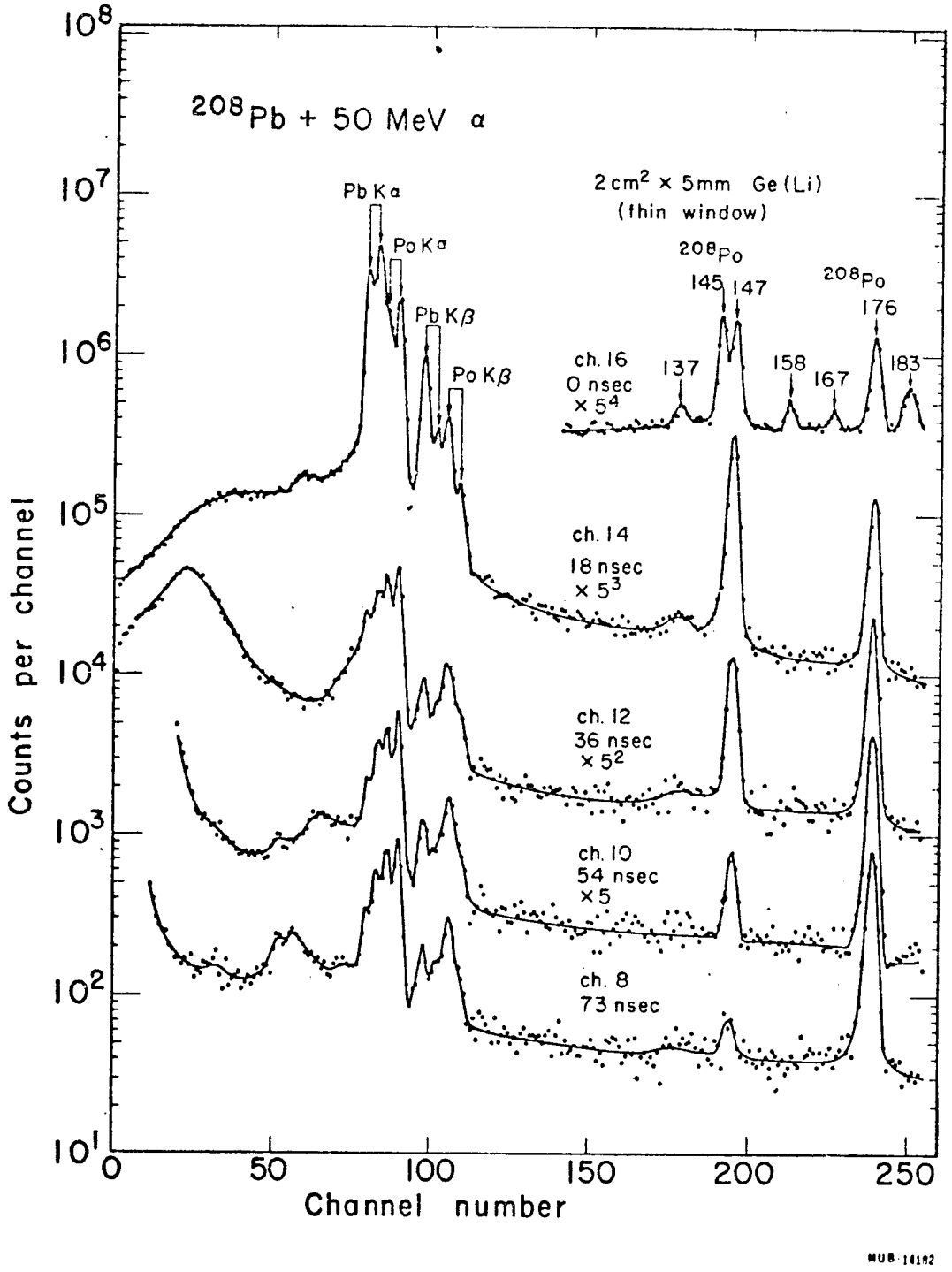

Fig.6 Part of the 256 channel (energy) x 16 channel (time) spectrum observed in the ^{208}Pb(α,4n)208Po reaction at 50 MeV, taken from ref.4). These data were obtained with a 2 cm² x 5 mm thick thin-window Ge(Li) detector. The 147 keV and 176 keV γ rays have delayed components with $t_{1/2}$ = 8 ± 2 nsec and $t_{1/2}$ = 400 nsec, respectively.

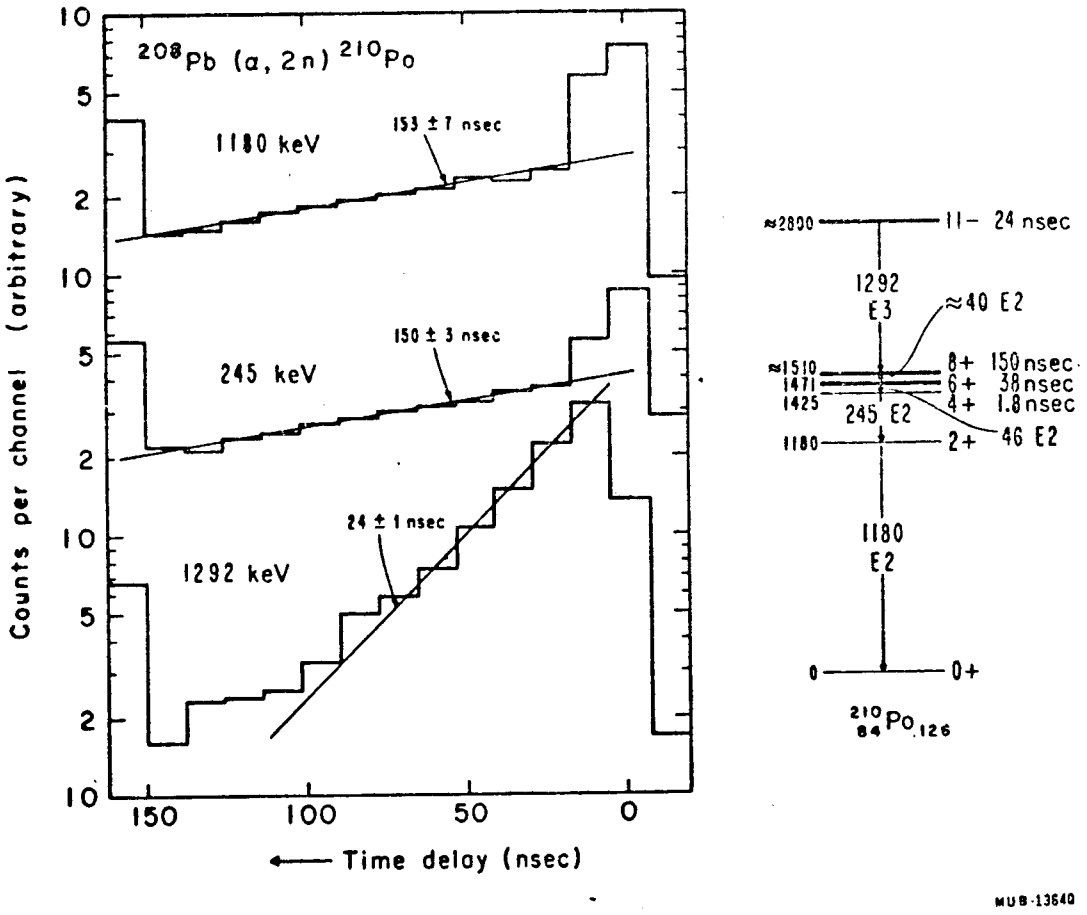

Fig.7 To the left are shown the time distribution curves of three transitions observed in the reaction $^{208}Pb(\alpha,2n)^{210}Po$ at 28 MeV. To the right is shown a tentative level scheme for ^{210}Po. Taken from ref.4)

The γ -ray signal from a Ge(Li) detector is amplified by a fast preamplifier, and then split into one pulse for energy analysis and one for time analysis. The pulse for time analysis is afterwards amplified by a fast amplifier, which triggers a fast discriminator to give a timing signal, whose threshold is slightly bigger than the noise level. The fast signal gives the start for a time-to-amplitude converter. The stop signal is generated from the cyclotron rf oscillator using a fast discriminator and a delay; only every second pulse from the cyclotron oscillator was used, for practical reasons, and

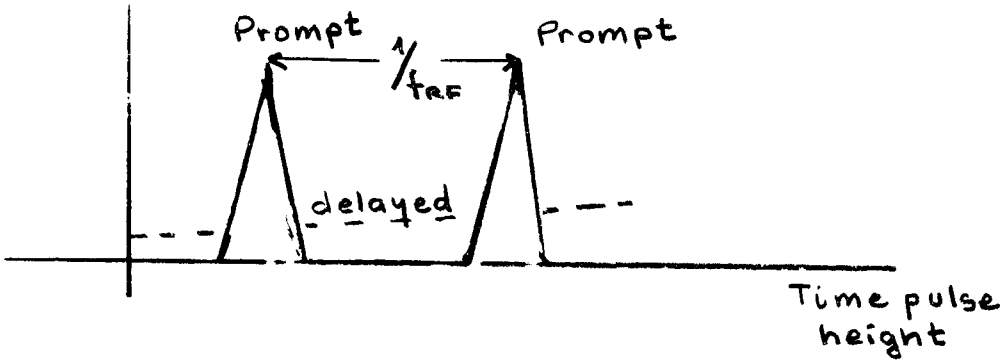

that gives rise to two prompt peaks with a time separation of $1/f_{RF}$. The overall width of a prompt curve was found to be 5 nsec. T. Yamazaki and G. Ewan determined in that way the spectrum in the $^{208}Pb(\alpha, 4n)^{208}Po$ at 50 Mev. The data were obtained with a $2 cm^2 \times 5 mm$ thick thin-window Ge(Li) detector. Only a few of the spectra are shown. Corresponding to five different time channels spaced by approximately 18 nsec. There are some peaks, like γ-145 , which decay very rapidly and give the prompt time distribution; others decay more slowly like γ-147 Kev and 176 Kev which have delayed components with $t_{1/2} = 8 \pm 2$ nsec and $t_{1/2} = 400$ nsec , respectively. The γ rays may either come directly from the isomeric state or from a level fed by an isomeric state.

Usually an isomeric decay involves more than one delayed γ- ray especially a high-spin and high-lying isomer emits many high-energy γ- rays, and the placement of these delayed γ- rays can be reasonably assured if one measures the whole time distributions, including prompt components and intensities of all the transitions. The isomeric transition itself can not have a prompt component, the prompt transitions that are preceded by an isomeric decay have both prompt and delayed components, so the relative intensities of the prompt components of transitions following the decay of an isomeric state give a powerful clue about the determination of the order of the transitions, since a lower lying level receives more prompt population than a higher-lying level.

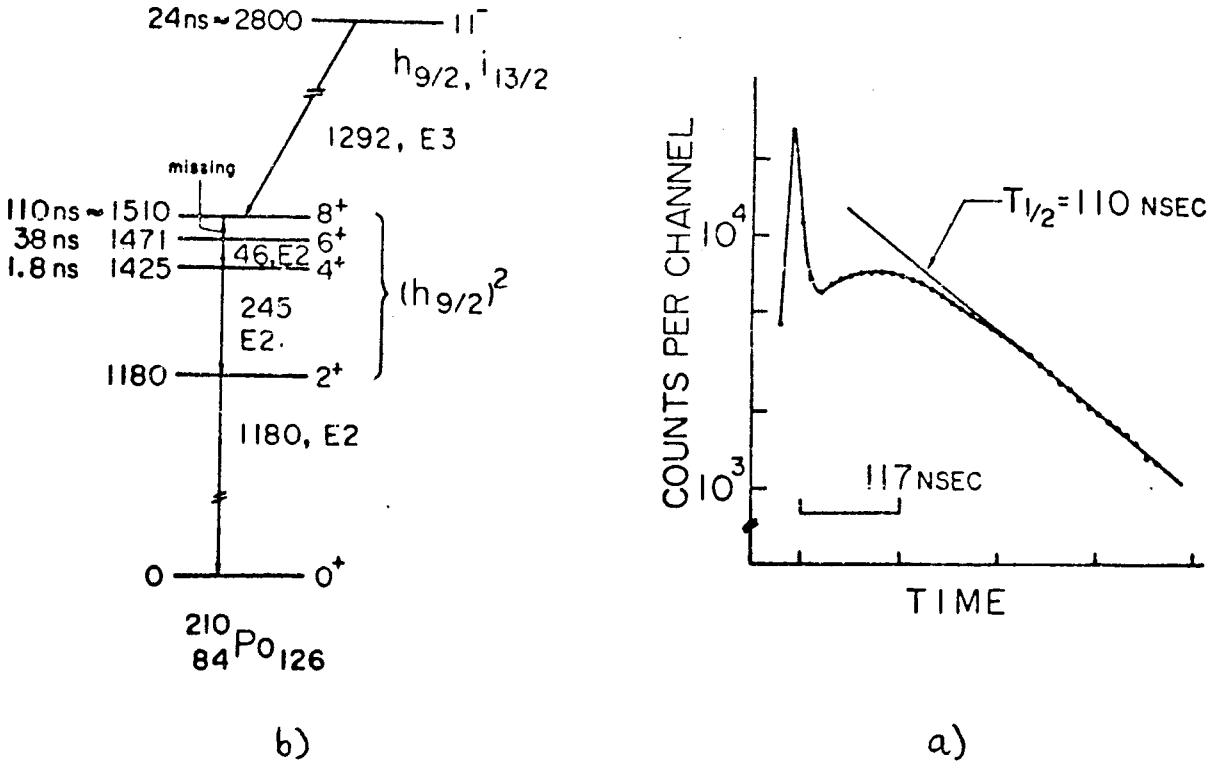

Fig.8 a) Time distribution of the 245 keV γ ray in the pulsed beam of 5-nsec width and 1.17 μsec inverval. The initial growth is due to the partial population of the 8+ state through the 24-nsec 11- state.

b) Level scheme of ^{210}Po established. Taken from ref.9).

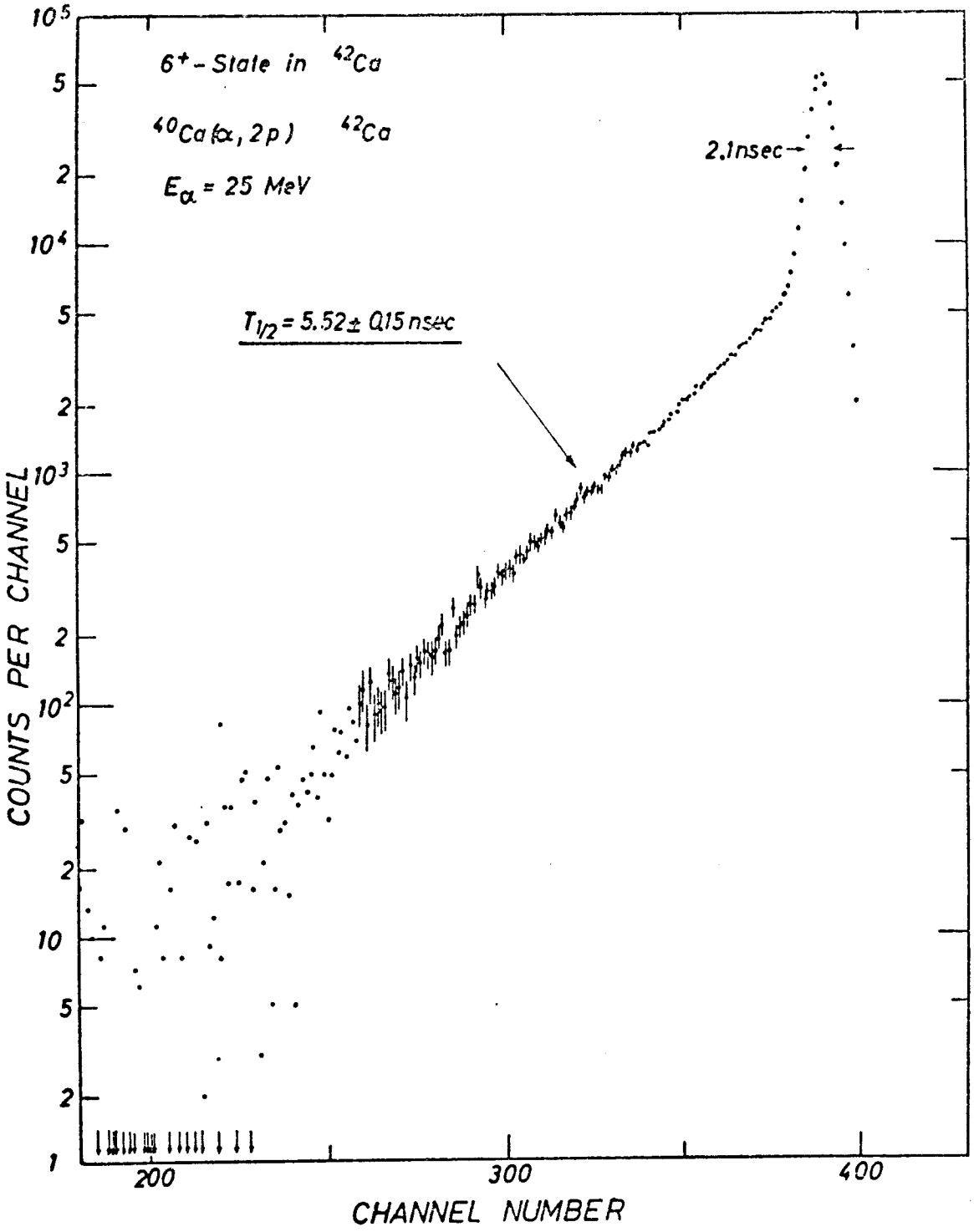

Fig.9 Time distribution of the 438 keV 6+ → 4+ γ ray emitted in the $^{40}Ca(\alpha,2p)^{42}Ca$ reaction at 25 MeV. A long-lived component due to the beta decay after the $^{40}Ca(\alpha,pn)^{42}Sc$ reaction has been subtracted. The prompt peak is due to the Compton background from prompt high-energy γ rays. Taken by Nomura et al.[10].

Naruma measured the time distributions of the $^{40}Ca(\alpha, 2p)^{42}Ca$ γ rays emitted for $E_\alpha = 25$ Mev . The figure shows the time spectrum of the 438 kev $6^+ \longrightarrow 4^+$ γ -ray; a long-lived components due to the beta decay after the $^{40}Ca(\alpha, pn)^{42}Sc$ reaction has been substracted. The prompt peak is due to the Compton background of higher energy γ rays, and the beam width is of the order of 2nsec in this case. Other posibilities of the time analysis method using pulsed γ beams is the measurement of the g-factor; by choosing the proper target and beam energy a large variety of new isomers can be reached, and very high spin states can be studied. This kind of study is in the beginning stage, and it seems there is a large number of unknown isomers. It is easy to find an isomer and to measure its half-life, but it is difficult to establish its isomeric decay scheme;coincidence studies and measurements of conversion electrons are often required in order to enable to draw some conclusion.

TIME OF FLIGHT SPECTROMETRY FOR CHARGED PARTICLES AND NEUTRONS

The nanosecond beam pulsing and precise time-of-flight techniques have improved during the last few years, so it is possible in many cases to resolve groups of charged particles or neutrons with a precision comparable to that obtained by the magnetic analysis of charged particles from nuclear reactions.

A survey of the literature shows that nanosecond work in the region of fast neutrons and charged particles is being done mainly in cyclotrons and dc accelerators such as tandems and Cockroft- Walton. Interest in fast neutron spectra comes from the necessity of data on nuclear energy levels to check models of the nucleus and from the fact that inelastic scattering cross sections are increasingly in demand for the design of fast reactors. The use of time of flight for charged particles is more recent, and has been used for particle identification.

As has been seen the flight time t for the flight path L and kinetic energy T is

$$t = L\sqrt{\frac{m}{2T}} = \frac{L}{c}\sqrt{\frac{mc^2}{2T}}$$

which, for neutrons, is

$$t = 72.3\, L\, T^{1/2} \quad \text{nsec}$$

where L is measured in metres and T in MeV,

The energy resolution $T/\Delta T$ equals $t/2\Delta t$, and we can increase it either by increasing t, (increasing the flight path) or by decreasing Δt ; since the beam flux reaching the detector varies inversely with the square of L, it seems better to decrease Δt rather than t . The choice of Δt is not simple: consider a ion burst of duration Δt_o which incides on the target. A particle originated in that target will then have an uncertainty Δt_o in the determination of its birth, and there are other sources of time uncertainty in the measurement of the time t which the particle needs to reach the detector.

The detector itself originates an uncertainty, Δt_d due to its thickness δ:

$$\Delta t_d = \frac{\delta}{L} t$$

since it is unknown at which point of the length δ the detecting signal arises.

The detection and electronic processes have a total time uncertainty which we call Δt_e . The value of the flight time t is fixed by the distance L, which is determined by the peak current available for the target, because that limits the flux of particles reaching the detector, and it is required to have a minimum acceptable signal to background ratio for the detector. Once fixed the values of L and t, the value of Δt_o is

fixed as the burst duration which gives the necessary precision of time determination, and the time between consicutive bursts, which is roughly equal to the flight time t. As an example, the figure gives the energy spread ΔT for neutrons as a function of neutron energy, for an uncertainty Δt of 1 nsec. The dashed curve shows the ΔT for L=5m which results from an additional Δt_d caused by an one inch thick detector.

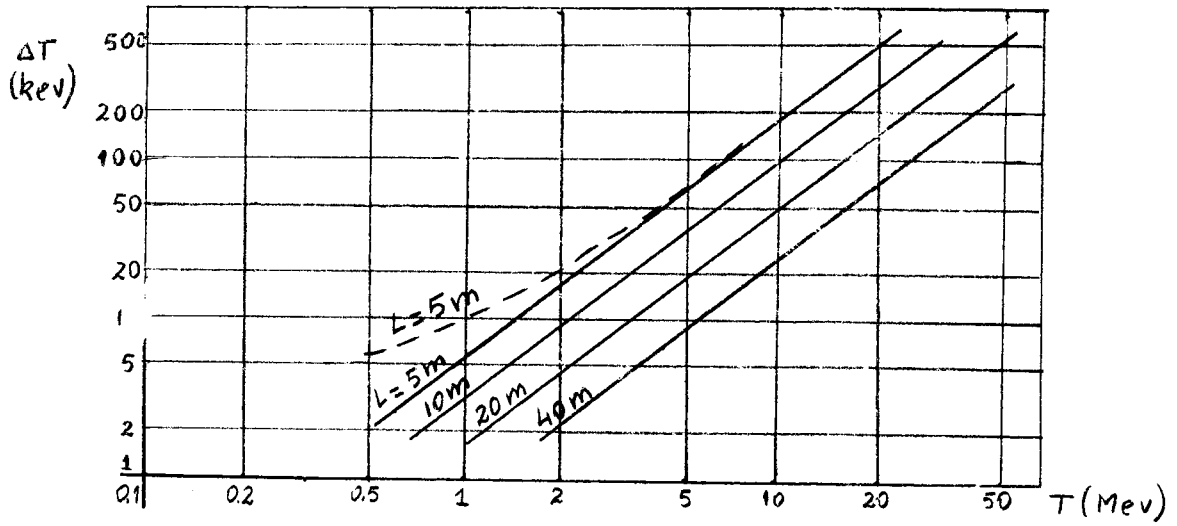

If Δt_o, Δt_d and Δt_e are smaller than the demanded by the peak current available and the precision in the measurement of time, the distance L can be shortened, so improving the signal to background ratio. That shows that the figure of merit to use for a time-of-flight spectrometer is the quantity instrumental resolving time per unit flight path, better than $\Delta t/t$, since a given energy will be measured with the same precision by two spectrometers having the same resolving time per unit flight path. For high energies the attainement of a good resolution implies time resolutions approaching the limit of the actual available techniques. For low energies the factor which determines the resolution is the beam homogeneity, and consequently the energy spread of the primary beam. Thus if the pulsed beam reaching the target has an energy spread ΔT, then the spread in the energy of the emerging particles or neutrons will be of the same order, if the yield curve for populating a certain level does not very appreciably over this energy internal.

Production of Pulsed Beams

As we have seen, it is necessary to produce beam bursts of time duration Δt_o with a peak current as large as possible. We will now review the methods used to obtain the pulsed beams:

Pulsed Electrostatic Accelerators

It is possible to produce the pulsed beam using a radio frequency ion source, in which the plasma gives a modulated beam with a frequency equal to the excitation radio frequency. This method has the disadvantage of needing to control the gas discharge, which is rather difficult.

The methods commonly employed are:

a) The beam chopping, in which one interrupts the beam chopping ~~in which one interrupts the beam, chopping~~ out parts which are discarded.

b) The bunching of the beam, in which the beam is divided into equal parts and then the parts are compressed in time, thereby producing a pulsed beam which has the same average current as the former dc beam.

Beam Chopping

The method consists in sweeping the beam across a slit by a radiofrequency voltage applied to two paralled plates, like in the Brookhaven National

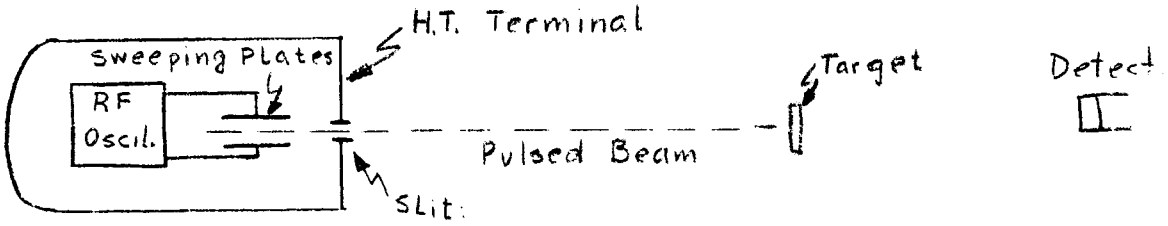

Laboratory experimental 4.5 MeV Van de Graaff, where the sweeping plates are located in the high voltage terminal.

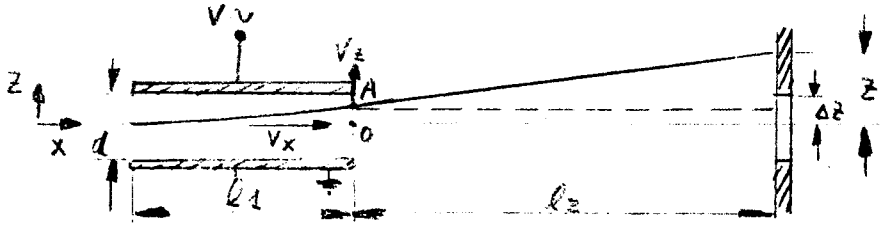

Let us suppose that the deflecting plates have a lenght l_1, and are at a distance l_2 from the slit. If the transit time through the plates is very small with respect to the period T of radiofrequency of voltage V, we consider that the accelerating electric field between plates, $\mathcal{E}_z$ is a function

$$\mathcal{E}_z = -\frac{V}{d} = \frac{V_0}{d}\left(\frac{2\pi t}{T} + w t_0\right)$$

If the beam enters the plates with the constant velocity V_x and energy $E = \frac{1}{2} m V_x^2$ the field E_z will displace it vertically with an acceleration

$$a_z = \frac{e\,\mathcal{E}_z}{m}$$

and wheh it reaches the exit of the deflector, the vertical displacement $\overline{OA}$ is, after the time $t = \frac{l_1}{V_x}$

$$\overline{OA} = \frac{e\,\mathcal{E}_z}{2m}\,\frac{l_1^2}{V_x^2}$$

The vertical velocity V_z is

$$V_z = \frac{e\,\mathcal{E}_z}{m}\,\frac{l_1}{V_0}$$

And the particles move from now on in a straight line towards the slit plane, where they hit the point Z. It can be seen in the figure that

$$\frac{z - \overline{OA}}{l_2} = \frac{v_z}{v_x}$$

and so

$$z = \frac{1}{2}\,\frac{l_2\, e\, \mathcal{E}_z\, l_1}{E} + \frac{1}{4}\,\frac{e\,\mathcal{E}_z\, l_1^2}{E}$$

where $E = \frac{1}{2} m v_x^2$

then, for an axial ray

$$\Delta z = \frac{1}{4}\, l_1 (l_1 + 2 l_2)\, \frac{e V_0}{E d}\, \Delta(\omega t_0)$$

or

$$\Delta t_0 = \frac{4 E d}{\omega e V_0}\, \frac{\Delta z}{l_1 (l_1 + l_2)}$$

As a typical example, for $E = 5$ keV, $d = 0.5$ cm

$\Delta z = 0{,}2$ cm $T = 10$ nsec l_1 and $l_2 = 5$ cm then $\Delta t_0 = 1$ nsec

An important remark has to be made about the RF sweeping: it may be obserbed that the pulsed beam is focused in two spots instead of one,

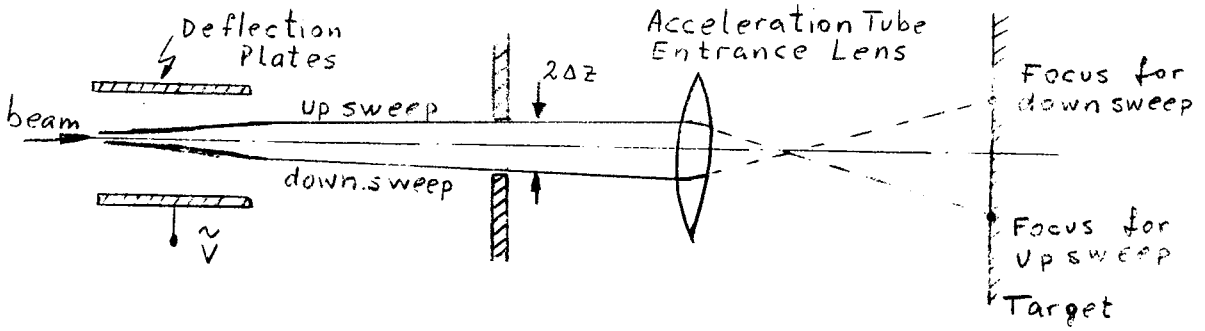

because the "up" sweep produces a virtual source which is displaced from the center by an amount equal and opposite to a similar source displacement produced by the "down" sweep. Thus two images are formed at the target, and this leads to ambiguities in the interpretation of data. This is usually corrected eliminating one of the sweeps, by following the pair of rf sweeping plates with a pair of de refractor plates, whose effect is to elevate or deppress the two virtual sources in the same direction, until one is directly on the optical axis and the other is suppressed by a collimator.

In general it seems that it is better to perform the pulsing between the ion source and the target, and not in the high-voltage terminal, because the pulse width Δt_0 is shorter in the former case. This is due to the fact that in the terminal the ion beam in general is not so well focused spatially and energetically as it is after acceleration

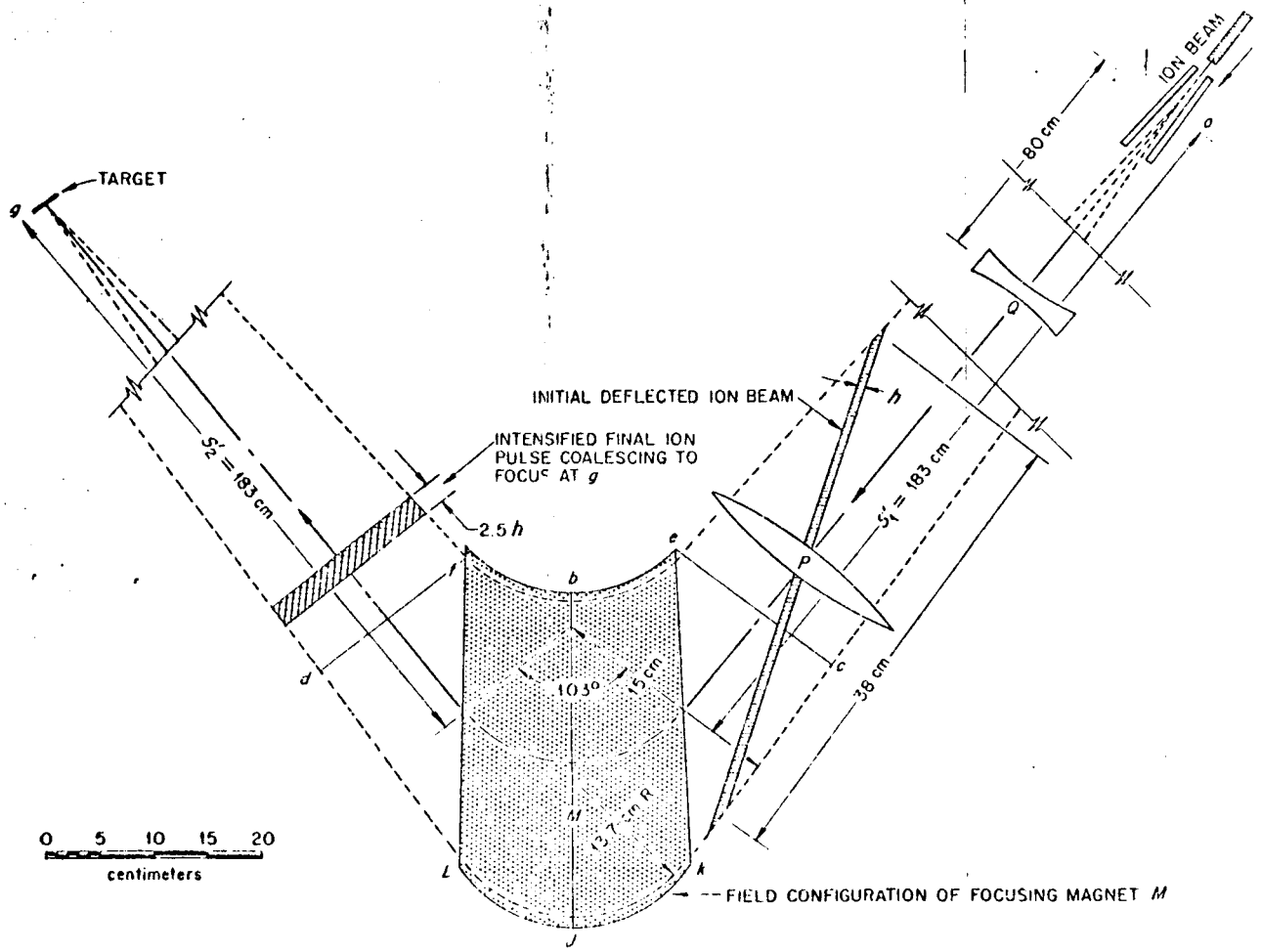
TARGET
g
INITIAL DEFLECTED ION BEAM
INTENSIFIED FINAL ION PULSE COALESCING TO FOCUS AT g
2.5 h
h
$S_2' = 183$ cm
$S_1' = 183$ cm
80 cm
ION BEAM
o
Q
P
a
b
c
d
e
f
L
M
k
j
103°
15 cm
13.7 cm R
38 cm
0 5 10 15 20
centimeters
FIELD CONFIGURATION OF FOCUSING MAGNET M

Beam Bunching

The compression of bursts of ions can be achieved in two different ways:

1) By speeding the last ions in a train of particles, so that after a certain time they catch up with the leading ions.

2) By causing the leading ions to take a longer path to get to a given point, where they meet the later ions. This second method was proposed by Mobley, and is usually known as the Mobley magnet buncher. It employs a double focusing magnet with deflector plates at one focus a and the target at the other focus g. The path lengths from a to g get progressively shorter for paths entering the magnetic field successively from K to e.

A triangular voltage pulse applied at a rf frequence to the deflector at a, will section the beam off

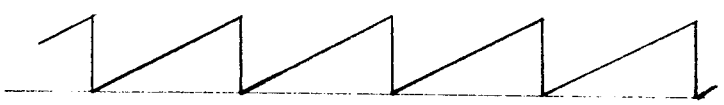

Triangular Voltage applied at deflector a

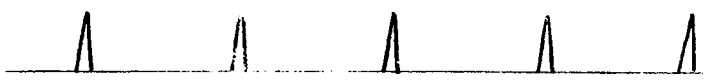

Beam Current at target Focus g

There is a limitation to this method: if one changes the the energy of the particles at the accelerator, it is necessary to change the sweep voltage and the magnetic field.

Also, there remains the problem of background arising from the unused beam.

The Mobley magnetic compression method has proved to be a popular and reliable method for achieving shatp ion bursts with Van de Graaff accelerators; as an example, a rf ion source and a beam chopper located in the high voltage terminal, produce pulses of 10 nsec width and 1000 nsec spacing; after acceleration the Mobley magnet system compresses the pulses to about 1 nsec width, and the peak current is several mA.

But this methods increases the beam divergence; also, the energy homogeneity deoreases, to 1:250 in the case cited, which is compared with values of 1:2000 common with dc beam from Van de Graaffs.

The Klystron Bunching

In that method a rf voltage is applied through a gap and increased during the passage of a train of ions in such a way that at a certain time or distance the consecutive ions in the initial burst arrive all simulataneously

Consider the Klystron buncher of the figure.

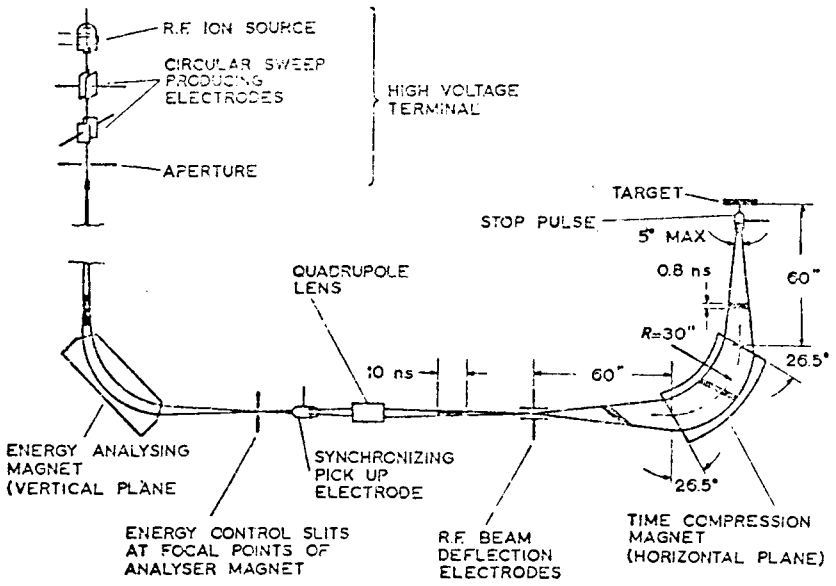

Fig. 1. Schematic diagram of pulsed-beam system.

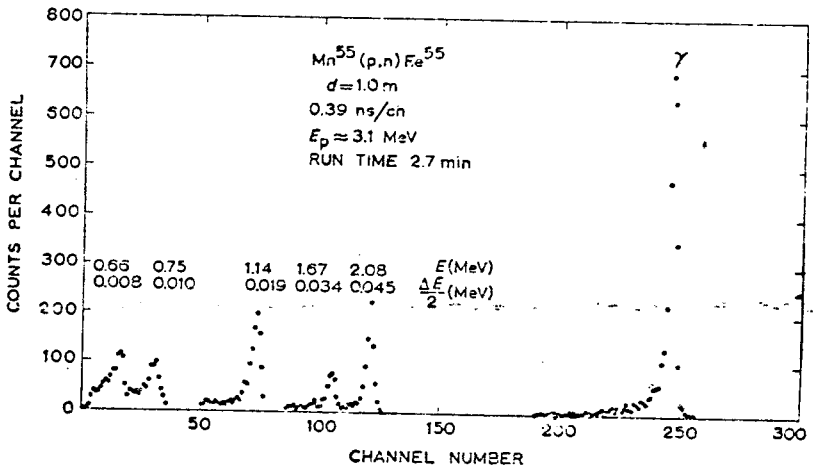

Fig. 2. Time spectrum for neutrons and gamma-rays from the reaction $Mn^{55}(p, n)Fe^{55}$ for zero-degree observation and the other conditions indicated on the figure.

a bunch of ions enters gap l_1 , with

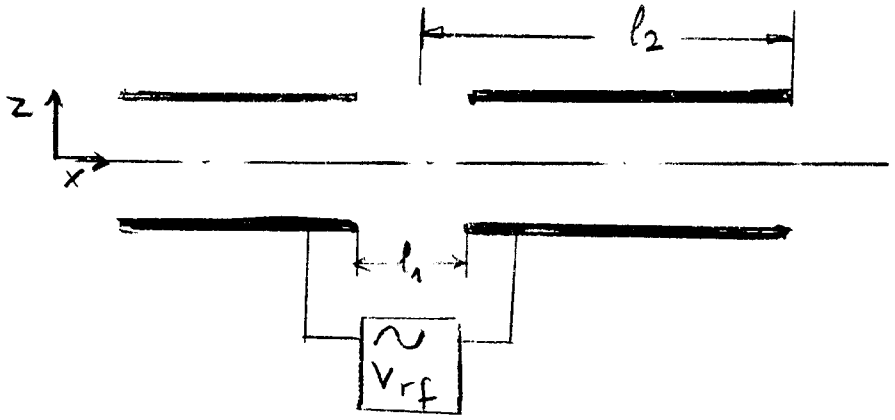

a potential across it

$$V = V_0 \cos \omega t$$

then the arrival time at a plane l_2 away is (ref. 7)

$$t' \approx t + \frac{l_2}{v_0}\left[1 + \frac{1}{2}\frac{eV_0}{E}\cos \omega t\right]$$

where E is the energy $\frac{1}{2} m v_0^2$ of the incidena particle.
Here $dt' = 0$ if $\omega \tau_2 eV_0 = 2E$
where

$$\tau_2 = \frac{l_2}{v_0} \qquad \sin \omega t \approx 1$$

The drift length l_2 is

$$l_2 = \frac{v_0 T E}{\pi e V_0}$$

where T is the period of bunching voltage.
A typical example of Klystron bunching is the compression of a 500 KeV deuteron beam, with 20nsec bursts, to 3 nsec bursts, and gaining a factor of a 6 in current. The bunching frequency was in that case 10 MHz, and ΔE across the bunching gap was 1 KeV.
A disadvantage of the Klystron bunching is that the method introduces a large energy spread in the incident ion beam.

R F Sweeping plus Klystron Bunching

At Livermore, Calif. a combined method was used in the Cockroft-Walton accelerator: a rf set of sweeping plates is followed by a Klystron buncher. About 95% of the beam is discarded on the rf sweeping slits, and the 5% remaining are bunched in bursts of 2 nsec. The diameter of the beam spot at the target is 1.5 cm, without any beam focusing after its entry into the pulsing apparatus.
A similar method is used in Tandem accelerators: a continuous negative ion beam from the Tandem ion injector is swept by

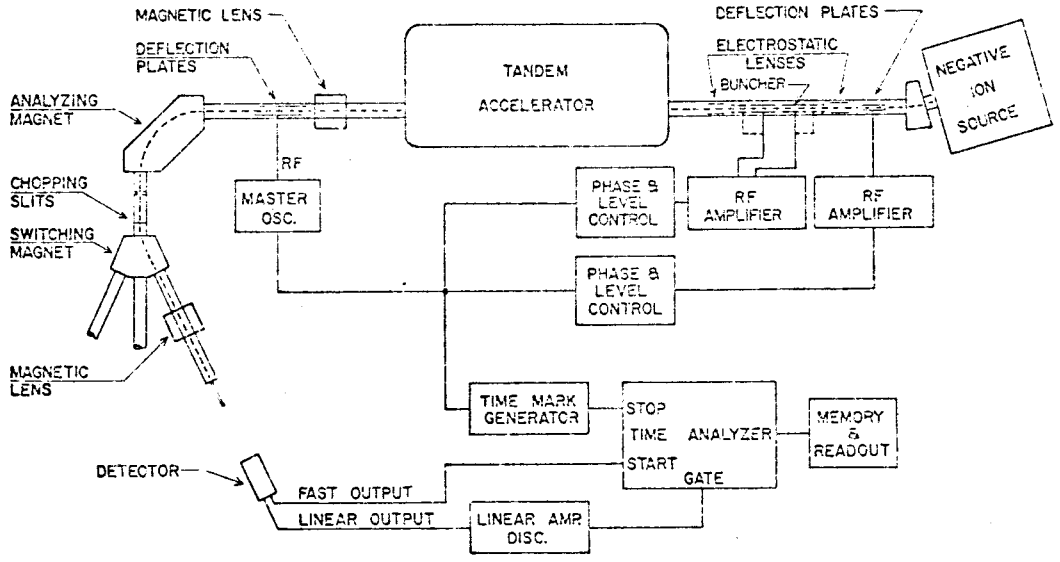

Fig. 1. Layout of tandem accelerator showing the neutron time-of-flight system (ref. 1).

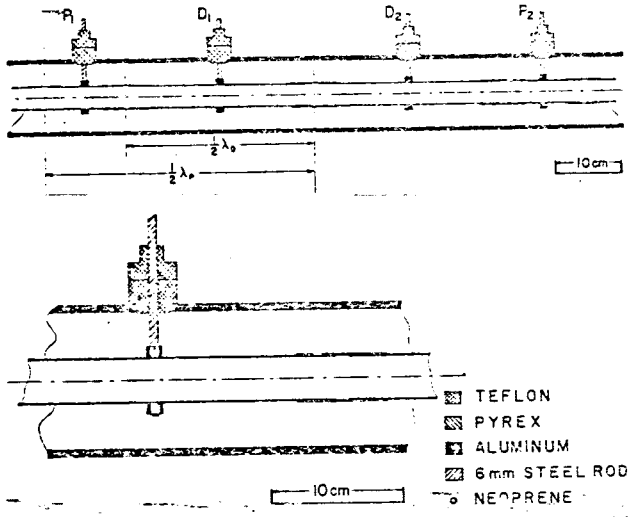

Fig. 2. Three-gap beam buncher. λ is the distance that ions will travel in one rf period. In order to bunch H^- ions electrodes P_1 and D_1 and electrodes P_2 and D_2 are connected. To bunch D^- ions electrodes P_1 and P_2 are grounded (ref. 1).

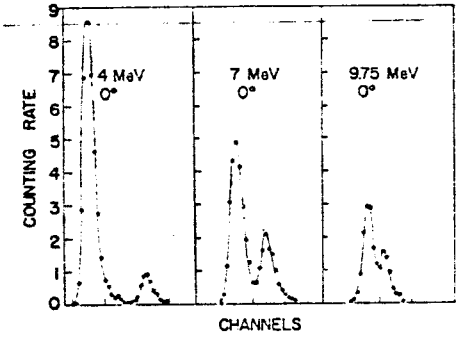

Fig. 3. Time spectra of neutrons emitted at 0° from the bombardment of Li by protons of energies at 4, 7, and 9.75 MeV. The two peaks are due to neutrons leaving the residual nucleus in the ground state and in the first excited state at 0.43 MeV (ref. 2).

means of deflection plates across an aperture to obtain pulses which may varied in duration from 25 te 70 nsec .
This pulsed beam is then passed through a bunching section where Klystron bunching techniques are utilized to obtain pulses of a few nanoseconds duration at the high end of the Tandem.
The minimum pulse length is limited primarily by the random energy spread present in the negative ion beam.
As an example, HVAC offers a nanosecond pulser for Model EN or FN tandems, with a pulse duration of 4.0 nsec and a bunching factor (ratio of the peak amplitude of the pulse to the available dc ion current at the same point of measurement) of 7.0, with a repetition rate of 2.5 MHz .
If the Tandem is equipped with a diode source, which provides negative ions by direct extraction, the pulse duration is 2 nsec and the bunching factor 15.0, for the same repetition rate of 2.5 MHz .

The Pulsed Beam of Cyclotrons

The cyclotron phase grouping was discussed by Bohm and Foldy in their theory of the Synchrocyclotron; the phase grouping is connected with the initial motion of the ions in a cyclotron before entry into the field-free region of the dees. In the fixed frequency cyclotron the complex motion of the ions before they enter into the dees results in a spatial and phase grouping which is mantained throughout the rest of its acceleration. The phase width in a cyclotron without feelers is (ref. 9.-)

$$\Delta\theta = \frac{eV_0}{2md^2\omega}$$

and with perfect feelers

$$\Delta\theta = 1{,}32 \left(\frac{eV_0}{2md^2\omega^2}\right)^{1/2}$$

where V_0 is the peak voltage between one of the dees and ground, d is the gap between dees, ω is the cyclotron radial frequency.
As an example, the Brookhaven Nat. Lab. 18 "cyclotron has a beam packet width of 1.2 nsec or 0.14 radians, and the Oak Ridge Nat. Lab. 80" cyclotron has a beam packet width of 3.5 nsec or 0.31 radians.
The repetition rates are usually of 50 to 100 nsec , and this in some cases causes difficulties, because the higher is the energy of the beam which bombards the target, the more complex is the velocity spectrum issuing from the target. When the period between target beam bursts is short, the slower velocity components will overlap one, two or more periods, producing a confusion in the measured spectrum. If the period between pulses is lenghtened, also the flight path will increase, and also the ener

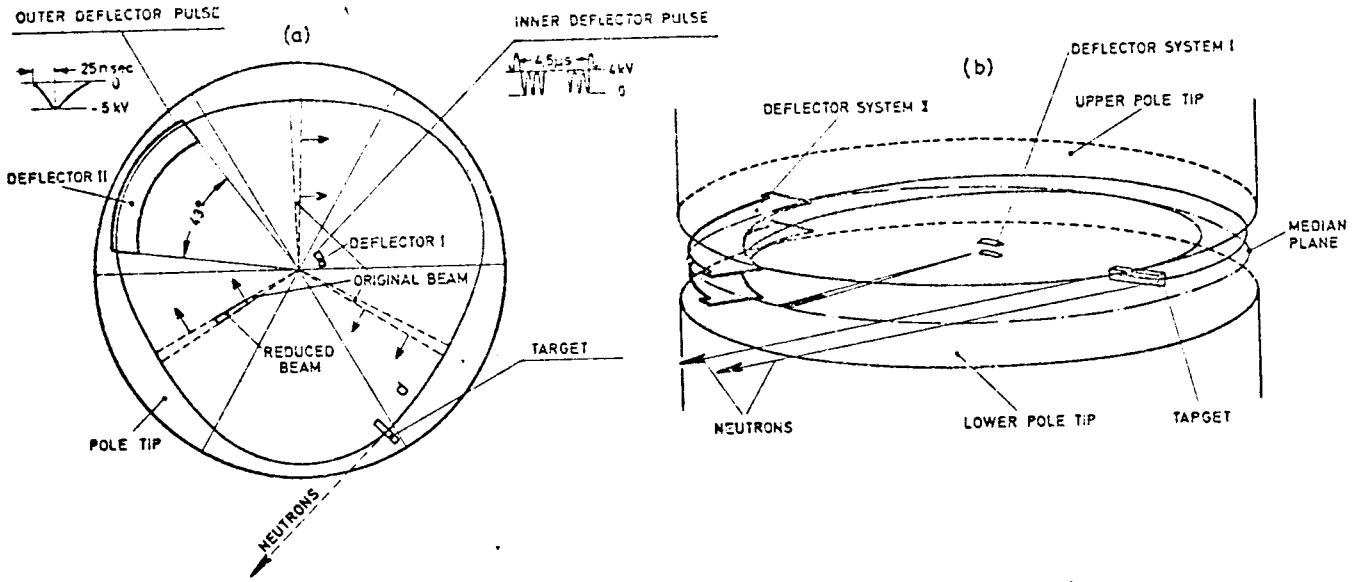

FIG. 1. Scheme of the bunching deflection system. (a) Top view. (b) Schematic drawing.

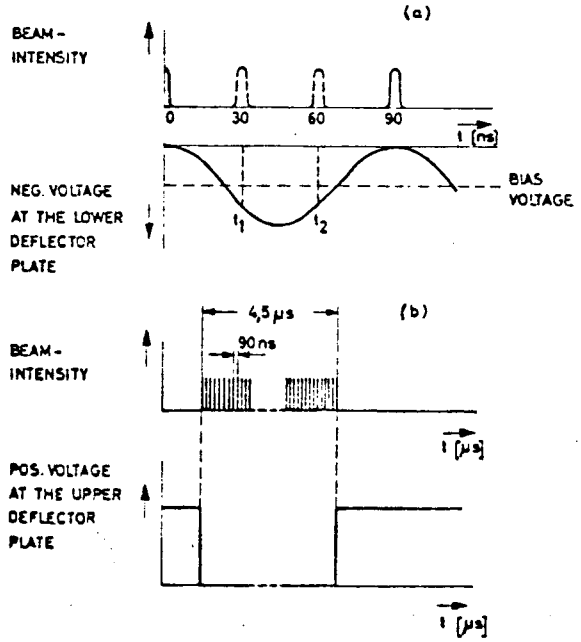

FIG. 2. Voltages of the deflector plates illustrating the principle of beam suppression. (a) Elimination of "two out of three" ion bunches. (b) Production of 4.5 μsec pulses.

gy resolution. This tends to lower the beam intensity, but at higher bombardment energies there is a tendency in most nuclear reactions towards a concentration in the forward direction of the particles emitted from the target, which compensates partly the inverse square law loss and thus encourages the use of longer flight paths and longer periods between bursts at higher energies.

The method of using the naturally pulsed beam of cyclotrons, without any change, has been frequently used, and for the experimentalist there is no important difference between it and a pulsed Van de Graaff or tandem. For instance, at the Brookhaven National Lab. the time-of-flight electronics used in the 18" cyclotron was installed without changes in the 4.5 MeV Van de Graaff. The only important difference was the rf fields which are in the vicinity of a cyclotron, and are picked up by the electronics. However, when considering the applications of the pulsed beam, it is usually desirable to have lower repetition rates, and for that it is necessary to eliminate one or more cyclotron bursts, by blocking the external beam or by stopping the beam near the ion source. The first method has the disadvantage that the stopped beam activates the metals it hits and gives a high radiation back ground.

The second method consists in stopping $N-n$ out of N particle micropulses by a collimator on the first turns, by applying a dc voltage to a deflector located near the dees.

When the repetition rate is high, as in the isochronous cyclotrons, it is necessary to introduce a device which eliminates pulses, such as described in references 10 and 11; the figure shows the central region of the Kalsruhe isochronous cyclotron, where the first orbit is defined by a set of slits mounted in the dees. Here the rf frequency is 33 MHz, so the spacing between beam bursts is 30 nsec, and the defining slits enable to achieve pulses of 0.2 to 0.5 nsec length. The reduction of pulse repetition rate and "bunching" was accomplished with two coupled pairs of deflection plates, as can be seen in the figure.

The deflector I is made of two tantalum plates separated by 10 mm, and it is located at the fourth ion orbit in a hill section of the magnet pole faces. The deflector II is made of copper plates separated by 14mm and it is located in the last remaining hill section. In the normal operation of the cyclotron, three ion bunches per revolution cycle are delivered from the source, and the deflector I eliminates two out of three pulses by deflection to a beam stop, and it also forms ion bunches of several microseconds duration, each consisting of about 50 microstructure pulses, with a repetition rate of 20 KHz.

The deflector II serves to deflect simultaneously the whole set of pulses to a neutron target above the median plane of the cyclotron.

For the elimination of two out of three microstructure pulses a

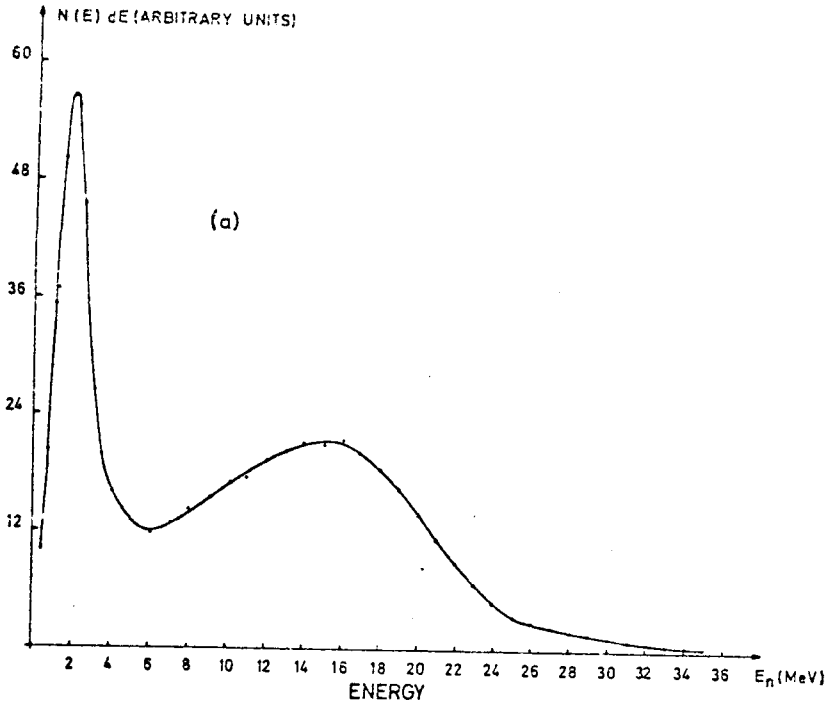

FIG. 9. (a) Typical energy spectrum. (b) Typical neutron time-of-flight spectrum.

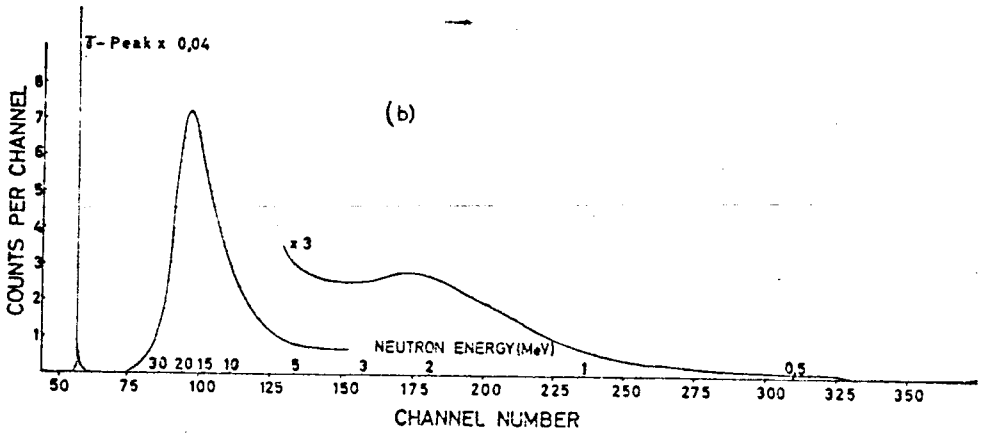

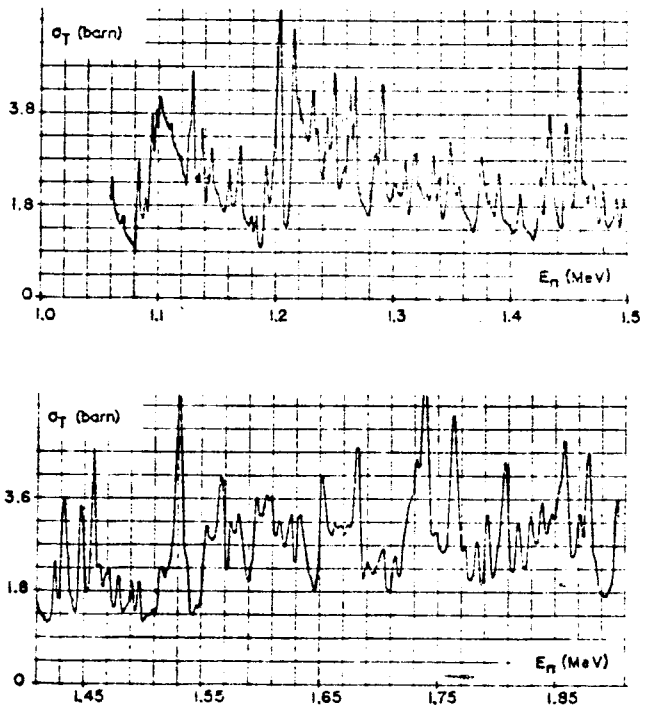

FIG. 11. Total neutron cross section of calcium.

sine wave as shown in t' figure is used. The first microstructure pulse passes the plates at a moment when the deflection voltage is zero, the two following pulses arrive after 30 and 60 nsec respectively and are removed from the beam.
For neutran production a natural uranium target, thick enough to stop the 50 Mev deuterons, is used.
The neutron time-of-flight spectrometer has a 57 meter flight path; there are two collimators defining a narrow neutron beam with a solid angle of about 2×10^{-6} srad.
The figure shows a typical spectrum obtained using a liquid scintillator at the end of the flight path. The maximun at about 16-20 Mev is due to neutrons from the deutron break-up in the coulomb field and at the nuclear surface.
The distribution at energies smaller than 6 Mev represents mainly the distribution of neutrons from evaporation and fission processes. The energy resolution for neutrons of 30 nev, $L = 57$ m, $\Delta t = 1$ nsec was determined as $\Delta E = 80.7$ KeV, for $\Delta t = 2$ nsec, $\Delta E = 161.4$ KeV, and for $\Delta t = 1$ nsec and $L = 180$ m is $\Delta E = 25.5$ KeV
so the overall resolution of the spectrometer is 0.025 nsec/m, with an integrated neutron flux at a 3 μA target current of $(5 \pm 2) \times 10^4$ neutrons - cm^{-2} - sec^{-1} above 250 keV at 57 meter.

The figure shows the total cross section for neutrons on calcium, measured with a 1-2% statistical error.

Measurement of the Flight Time

The measurement of the flight time is esentially a determination of a delayed coincidence between a reference time and the time at the event; in contrast with the nuclear decay determinations, it involves the precise and simultaneous determination of the positions of the peaks in a energy spectrum. This can be done by means of a multichannel coincidence system, where the number of channels depends on the characteristics of the experiment. When dealing with times of the order of monoseconds, it is necessary to determine accurately the initial time at which the burst starts; in principle this can be determined from the radiofrequency deflection pattern, but in practice it is done by calibrating the time scale with a known structure which is readily identifiable, such as the γ-rays from inelastic scattering, the elastically scattered neutrons, etc. Another technique for determining the start time is the associated particle method. As an example, let us consider the reaction $^3H(d,n)^4He$; here a neutron and an alpha particle are produced at the same time, and the pulse from the alpha particle detector, which is close to the source, gives the start for the time-of-flight measurement. The stop signal is obtained when a scattered neutron is subsequently detected. These pulses are then sent to a time to amplitude converter.
This method can also be employed with some difficulty with the

$D(d,n)^3He$ reaction.

In order to measure the time interval it is important to evaluate the resolving time or full-width at half maximun of the delayed coincidence curve; for multichannel systems the curve can be directly obtained when coincident signals are used to operate the two inputs. The coincident signals may be obtained from a fast pulser, from two separate detectors which observe coincident γ rays such as annihilation radiation, or alternatively a single detector may be used to observe the γ rays or neutrons produced from the pulsed accelerator.

An ideal time analyzer should have (ref. 3): time resolution of 1 nsec for detector signals, a differential linearity of about 5%, an integral linearity of about 1% over each of the time scales, sufficient number of channels to cover each time scale, insensivity to variations in counting rates over the range 10 to 10^4 counts per second, short term stability of the order of 0.1 of the channel resolution, and long term stability comparable to the channel resolution.

A special device for the delayed coincidences is the chronotron, which operates by determining the superposition locus along a transmission line of two pulses whose relative time interval is to be measured: the pulses of the particle detectors are applied one to each end of the transmission line, and they travel towards each other, their point of intersection being determined by a suitable array of detectors along the line. If one pulse is delayed with respect to the other, the meeting point will not be in the middle of the line, but it will be shifted towards the side of the delayed pulse. The time between the two pulses is 2 x/c where x is the distance from the center of the line to the point of intersection and c is the velocity of propagation of pulses on the line. Lefevre and Russell (ref. 12) have developed a chronotron which has gate widths of the order of 0.5 nsec, which are stable to 10^{-4} nsec.

The systems normally used are not as complicated as the chronotron; a time to voltage converter usually suffices. This device operates by the conversion of relatively short time intervals to pulse heights proportional to the intervals, and the pulse heights may then be analyzed in an ordinary commercial multichannel analyzer.

Usually it is not the electronic timing system that limits the resolution which can be obtained but the size and jitter of the detector.

Detectors for Time of Flight Spectrometry.

Most of the detectors used for fast timing have been liquid or plastic scintillators, although the solid state detector is being increasingly used. Several characteristics should be considered in discussing the different types of detectors:

a) The energy proportionality.
b) Efficiency
c) Background sensitivity
d) Speed of recovery

Some of the most used liquid or plastic organic scintillators are listed bellow

Phosphor	Electrons/cm^3 x 10^{23}	Hydrogen atoms/ cm x 10^{23}	Scintillation decay time nsec
Anthrancene	4.0	4.2	35
Stilbene	4.0	4.7	6
Tolvene + p-terphenyl	2.8	4.5	22

For energies above 100 keV the pulse amplitude response is linear with the recoil electron energy; the response to heavy charged particles is not linear, although the differential response approaches linearity for protons of 5 MeV. In order to detect a large number of neutrons, the detector shall be as large

as possible; but if too large, the difference in time between a neutron arriving at the point in the detector which is nearest to the source and one arriving at the furthest extremity of the detector can be large compared with the desired resolving time. Thus, if a plastic scintillator which has a thickness of 2 cm detects a 1 MeV neutron, that particle needs 1.4 nsec to traverse the detector and this means that a neutron detected at the front of the scintillator will be 1.4 nsec in front of a neutron detected at the rear, thus introducing a 1.4 nsec time spread. In order to obtain better time resolution , it is neccesary to use smaller detectors. Plastic or liquid organic scintillators coupled to fast photomultipliers are widely used to detect fast neutrons. A flat continuous distribution of pulse heights result from the fast neutron interaction with the scintillator, and in order to mantain a high counting rate it is desirable to use a wide dynamic range of pulse heights for timing.

If the scintillator area is not large and the pulses used for timing are a small range of the larger pulses, it is possible to detect neutrons of several MeV energy with a time jitter well under 1nsec.

The rise time of the pulse from the detector is governed by the decay time of the scintillator (2-4 nsec), the time taken by the photons to arrive at the photocathode, and the rise time of the photomultiplier (typically 2 nsec).

In 1957 L. Cranberg suggested that an effective method to reduce background would be to detect γ rays in coincidence with the source neutrons. Efficient detection of the γ ray requires that the detector be $NaI(Tl)$ or some other dense, high Z scintillator.

The list below shows the characteristics of some neutron detectors which use $(n,\alpha\gamma)$ reactions:

$^{10}B(n,\alpha\gamma)^{7}Li$, with a scintillator of $NaI(Tl)$, whose scintillation decay time τ is of 250 nsec, and which detects γ rays

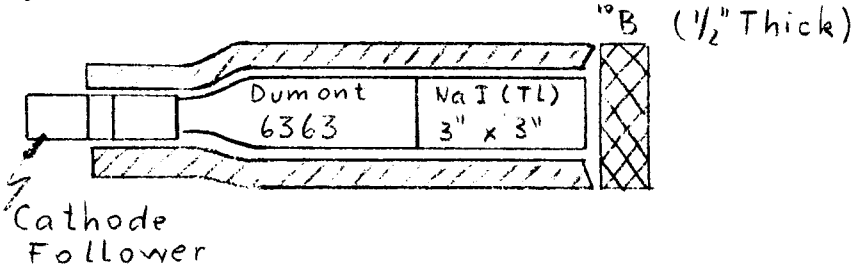

Neutron detector utilizing the reaction $^{10}B(n,\alpha\gamma)^{7}Li$

$^{6}Li(n,\alpha)T$ detects γ and T, with a scintillator of $LiI(Eu)$ and a decay time τ of 2000 nsec. $^{10}B(n,\alpha\gamma)^{7}Li$, detects γ when a $He + Xe\ (> 10\%)$ scintillator is used, and where a quaterphenyl wave length shifter is used. Here τ is less than 15 nsec.

A solid state detector which is used for experiments such as $(n,n'\gamma)$ is the $Ge(Li)$ detector.

Applications in Nuclear Reaction Studies

As an example we can discuss the method developed by H. Brückmann (ref.11) to study the reaction products n,p,d,t, He^3 and α in the energy range between* 0.5 and 6 m, the corresponding times of flight extend from 10 nsec to 200 nsec; but the separation between bursts of the primary beam is only 30 nsec, and the particles created by different beam pulses will overtake each other, as seen in the figure, were it

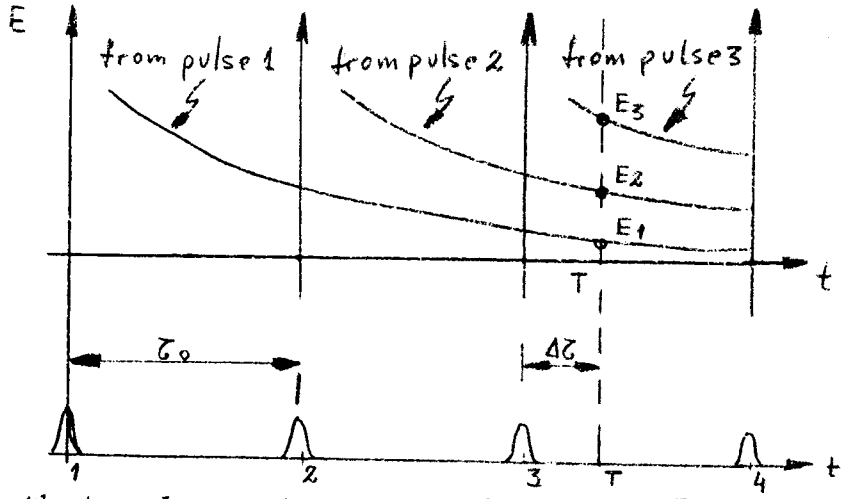

is assumed that only neutrons are detected. In the upper part the neutron energy versus time of flight is shown, and in the lower part the arrival time for successive beam pulses 1,2...
The point T marks the arrival time of a neutron at the detector and $\Delta\tau$ is the time difference with the preceding beam pulse.

The neutrons with energies E_1, E_2, E_3 from pulses 1,2,3 arrive simultaneously to the detector. The total time of flight is evaluated from

$$\tau = \Delta\tau + n\tau_0$$

where the integer n=1,2... is determined by a second independent measurement, and using the relativistic expression for the relation between time of flight, lenght of flight path, mass and energy, the exact energy of the particle is calculated.

In this determination the energy resolution has to be good enough only to separate the different branches at time T; the position of the reference pulses n is calibrated using the prompt γ radiation from the target. The measurement of the neutron energy is made with a proton recoil telescope, consisting of two flat scintillators: the first one of 0.5 to 2 cm thickness emits the recoil protons, which lose part of their energy in the scintillator, and the rest of the recoil energy is lost in a second scintillator of the same size placed 20 to 40 cm behind the first one. The pulses of the two detectors are added, giving a sum which measures the total proton recoil energy and determines the neutron energy with a precision which depends on the geometry. For the

* 10 and 100 Mev, using the isochronous cyclotron at Karlsruhe

For flight paths between...

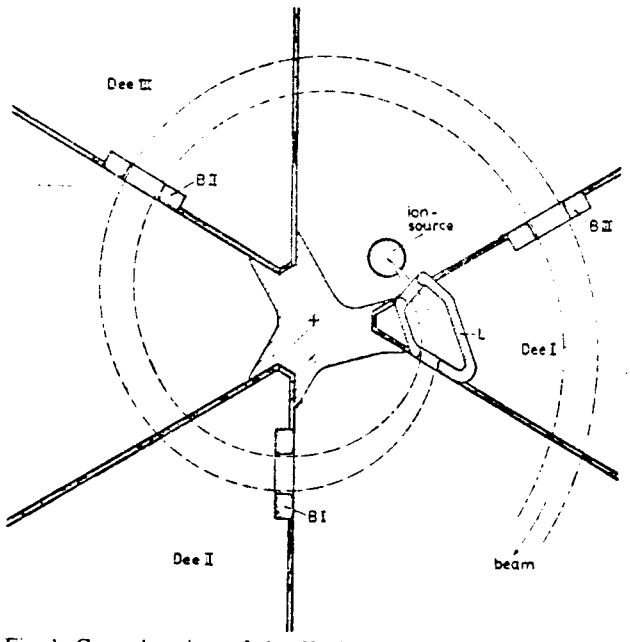

Fig. 1. Central region of the Karlsruhe isochronous cyclotron Schematically shown are the three dees I, II and III, the ion source and the beam defining slits L, B I, B II and B III.

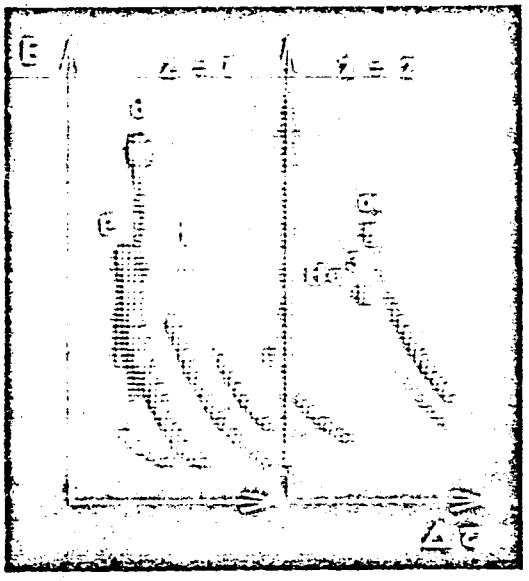

Fig. 9. Map display of protons, deuterons, tritons, ^{3}He and α-particles. These reaction products were sorted according to their charge into the right and left halves of the memory. The mass separation is achieved with the time-of-flight technique.

determination of the time of flight the timing signal is taken from the first scintillator. When determining the energy spectrum of charged particles, a solid state detector is used to give the energy signal. Since the time τ_0 is fixed by the radiofrequency of the cyclotron and is then known with an accuracy of 10^{-5} to 10^{-6}, the error introduced by the term $n\tau_0$, where n is large, is very small, and the main contribution corresponds to the accuracy in the determination of $\Delta\tau$.

The determination of the time difference $\Delta\tau$ implies that for each event the preceding beam pulse is selected out of the structure of rf pulses, and that $\Delta\tau$ is converted into an amplitude. When T is very close to a beam pulse, special care must be taken to avoid errors, since there a very small change in the position of T relative to the reference pulses will switch the output signal for $\Delta\tau$ from the maximum value to nearly zero. If a conventional time-to-pulse-height converter is used to measure $\Delta\tau$, the single pulse T starts the converter and the pulse chain of radio frequency has to stop it; but this mode of operation is nonlinear, so a more elaborate method is used.

The time-of-flight method can give a very accurate determination of absolute energies; at last as precise as using a magnetic analyzer, since only two absolute quantities, the distance L and the time-of-flight T have to be determined. As an example, the measurement of the time τ may have an error of 1.5×10^{-4} for L=10m and 50 MeV deuterons, so the absolute energy of the beam is determined with an uncertainty of $\pm 3 \times 10^{-4}$, or $E = 50\,MeV \pm 15\,keV$.

The method can be also used for particle identification: since it is only able to discriminate between different masses of the reaction products, it is necessary to combine a dE/dx measurement,* and so determine the charge and the mass of a particle separately.

A thin silicon transmission detector gives the timing signal as well as the dE/dx signal. This dE/dx generates a routing signal for particles with charge two, and the E signal is obtained from the sum of the dE/dx counter and a solid state counter placed directly behind the transmission detector.

The figure represents a 64 x 64 channel map display of particle energy vs. time-of-flight; on the left side particles with charge one are displayed; on the right side with charge two; buth spectra were taken simultaneously, using a gas target filled with ^4He bombarded with 50 MeV deuterons. In this case the reaction $^4He(d,t)^3He$ was of special interest, since the comparison of reactions (d,t) and $(d,^3He)$ was being realized.

Other applications of the time-of-flight method for charged particles consist in the measurement of differential cross sections, coincidence experiments for the study of three-particle reactions, polarization phenomena.

* with the time-of-flight measurament,...

NEUTRON MEASUREMENTS BY TIME OF FLIGHT

The use of time-of-flight in the one percent energy region for neutrons up to 100 MeV is increasing; this technique has been used to study neutrons of energies from 0.2 MeV up to 5 GeV. Since the range of energy is so wide, the equipment used to measure the time of flight varies enough to justify the division in three different energy intervals: slow neutrons, up to 10 keV; fast neutrons, up to about 100 MeV, and high-energy neutrons, for more than 100 MeV. We will consider the characteristics of slow and fast neutrons techniques.

Slow neutrons

Neutrons produced in nuclear reactions are usually fast, and it is necessary to slow them down before their interactions can be studied. The thermal neutrons of energies below about 0.5 eV are used primarily to obtain information about solid and liquid state; for energies between 0.5 eV and 10 keV the main use is the study of nuclear structure. In that range, the cross sections are comparatively simple to measure and analyse, since mainly 1=0 interactions take place, the scattering is always elastic and usually all angular distributions are isotropic. Nevertheless, many resonances are observed in each nuclide, and the spacing between the peaks is of a few eV, so the analysis of a large number of levels may result complicate. The use of those neutrons is primarily to study resonances in the compound nucleus for nuclei of intermediate and heavy mass, which give a description of the levels of the compound nucleus near the binding energy of the neutron; and the time-of-flight method is the only one giving enough high resolution to investigate these levels.

Since there is an inevitable intensity loss resulting from the method, the production of neutrons in sharp bursts of the highest possible intensity is necessary. The time-of-flight technique is the same whether the burst is produced by the modulation of the beam of an accelerator or by a mechanical chopper in a reactor, although in the last case the flux of thermal neutrons is about two orders of magnitude higher.

The counting rate is constant with energy for the time-of-flight method, and if we compare this method with the alternative one of using a crystal monochromator as a spectrometer, we see that the crystal has a very good intensity in the 0.1 to 10 eV region, and it rapidly becomes worse than the time of flight due to the decreasing of crystal reflectivity as the energy is increased.

The measurement of the time of arrival at the detector is usually done with a path lenght of 5 to 100 meters, and the

As can be seen, most of the measurements have been done for energies up to about 20 MeV, which corresponds to beams delivered from tandem Van de Graaf accelerators. Very little experiments have been done for higher energies, which can be obtained using cyclotrons.

Neutron sources

By bombarding targets with charged particles, or with photons, fast neutrons are generated in reactions like (p,n) (d,n), (α,n), (t,n), (γ, n) and fission. If the ion beam is monoenergetic, the neutrons are also monoenergetic; the reactions most frequently used are:

$D(d,n)He^3$ This reaction has a Q value of + 3.3 MeV, a range of monoenergetic neutrons at 0° of 2.45 to 7.70 MeV, and a threshold of 4.5 MeV for the competing reaction D (d, np) D, which becomes more possible as the bombarding energy is increased.

$T(p,n)He^3$ The Q is -0.76 MeV, with a laboratory threshold of 1.02 MeV. The monoenergetic neutrons emitted in the forward direction are produced for a range of energies from 0.3 to 7.58 MeV. The competing reaction is T(p,np)D with a threshold of 8.4 MeV.

$Li^7(p,n)Be^7$ The Q is -1.65 MeV, with a threshold of 1.88 MeV. The range of energies within which monoenergetic neutrons are produced at 0° is 0.12 to 0.65 MeV; since tritium became available, the T(p,n) He^3 reaction has replaced the $Li^7(p,n)Be^7$ as a neutron source in the 0.6 to 4 MeV energy range. The competing reaction is $Li^7(p,n)Be^{7*}$ with a threshold of 2.4 MeV.

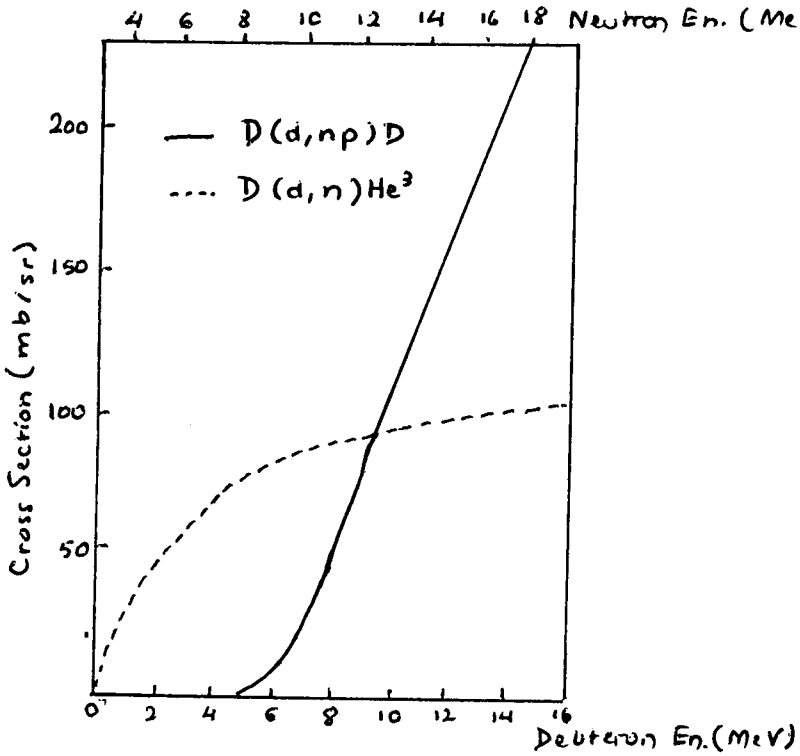

Zero degree differential cross sections for the production of neutrons from the D-D reaction (Ref.37).

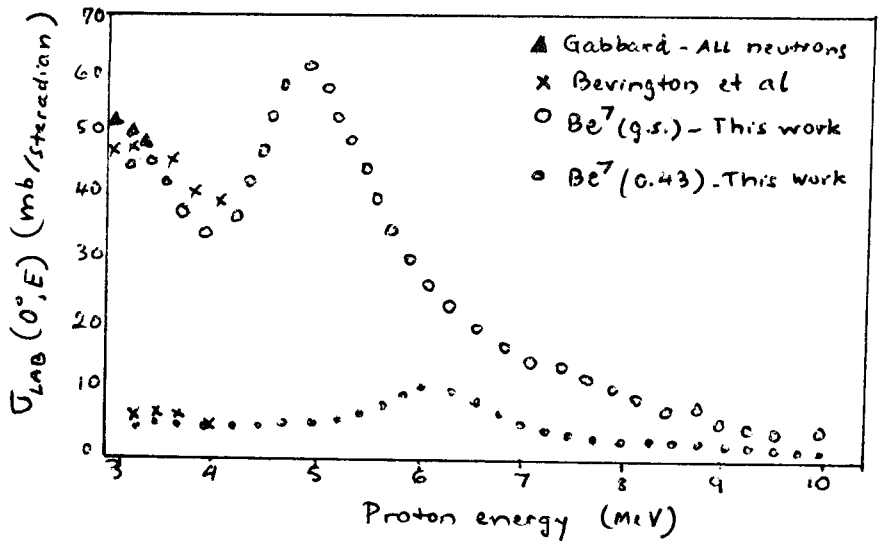

Zero degree differential cross section for neutrons from $Li^7 + p$. The upper points refer to neutrons leaving Be^7 in the ground state. The lower to the formation of Be^{7*} (Ref. 50)

$C^{12}(d,n)N^{13}$

Has a Q of -0.28 MeV, a threshold of 0.33 MeV, a range of monoenergetic neutrons at 0° of 0.03 to 2.76 MeV, and a threshold for the competing reaction $C^{12}(d,n)N^{13*}$ of 3.03 MeV.

$Be^9(\alpha,n)C^{12}$

The relatively large Q value of this reaction, 5.71 MeV permits experiments in the 7.7 to 10.6 MeV neutrons energy range by use of 2.5 MeV α particles. Below 2 MeV, the small cross section limits its usefulness as a neutron source. The competing reaction is $Be^9(\alpha,n)C^{12*}$, with a 0 threshold.

$C^{13}(\alpha,n)O^{16}$

With a Q=2.2 MeV, it is monoenergetic up to an α particle bombarding energy of 5.05 MeV, in which case the neutron energy at 0° is 7.06 MeV; this bombarding energy is the [illegible] 7.06 , this bombarding energy is the threshold for the competing reaction $C^{13}(d,n)O^{16*}$

$T(d,n)He^4$

Monoenergetic neutrons from 14.0 to 20.7 MeV at 0° are supplied by this reaction, which has the exceptionally large Q value of 17.6 MeV, and due to this high Q the neutron energy is relatively insensitive to the angle of emission for the region of low deuteron bombarding energy. The competing reactions are $T(d,n)pT$ and $T(d,n)nHe^3$, with threshold values of 3.71 MeV and 4.99 MeV respectively.

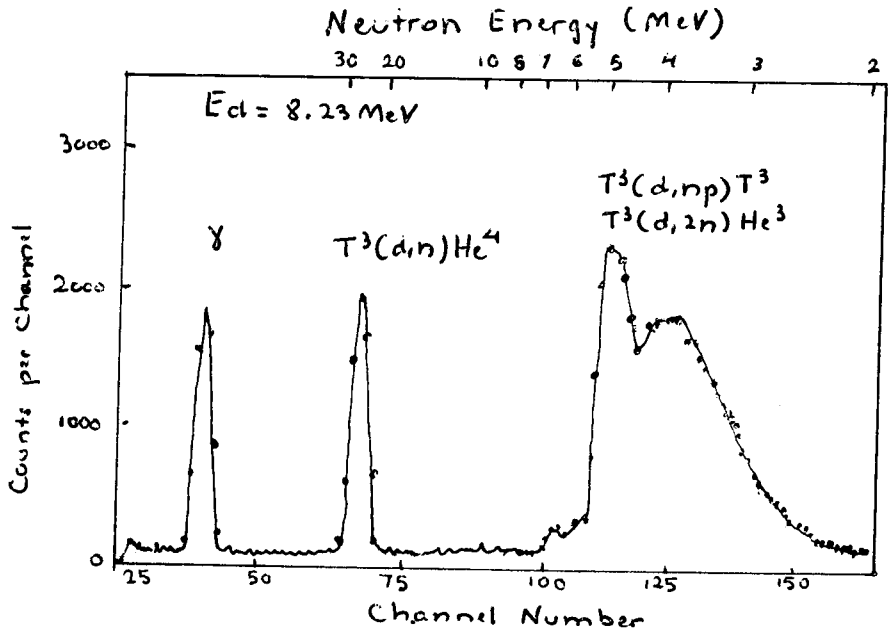

Time spectrum for neutrons from 8.23 MeV deuterons on tritium (Ref.51).

NEUTRONS OF MORE THAN 20 MeV

The increase of energy of the incident charged particle allows other neutron producing reactions; however those have an increasingly large energy spread, since many competing reactions become energetically possible. The most convenient way to work with these large energy spreads is to use the time of flight to define the energy of the incident neutron beam.

A technique for generating high energy neutrons uses the charge exchange in nucleon-nucleon collision. The figure shows the neutron energy spectra obtained at several angles bombarding LiH with 95 MeV protons (Ref. 52). At 0° the peak yield appears at about 85 MeV. Similar Results were obtained for LiD and Be.

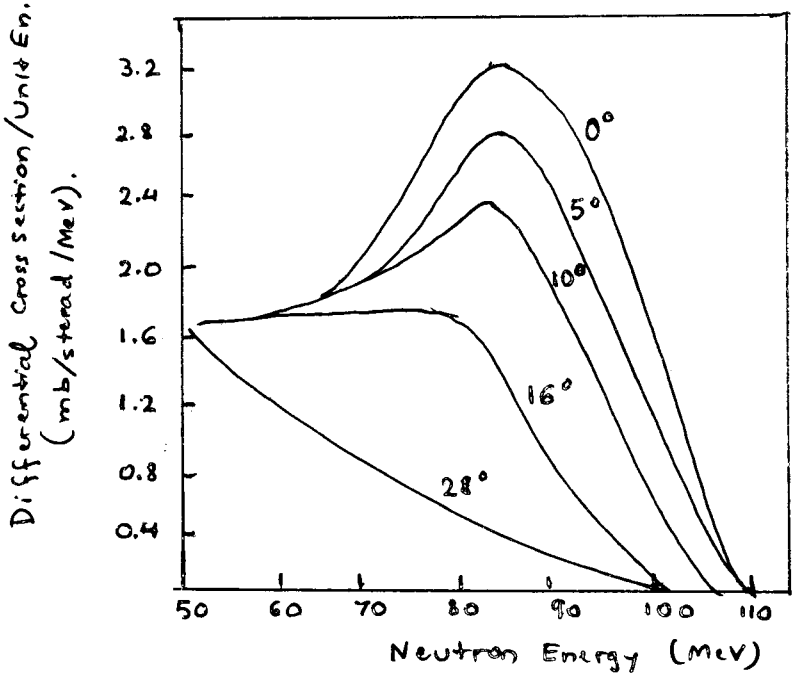

Neutron energy distribution observed at various angles from LiH bombarded with 95 MeV protons (Ref. 52).

ACCELERATORS USED FOR NEUTRON PRODUCTION

The tandem accelerator with pulsed beam can yield beam pulses lengts of about 1 nsec at a current of several miliamperes and a repetition rate of 10^6 per second; the high intensity pulsed beam has permitted considerable progress in inelastic scattering studies, particle induced neutron reactions and fast neutron capture.

The epithermal energy region up to several keV can be studied by means of the linear electron accelerator, which is a pulsed machine providing gamma rays and, through the nuclear photo effect, neutron bursts of great intensity. With this type of machine it is possible to carry out studies of the total, radiative, capture and scattering effects, involving angular momenta l=0,1,2 and to allocate the spin involved in a particular resonance interaction.

Another useful accelerator is the synchrocyclotron, which has a high instantaneous intensity and a pulse length of about one nsec. If instead of fast neutrons, low energy ones are wanted, it is necessary to place a moderator into the cyclotron tank to modify the original neutron spectrum; the slowing down in the moderator increases the pulse length.

The isochronous cyclotron is an intense neutron source for fast neutron time of flight experiments; utilizing a bunching system, it has been possible to obtain 10^9 neutrons in a 1.5 nsec burst (Ref. 5), and that converts the cyclotron into a time-of-flight facility with a very impressive perfomance.

Cyclotrons, both FM and SF, have been used for total cross section measurements of nucleons and nuclei as a function of energy, polarization experiments, and nuclear reactions. The neutron energy distribution corresponds to that of an evaporation spectrum with a peak of about 1 MeV, and a tail reaching into the 100 MeV region.

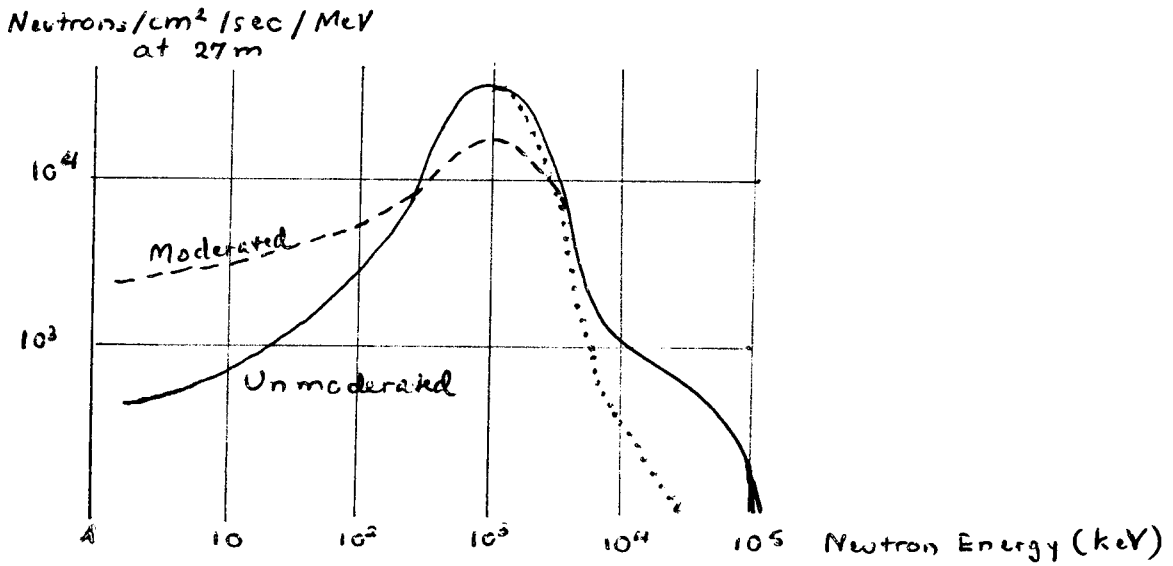

The figure shows the neuron spectrum of the Harwell 150 Mev synchrocyclotron (Ref.40). The dotted curve shows the unmoderated neutrons emitted in the backward direction.

The following table compares order of magnitude performance figures for a number of very intense neutron sources (Ref.5) They are arranged in order of increasing efficiency, measured in neutrons per MWatt-sec. The columns are: efficiency in n MW^{-1} sec^{-1}, pulse width τ in sec, repitition rate f, 4π peak neutron intensity I_p, average neutron intensity I_a, where $I_a = I_p \tau f = N f$, neutron yield per burst N, and figure of merit M, where $M = N f \tau^{-2}$.

Parameters of very intense neutron sources

FACILITY	n per MW sec	τ (sec)	f (sec^{-1})	I_p (sec^{-1})	I_a (sec^{-1})	N	M (sec^{-3})
RPI Linac	3×10^{15}	9×10^{-9}	720	4×10^{17}	3×10^{12}	4×10^{9}	3×10^{28}
GA Linac (pulsed fast booster)	3×10^{16}	1×10^{-5}	100	5×10^{20}	5×10^{17}	5×10^{15}	5×10^{27}
Harwell FM Cyclotron	7×10^{16}	1×10^{-8}	200	5×10^{18}	1×10^{13}	5×10^{10}	1×10^{29}
Karlsruhe Isochr. Cycl.	8×10^{16}	2×10^{-3}	2×10^{4}	7×10^{17}	2×10^{13}	1×10^{9}	1×10^{31}
IB. Reactor	3×10^{16}	4×10^{-5}	83	6×10^{16}	2×10^{14}	2×10^{12}	1×10^{23}

As may be concluded from the different values of τ, the research areas suitable for those intense neutron sources are:

1) $\tau \simeq 20 - 40$ μsec (pulsed reactors): solid state studies, radiation effects including relaxation effects, isotope production.

2) $\tau \simeq 5 - 10$ μsec (electron linacs): solid state studies (same as pulsed reactor but with higher resolution), nuclear systematics below 100 eV, radiation effects, isotope production, experiments on properties of fast neutron assemblies.

3) $\tau \simeq 0{,}001 - 5$ μsec (cyclotrons).

Nuclear reactions and nuclear structure, neutron resonance spectroscopy, solid state studies, isotope production, radiation effects, fast neutron parameters measured with high resolution.

Experiments in Neutron Physics

Fast neutron time-of-flight spectroscopy is able to supply unique data on nuclear levels; during the last decade the resolution has been improved by an order of magnitude, using the increased intensity of the new pulsed accelerators, and it is now possible to separate low-lying nuclear levels. Experiments which can give information on nuclear structure are the following:

Measurements of total cross sections.

The total cross section of nuclei is usually measured by means of a transmission experiment in which relative neutron flux measurements are made. The behavior of the total cross sections of nuclei for fast neutrons as a function of atomic weight and bombarding energy is well known, particularly below 15 MeV. Further experiments up to 100 MeV are interesting, to examine the maxima and minima which appear in this range. The existing results have given information concerning the properties of individual excited states in the coumpound nuclei formed in various reactions, and also have given important information about the character of the average interaction between a neutron and a nucleus.

As an example, the time-of-flight facility at the Karlsruhe Isochronous Cyclotron has been used for the total cross sections of ^{23}Na and Ca, for the energy range from 290 keV to 40 MeV (Ref. 20). The fast neutrons were produced in bursts of about 1 nsec by bombarding a U target with deuterons of the internal beam at a repetition rate of 2×10^4 Hz. With a flight path of about 57 m an overall resolution better than 0.05 nsec/m was obtained which corresponds to an energy resolution of 0.22 keV at 300 keV and 2.5 keV at 1.5 MeV.

The cross sections measurements were analyzed below 1 MeV using the multilevel R-matrix description with a single open channel for elastic scattering, since the resonance widths approach the level spacings for Na and Ca in that energy region, so making impossible the application of the usual Breit-Wigner single level formulae.

The results for Na from 0.28 to 1.02 MeV are shown in the figure, where the solid curve was calculated using resonance parameters. Here the inelastic scattering cross section is $\sigma_{n,n'} \simeq 300$ mb and since a satisfactory two channel fitting procedure was not available it was decided to extend the elastic scattering formulae. Due to inelastic scattering, the true total cross section was reduced from that given by the one-channel formalism by a factor of approximately

$$\frac{\Gamma_n}{\Gamma_n + \Gamma_{n'}}$$

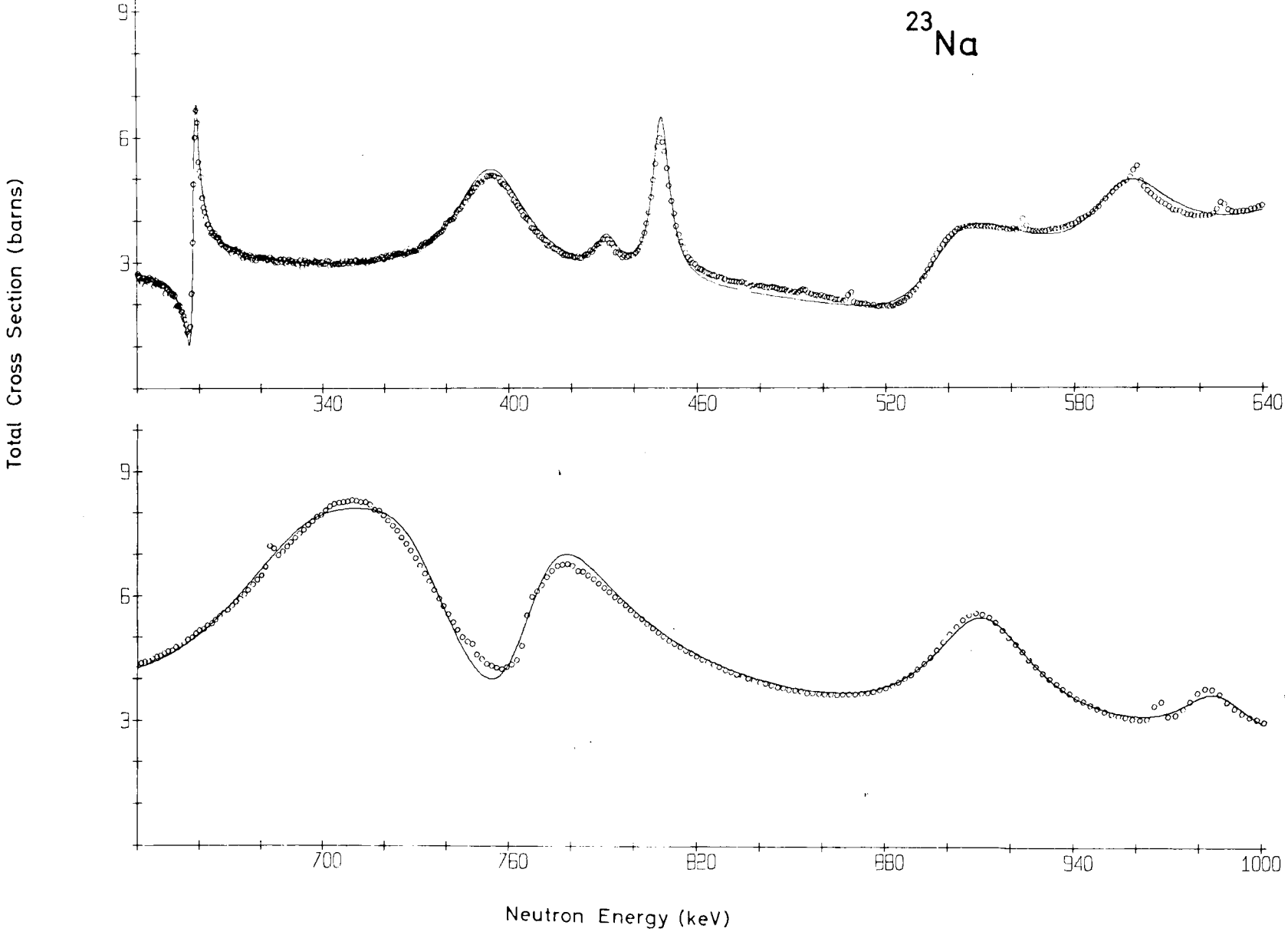

(Reference 54)

ELASTIC SCATTERING

The experimental values of the differential cross sections for elastic scattering of fast neutrons by nuclei can provide considerable information concerning the neutron-nucleus interaction in the entrance channel; because of the interference effects between the scattered wave and the incident wave, the differential cross section gives an indication of the properties of the interaction .

Two methods are used to obtain the angular distribution of elastically scattered neutrons: observation of the energy or the emission angle of the recoiling nucleus, and direct detection of the scattered neutrons. The former method has been used extensively with light nuclei where the momentum transfered to the recoil nucleus is sufficient to allow an accurate determination of its energy.

INELASTIC SCATTERING

At low energies the elastic and inelastic scattering are coupled through the compound nucleus, since an incoming neutron of energy E may form a compound nucleus with the subsequent emission of a neutron of equal energy E; in this case there is a compound elastic scattering, and not a shape elastic scattering and the cross section for this process may be of the same order of magnitude as for inelastic scattering. Experimentally both types of elastic scattering are difficult to separate, although they may be differentiated in part by a study of the angular distribution of the scattered neutrons. For neutron energies above 10 MeV the $(n,2n)$ reaction compates favorably with the (n,n') reaction, but at all energies the elastic scattering guides the selection of the potential to be employed in the interpretation of the inelastic results.

As the energy and scattering mass increases the levels become broad and closely spaced and finally overlap. Were the average resonance width Γ is much smaller than the level spacing D, and D is much smaller than the incident energy spread ΔE, many compound states are excited resulting in average cross sections that are symmetric about 90° and relatively smooth functions of energy though small fluctuations will remain. The average CN cross sections are given in the Hauser and Feshbach theory as

$$\sigma_c = \sum_\ell \sigma_c^{(\ell)} = \sum_\ell (2\ell+1)\,\pi\lambda^2 T_\ell(E)$$

Where $\sigma_c^{(\ell)}$ is the cross section for incoming partial waves of angular momentum l, λ the wavelength of the incoming neutron, and $T_\ell(E)$ is the transmission coefficient for the target nucleus for this ℓ and λ. As the incident neutron enrgy increases, direct inelastic scattering becomes more probable and the compound excitation of single states drops as the number of available exit channels increases.

When neutron inelastic scattering occurs, the residual nucleus is left in one of its excited states, and it decays either directly or by a cascade process, with the emission of γ rays;

therefore the nature and decay properties of the state ca. tained studying this radiation, which will also give the pr bility of inelastic neutron scattering to this particular st. te. Using the time-of-flight method, it is possible to discrimi. nate between γ rays due to inelastic scattering in the target, and the background due to neutrons scattered from the target into the detector.

NEUTRON INDUCED REACTIONS

Those are reactions in which charged particles are emitted as a result of bombarding target nuclei with fast neutrons. In general the neutron induced reactions are simpler than their charged particle counterpart; other advantages of stydying them are: the fact that neutron rich isotopes can be formed, and consequently they are used to determine the stability curve on the $N>Z$ side. A few examples of the neutron induced reactions are:

(n,p), where the total (n,p) emission cross section is not limited to the exchange between a target proton for a bombarding neutron, but includes such processes as (n,np) and (n,pp). The most elementary processes are conventionally described by the symbol $(n,p\gamma)$ .., corresponding to processes whose inverse is β^- decay. The mechanism of the (n,pp) reaction depends strongly in the incident neutron energy; at low energies and for heavy targets the Coulomb barrier binders proton evaporation, so a direct interaction mechanism is important.

(n,α) reactions.

Here the technique for measuring cross sections is similar to the one used for (n,p) reactions, with direct detection of the emitted alfa particles.

(n,d) , which can be related to the reaction (d,He^3) or (t,α) which deals with the same residual nucleus, similarly to (n,t) , which has as counter_part the reaction (p,He^3) .

In general the nuclear reactions which lead to three, four or more reaction products have been little studied because of their complexity, but many of them can give interesting information.

FUTURE OF NEUTRON PHYSICS.

Neutron physics is becoming a more and more important chapter in physics, not only because of the information it gives about nuclear structure, solid state and astrophysics, but also for its application to technological fiels, like reactor theory. Here there is required neutron nuclear data for the energy range from almost 0 to at least 15 MeV. The Panel on Neutron Data Compilation, in a meeting at Brookhaven in February 1969, reported the necessity of the following data types (Ref. 53):

a) microscopic cross sections for all neutron induced reactions between 0 and al teast 15 meV (for example (n,f),(n,γ), (n,n), (n,n'),(n,p),(n,α),$(n,2n)$ and other threebody-break-up reactions) together with quantities involving cross section ratios such as $\alpha = \delta n\gamma / \delta nf$ and $\eta = \nu / 1+\alpha$;

b) angular distributions for elastically scattered neutrons and elastic scattering polarization data;

c) angular and energy distributions for inellasticaly scattered neutrons;

d) differential angular and energy dependent excitation data for outgoing neutrons, protons, α particles, gamma-rays, etc., outgoing combination of these particles;

e) number, energy spectra and angular distributions of prompt and delayed fission neutrons and the half-lives of delayed neutron precursors;

f) resolved and statistical resonance parameters, statistical distributions of resonance partial half widths and level spacings;

g) Legendre polynomial coefficients of scattering angular distributions;

h) nuclear temperatures and single particle levels densities derived, e.g., from neutron inelastic scattering to the "continuum" range of residual nuclear energy levels and similar physically significant parameters derived by experimenters from their measurements;

i) fission product yields and cross sections;

j) "clean" integral data having immediate application in experimental neutron physics and in evaluation. The principal types are average cross sections measured in well-defined neutron spectra, such as thermal reactor and neutron fission spectra, together with so called 00 dilution resonance integrals for neutron absorption and fission processes.

REFERENCES

1.- P.H. Rose and A. Balejs- Progress in Nucl. Tech, and Instr. Vol. 2 - Edited by F. J. M Farley, North Holland, (1967).

2.- Third Accelerator Conference, Boston 1963, Nucl. Instr. Meth. 28, (1964).

3.- Particle Accelerator Conference, Washington, 1967, IEEE Trans. Nucl. Sci. NS-14.

4.- Particle Accelerator Conference, Washington, 1969, IEEE Trans. Nucl. Sc. Ns-16

5.- Brooks. N.B., A.B. Wittkower and R.P. Bastide, Rev. Sce. Instr. 35 , 894, (1964)

6.- Rose, P.H., A.J. Gale and R. J. Connor, Kerntechnik. 4, 246, (1962)

7.- Lawrence, A.P., R.K. Beauchman and J.L. Mc. Kibben, Nucl. Instr. and Meth 32, 357, (1966).

8.- N.J. Caling. H. Fauska and F.H. Schmidt. IEEE Trans. on Nucl. Sc. NS-16, 96,(1969).

9.- J. Reginald Richardson, Prog. in Nucl. Techn. and Instr. vol.1 edited by F.J. M. Farley, North Holland (1965).

10.-John J. Livingood, Principles of Cyclic Particle Accelerators, Van Nostrand (1961).

11.- L.H. Thomas, Phys. Rev. 54, 580 (1938)

12.- M. Stanley Livingston and John P. Blewett, Particle Accelerators, Chapters 9 and 11, Mc Graw Hill Co., New York (1962).

13.- S.S.Kolomensky and A.N. Lebedev, Theory of Cyclic Accelerators, Chapters 1, 2 and 4- North-Holland (1966).

14.- Henry Bruck, Accélérateurs Circulaires de Particules-Presses Universitaires de France, Paris.(1966).

15.-T.J Khoe and J.J. Livingood, IEEE Trans. on Nucl. Sci., NS-14 23, June 1967.

16.- H.G. Blosser, IEEE Trans. on Nucl. Sci. NS-16, 405, June 1969.

17.- B.L. Cohen, Cyclotrons and Synchrocyclotrons, Handbuch der Physik., XLIV, Springer, Berlin (1959)

18.-E.D. Courant andH.S. Snyder-Annals of Physics, 3, 1 (1958)

19.-P.S.Sturrock- Static and Dynamic Electron Optics, Cambridge University Press (1955)

20.-G.J. [illegible] Phys Rev 113, 311 (1959).

21.-B.L. Cohen, Rev. Sci. Instr. 30, 415 (1959)

22.-Bo Sjögren, Nucl. Instr. and Meth. 7, 76 (1960)

23.-H.S. Enge, Nucl. Instr. and Meth. 28, 119 (1964)

24.-W.C. Parkinson and J. Bardwick, Nucl. Inst. and Meth 78, 245 (1970)

25.-B. Kiani, D.A. Lind and R.R. Jonhson-Nucl, Instr. and Meth. 67 61 (1969).

26.- G.H. Mackenzie, E. Bashy, M.M. Gordon and H.G. Blosser, IEEE Trans. on Nucl. SC. NS-14, 450, June 1967.

27.-E. Jaitschke, W. Reichardt, G. Ischenko, F. Frosch, B. Huber and E. Reinsdorff, Nucl. Instr. 71, 29 (1969).

28.- D. Bohm and L. Foldy, Phys. Rev. 72 (1947) 649.
29.- Bernard L. Cohen Rev. Sci. Instr. 24 (1953) 589.
30.- Stewart D. Bloom "Nuclear Reactions" Vol. II ed. P.M. Endt and P.B Smith (North Holland Pub. Co. Amsterdam 1962).
31.- T. Yamazaki International Conference on Radiactivity in Nuclear Spectroscopy Nashville August 11-15 1969.
32.-A.L. Mc Carthy Bernard L. Cohen and L. H Goldman Phys. Rev. 137B 250 (1965)
33.-T.W Conlon R.A. Newman and A.L. Mc. Carthy Nucl. Phys. A104, 213 (1967)
34.-H.F. Birkmann C. Heiser and W.D. Fromm Nucl. Phys. A96 318 (1967)
35.-T. Yamazaki and G.T.Ewan Nucl. Instr. 62 101 (1969).
36.-W.W. Havens, Jr.- Time of Flight Method in "Methods of Experimental Physics" Vol. 5A Ed. L.C.L. Yuan and Chien-Shiung Wu, Academic Press, N. York, 1961.
37.- H.H. Barschall, Nucl. Instr. a Meth. 28 (1964) 44.
38.-P.H. Stelson, Nucl. Research with Low. En. Accelerators, Ed. J. Marion and D. Van Patter, Academic Press. N. York (1967)
39.- D. Dandy and D.P. Hammond Nucl. Instr. and Meth. 32, 23 (1964).
40.- Proceedings of the Intern. Conf. on the Study of Nuclear Structure with Neutrons, Antwerp. 1965 North Holland Co., Amsterdam 1966.
41.- R.C. Mobley, Phys. Rev. 88 (1952) 360
42.- J.M. Neiler and W.M. Good, Fast Neutron Physics, Vol. I Ed J. B. Marion and J.L. Fowler, Interscience Publ. Inc. New York, (1960)
43.-L. Cranberg, R.A. Fernald. F.S. Hahn, Nucl. Instr. and Meth 12 (1961) 335.
44.- Bernard L. Cohen, Rev. Sci. Instr. 24 (1953) 589.
45.- S. Cierjacks, et al. Rev. Sci. Instr. 39 (1968) 1279.
46.- H. Brückmann, E.L. Haase, W. KLuge and K. Schänzler. Nuclear Instr. and Met. 67 (1969) 29.
47.-H.W. Lefevre and J.T. Russell Bull. Am. Phys. Soc. 2 (1957).
48.- Ivo Slaus, Some Problems in Fast Neutron Physics IX Latin American School of Physics, Chile (1967)
49.- K.B. Mather and P. Swan Nuclear Scattering Cambridge Univ Press. (1958)
50.- R.R. Borchers and C. H. Poppe Phys. Rev. 129 2679 (1963)
51.- W.E. Wilson R.L. Walter and D. B. Fossan Nucl. Phys. 27 421 (1961)
52.- J.A. Hofmann and K. Strauch, Phys. Rev. 90, 449, (1953)
53.- JJ Schmidt, CODATA Newsletter. Dic. 1969.
54.-J. Nebe and G.J. Kirouac Second Internat. Confer. on Nuclear Data for Reactors, Helsinki (1970).